The role of medial septal neurons in orchestrating locomotion-related dynamics, and their projections to the hippocampus

Thesis

for the degree of

doctor rerum naturalium (Dr. rer. nat.)

approved by the Faculty of Natural Sciences of Otto von Guericke University Magdeburg

by MSc. Endre Levente Marosi

born on 28.03.1996 in Budapest, Hungary

Examiner: Prof. Dr. Stefan Remy

Prof. Dr. Tatiana Korotkova

submitted on: 17.12.2024

defended on: 18.08.2025

Preamble

I frequently hear nowadays how common it has become to deviate from the original goals outlined in our PhD proposals. This was mine 4 years ago: “My PhD aim is to gain deeper insight into two aspects of the role of Medial Septum and Diagonal Band of Broca complex (MSDB) in locomotion, learning and memory. Namely, I will investigate (1) the electrophysiological characteristics of VGluT2+ neurons in the MSDB, and (2) identify the role of the septo-hippocampal projections of specific MSDB cell types along the dorsoventral axis.” Today, after gaining valuable insights along my journey, I would slightly rephrase this paragraph—acknowledging that here I do not provide direct evidence regarding the functional role of septo-hippocampal projections. Instead, I invite you to dig deeper into (1) the in vivo electrophysiological characteristics of neurons in the MSDB, and (2) the identification of a projection gradient of MSDB VGluT2+ cells along the dorsoventral axis of the hippocampus. Although the wording of my aims evolved slightly over time, their significance transformed profoundly in my hands. In those early days, I couldn't fully appreciate the complexity of the questions we were exploring. However, as I delved deeper into the study of the septum, I came to realize how much valuable work had already been done, while also uncovering gaps in our understanding—gaps that I sought to address through the discoveries made in this thesis. This thesis does not aspire to solve the Rubik’s cube of neuroscience. Instead, it takes a modest yet confident approach, contributing a small but meaningful building block to the ever-growing structure of human understanding.

I can only imagine how challenging it might be to navigate through long pages of dry data. To ease this experience, I aimed to soften the tone of my descriptions and, from time to time, add a spark of interest with occasional personal notes to engage the reader. I find this important for the sake of captivity, hereby not only pleasing the reviewers, but my friend, Benjamin, and hopefully some of the upcoming generation of master or PhD students in the Mikulovic lab, where this whole story thrived.

During the last 4 years, I had the chance to get in touch with several techniques through different projects. However, the highest improvement I reached by changing from *in vitro* single cell electrophysiology to population recordings in living animals methodically (*in vivo* veritas?),

and also acquired the subsequent coding skill that was important for the data analysis. I am humbly grateful for this experience.

The analysis of our behavior videos, anatomical sections, and the literature formed my view on subcortical circuits. I think, that these pathways are in delicate synchrony, which leads to cortical neuromodulatory changes, their balance may influence different behaviors and motivations. Exploring subcortico-cortical interactions during locomotion is, to me, an incredibly exciting avenue for further research. If I were to draft a starting grant proposal to establish a lab dedicated to subcortico-cortical interactions (SCI Lab), this topic would undoubtedly be at the heart of its focus. Join me on the journey of my Phd thesis, and I hope to show you why this topic is so compelling.

Table of content

List of abreviations

$[Ca^{2+}]_o$:	extracellular calcium concentration
4-AP:	4-amynopyridin
5-HT:	5-hydroxytryptamine
AAV:	adeno-associated virus
ac:	autocorrelation function
ACh:	acetylcholine
AChE:	acetylcholinesterase
ACSF:	artificial cerebrospinal fluid
AMPA:	α-amino-3-hydroxy-5-methyl-4-isoxazolepropionic acid
Amy:	amygdala
AP:	action potential
AUC:	area under the curve
bAP:	backpropagating action potential
BF:	basal forebrain
BG:	basal ganglia
BI:	burst index
BLA:	basolateral amygdala
BNST:	bed nucleus of the stria terminalis
CA1/2/3:	Cornu Ammonis 1/2/3
Ca^{2+}:	calcium
CaMKII:	calcium/calmodulin-dependent protein kinase II
CB:	calbindin
CCK:	cholecystokinin
ChAT:	choline acetyltransferase
ChR2:	channelrhodopsin-2
CME:	camera motion energy
CNS:	central nervous system
CPG:	central pattern generator
CR:	calretinin
CRH:	corticotropin-releasing hormone
Ctrl:	control
cw:	continuous wave
DA:	dopamine
D-AP5:	D-2-amino-5-phosphonopentanoate
dHC:	dorsal hippocampus
DLC:	DeepLabCut
DNQX:	6,7-dinitroquinoxaline-2,3-dione
E/I balance:	excitatory/inhibitory balance
EC:	entorhinal cortex
FC:	fear conditioning
GABA:	γ-aminobutyric acid
GAD:	glutamic acid decarboxylase
GECI:	genetically encoded calcium indicator
GFP:	green fluorescent protein
GLM:	generalized linear model
HC:	hippocampus
HCN:	hyperpolarization-activated, cyclic nucleotide-gated channels
I_{CAN}:	calcium-activated non-selective cation current
I_h:	hyperpolarization-activated current
IR:	input resistance
ISI:	inter-spike interval
IStI:	inter-stimulus interval
LFP:	local field potential

LH:	lateral hypothalamus
LHb:	lateral habenula
LIN:	Leibniz Institute for Neurobiology
LS:	lateral septum
mAChR:	muscarinic acetylcholine receptor
MCPG:	(RS)-α-Methyl-4-carboxyphenylglycine
MEA:	multielectrode array
mGluR:	metabotropic glutamate receptor
MLR:	mesencephalic locomotor region
MSDB:	medial septum and diagonal band of Broca
MTL:	medial temporal lobe
Na^+:	natrium
NAAG:	N-acetyl-aspartyl-glutamate
NAc:	nucleus accumbens
nAChR:	nicotinic acetylcholine receptor
NBQX:	2,3-Dioxo-6-nitro-1,2,3,4-tetrahydrobenzo[f]quinoxaline-7-sulfonamide
NE:	noradrenaline/norepinephrine
NI:	nucleus incertus
NMDA:	N-methyl-D-aspartate
NPX:	Neuropixels
NPY:	neuropeptide Y
NR:	nucleus reticularis
NREM:	non-rapid eye movement
ORX:	orexinergic
PAG:	periaqueductal gray
PBS:	phosphate-buffered saline
PC:	pyramidal cell
PCR:	polymerase chain reaction
PF:	persistent firing
PFA:	paraformaldehyde
PFC:	prefrontal cortex
POA:	preoptic area
PPN:	pedunculopontine nucleus
PR:	paired ratio
PV:	parvalbumin
PVN:	paraventricular nucleus
RF:	reticular formation
RI:	rhythmicity index
R_{in}:	input resistance
SOM:	somatostatin
sPUPr/nr:	stimulated pupil dilation with running/ no running (successful/non-successful run initiation)
SWR:	sharp wave ripple
TRP:	transient receptor potential
V1:	primary visual cortex
VGluT(1/2/3):	vesicular glutamate transporter (type 1/ type 2/ type 3)
vHC:	ventral hippocampus
VIP:	vasoactive intestinal peptide
VMH:	ventromedial hypothalamus
VTA:	ventral tegmental area

Summary

Locomotion is a fundamental behavior critical for the survival of many species. Beyond mere movement, locomotion is tightly linked to sensory processing, motivation, and cognition. Locomotion-driven sensory input, such as tactile, visual, or auditory cues, informs an organism about its surroundings, and these inputs are integrated to guide learning and memory processes. The medial septum and diagonal band of Broca (MSDB), a crucial hub in the basal forebrain, has emerged as a key player in these processes, facilitating communication between cortical and subcortical regions. The MSDB plays pivotal role in synchronizing neural activity in brain areas, like the hippocampus (HC), a structure central to memory and navigation.

The HC extends along a dorsoventral (dHC, vHC) axis exhibiting functional specialization. Despite decades of research on the MSDB-dHC pathway and its role in cognitive memory formation, far less is understood about the MSDB-vHC projection and how these connections contribute to emotional behaviors. Exploring the molecular and anatomical differences between MSDB cells projecting to these hippocampal subregions is vital for understanding how this brain region regulates distinct aspects of cognition and emotion.

The functional role of the MSDB extends beyond hippocampal interactions. MSDB neurons are uniquely positioned to integrate sensory and motor information, but whether they facilitate synchronization among behaviors such as whisking, running, and pupil dilation is still an open question.

Persistent firing (PF), a phenomenon in which neurons maintain activity beyond a stimulus, offers a potential mechanism for the MSDB's coordination of motor and cognitive processes. Intriguingly, rhythmic phenomena such as whisking, pupil dilation, and locomotion often align with cortical state modulation. PF in the MSDB may serve as a bridge between motor behaviors and neural state changes.

This thesis investigates the MSDB's role in coordinating locomotor-related neural and behavioral mechanisms and its anatomical projections to the hippocampus. By addressing these aspects, this work aims to clarify the MSDB's integrative role in linking sensory, motor, and cognitive functions, contributing to a deeper understanding of its functions in health and disease.

Zusammenfassung

Lokomotion ist ein fundamentales Verhalten, das für das Überleben vieler Spezies entscheidend ist. Über die reine Bewegung hinaus ist Lokomotion eng mit sensorischer Verarbeitung, Motivation und Kognition verknüpft. Sensorische Eingaben wie taktile, visuelle oder auditive Reize, die durch Lokomotion ausgelöst werden, informieren den Organismus über seine Umgebung und steuern Lern- und Gedächtnisprozesse. Das mediale Septum und der diagonale Band von Broca (MSDB), ein zentraler Knotenpunkt im basalen Vorderhirn, erleichtert die Kommunikation zwischen kortikalen und subkortikalen Regionen. Es spielt eine Schlüsselrolle bei der Synchronisierung neuronaler Aktivität in Bereichen wie dem Hippocampus (HC), einer Struktur, die für Gedächtnis und Navigation essenziell ist.

Der Hippocampus zeigt eine funktionelle Spezialisierung entlang seiner dorsoventralen Achse. Während die MSDB-dHC-Verbindung intensiv in der kognitiven Gedächtnisbildung erforscht wurde, ist über die MSDB-vHC-Projektion und ihren Beitrag zu emotionalem Verhalten wenig bekannt. Die Untersuchung der molekularen und anatomischen Unterschiede von MSDB-Zellen, die zu diesen Hippocampus-Unterregionen projizieren, ist entscheidend, um die Regulation von Kognition und Emotion durch das MSDB zu verstehen.

MSDB-Neuronen integrieren sensorische und motorische Informationen, doch ihre Rolle bei der Synchronisierung von Verhaltensweisen wie Schnurrhaarbewegung (whisking), Laufen und Pupillenerweiterung bleibt unklar. Persistente Feuerraten (PF), bei denen Neuronen ihre Aktivität über einen Reiz hinaus aufrechterhalten, könnten ein Mechanismus sein, der motorische und kognitive Prozesse im MSDB koordiniert. Rhythmische Phänomene wie Schnurrhaarbewegungen und Pupillenerweiterung stimmen oft mit kortikalen Zustandsänderungen überein. PF im MSDB könnte dabei eine Brücke zwischen motorischen Verhaltensweisen und neuronalen Zustandsänderungen bilden.

Diese Arbeit untersucht die Rolle des MSDB bei der Koordination lokomotionsbezogener neuronaler und behavioraler Mechanismen sowie seine anatomischen Projektionen zum Hippocampus. Ziel ist es, die integrative Rolle des MSDB bei der Verknüpfung sensorischer, motorischer und kognitiver Funktionen besser zu verstehen und neue Einblicke in seine Funktionen in Gesundheit und Krankheit zu gewinnen.

1. Introduction

Movement, particularly locomotion, is crucial for the survival of most species. Locomotion can be driven by various motivations, and its speed significantly influences how we process sensory information from our environment, thereby further impacting our learning and memory processes. A key challenge in neuroscience is understanding how the same brain regions involved in different behaviors, such as locomotion, learning, or memory, are functionally connected and synchronized to each other. Several brain regions are known to regulate these behaviors including thalamic and hypothalamic nuclei, the ventral tegmental area, the hippocampus, and the amygdala. Among these, the medial septum and diagonal band of Broca complex (MSDB) in the basal forebrain (BF) is a critical hub that integrates sensory and motor information across subcortical and cortical areas (Bland and Oddie, 2001).

To effectively internalize the heightened sensory input experienced during locomotion compared to a stationary state, several brain and body systems must synchronize seamlessly. In rodents, for instance, whisking—a tactile sensory behavior—precedes locomotion by several milliseconds and shows correlation locomotor speed (Sofroniew et al., 2014). Additionally, locomotion is also linked to pupil dilation, which facilitates enhanced visual input. This pupil dilation correlates with the activity of neuromodulatory systems, particularly noradrenaline (NE) and acetylcholine (ACh) pathways, which are tightly linked to both arousal and movement (Reimer et al., 2016). In parallel with these, MSDB neurons show step-locked firing patterns (A. Joshi et al., 2023; A. Joshi & Somogyi, 2020), and entrain theta oscillation, a low rhythmic field activity in the hippocampal formation (Fuhrmann et al., 2015; J. Robinson et al., 2016). This rhythm synchronizes hippocampal and entorhinal cells by gating their intercommunication, and loss of theta oscillation impairs spatial memory (Boyce et al., 2016; Brandon et al., 2011; Etter et al., 2023; Koenig et al., 2011; Mitchell et al., 1982; Quirk et al., 2021; J. C. Robinson et al., 2023; Zutshi et al., 2018). Despite these findings, it remains unclear whether a specific population of brain cells orchestrates the synchronization of these diverse locomotor-related mechanisms.

Uncovering the cellular mechanisms that enable the brain to integrate sensory, motor, and cognitive functions is essential. One important aspect of neuronal physiology is persistent firing (PF), a phenomenon that allows neurons to maintain activity beyond the stimulus duration, supporting cognitive functions like working memory, spatial navigation, and sensory processing.

While persistent firing has been extensively studied in regions like the prefrontal cortex and hippocampus and classically related to working memory (Fuster, 1973; Funahashi et al., 1989; Yoshida & Hasselmo, 2009; Knauer et al., 2013), it also plays a crucial role in motor behaviors, where sustained neural activity supports the execution of planned movements and adaptive responses (Di Prisco et al., 2000; N. Li et al., 2016). Additionally, behaviors such as pupil dilation, whisking and locomotion are not isolated phenomena but are closely interrelated, often coupled with cortical state modulation and sensory feedback loops (Bradshaw, 1967; Beatty, 1982; Vinck et al., 2015a; Busse, 2018). Whisking and locomotion are tightly coordinated with rhythmic brain activity (Buzsáki, 2002; Brandon et al., 2011; Koenig et al., 2011; Fuhrmann et al., 2015; Sofroniew & Svoboda, 2015; A. Joshi & Somogyi, 2020). Consequently, understanding how these oscillatory phenomena coordinate is essential for understanding the brain's flexible adaptation to environmental demands that intensifies with increasing locomotion velocity.

The MSDB plays a critical role in linking motivation, sensory input, motor planning, and behavior execution to cognitive and emotional learning and memory (Bland & Oddie, 2001; Vertes & Kocsis, 1997). These processes are regulated through MSDB interconnection with downstream areas (Buzsáki, 2002; Petsche et al., 1962; Teles-Grilo Ruivo & Mellor, 2013). The pathway between the MSDB and the hippocampus is among the most extensively studied (Müller & Remy, 2018). For decades, research has primarily focused on the dorsal hippocampus (dHC), well-known for its role in cognitive functions, such as spatial navigation and memory encoding (O'Keefe & Dostrovsky, 1971; O'Keefe & Nadel, 1979; Moser, 1995). However, it is now clear that the hippocampus exhibits functional differentiation along its dorsoventral axis, with the ventral hippocampus (vHC) showing a stronger association with emotional behaviors (Fanselow & Dong, 2010; Strange et al., 2014). While the MSDB–dHC connection has been thoroughly investigated in the context of cognitive memory formation (Vertes & Kocsis, 1997; Korotkova et al., 2018), much less is known about the molecular profiles and biophysical properties of MSDB cells associated with projections to either the dHC or vHC. Acquiring this knowledge is crucial for further elucidating the functional roles of MSDB cell populations based on their projection patterns (Teles-Grilo Ruivo & Mellor, 2013; Unal et al., 2015, 2018).

To understand how the MSDB orchestrates the large number functions it has shownd to be associated with, this thesis investigates two major aspects: (1) single-unit activity dynamics

and interactions of MSDB neuronal population during stereotyped behaviors such as running, whisking, and pupil dilation proposing a candidate cell type acting as the conductor of the locomotor orchestra, and (2) anatomical distinctions in septo-hippocampal projections to dorsal and ventral hippocampal subfields (dHC and vHC). The investigations presented in this thesis aim to clarify how the MSDB coordinates locomotor-related neural mechanisms and links them to hippocampal circuits. Here, I aim to provide an introduction that offers context and explains the rationale behind these investigations.

1.1 Medial Septum and Diagonal band of Broca complex (MSDB)

We move to reach specific locations, acquire rewards, engage socially and sexually, flee predators, or pursue prey. However, while extensive research has been conducted on the neuronal circuits underlying locomotion (Fuhrmann et al., 2015; Howe & Dombeck, 2016; Justus et al., 2017; Caggiano et al., 2018), comparatively little is known about how internal states influence specific motor performance (Ferreira-Pinto et al., 2018). For instance, the vigor of movement may reflect the cumulative integration of individual sensory modalities (Bland & Oddie, 2001) or draw upon prior experiences encoded in memory. This suggests that identical motor outputs can emerge from distinct combinations of neural information processed across different brain regions and circuits.

The MSDB receives inputs from the supra-mammillary nucleus, the thalamus; projects to the hypothalamus, the nucleus incertus (Haghdoost-Yazdi et al., 2009; Müller & Remy, 2018), and the cerebellum (Watson et al., 2019), and projects to the hippocampus, the hypothalamus, the amygdala and the ventral tegmental area (VTA) (Fuhrmann et al., 2015; Swanson & Cowan, 1979). These connections ideally position MSDB to play a pivotal role in locomotion (Bland and Oddie, 2001; Fuhrmann et al., 2015; Justus et al., 2017), learning (Brioni et al., 1990; Hagan et al., 1988; Loureiro et al., 2012; Pang et al., 2011), fear memory generalization and extinction (Calandreau et al., 2007; Knox & Keller, 2016; Staib et al., 2018) and other cognitive and emotional behaviors (Colom, 2006; Roland et al., 2014). Due to its extensive reciprocal connectivity, the MSDB has been frequently described as a central subcortical hub for information processing within the brain.

To understand how the MSDB coordinates those diverse functions, it is important to explore its influence on downstream regions with more specialized roles. A key mechanism by

which the MSDB integrates and orchestrates these behaviors is through theta oscillations, a rhythmic neural activity in the 4–12 Hz range. Theta provides a temporal framework that synchronizes neural activity across brain regions involved in memory, attention, sensory processing, and motor coordination (Buzsáki, 2002), which is supported by the observation that disruption of theta is associated with impairments in memory and navigation (Boyce et al., 2016; Brandon et al., 2011; Koenig et al., 2011; Zutshi et al., 2018). This oscillatory mechanism will be a recurring theme throughout this thesis. To understand its emergence, we must first examine the individual cellular composition and organizational structure of the MSDB.

1.1.1 *Cell types, conductances, and rhythms*

Since the early days of neuroscience, researchers have sought to classify nerve cells. However, during the classical era, the limited availability of methodological tools constrained these efforts to relatively broad categorizations. The first studies, for instance, divided MSDB cells into cholinergic and non-cholinergic subgroups (Armstrong et al., 1983; Amaral & Kurz, 1985; Markram & Segal, 1990). For several decades, research in the field has focused on three primary cell populations within the MSDB: cholinergic, GABAergic, and glutamatergic cells (Müller & Remy, 2018; Mocellin & Mikulovic, 2021). However, the recent advancements in molecular techniques such as mRNA profiling have started to significantly refine our ability to classify these cells with greater precision (Kuhn et al., 2024). My first insights into cellular classification approaches comes from my early years in Oxford, where I could study the work of my first mentor, Peter Somogyi and his team. I learnt the importance of molecular markers. These can be different types of Ca^{2+} binding proteins like parvalbumin (PV), calbindin (CB), calretinin (CR), various neuropeptides as neuropeptide Y (NPY), cholecystokinin (CCK), somatostatin (SOM) for example (Gritti et al., 2003), or ion channels, like voltage gated potassium channels (Henderson et al., 2010), as well as projection patterns defining a cell type. Later, working with János Szabadics, I experienced cell type differences in intracellular electrophysiology, and gained insights into the mechanisms behind their unique properties. Drawing from this background, I will outline the markers that have proven significant in MSDB function.

One of the earliest classifications of MSDB neurons relied on the histological markers for choline acetyltransferase (ChAT), identified cholinergic (ChAT+) and non-cholinergic (ChAT−) subpopulations (Armstrong et al., 1983; Amaral & Kurz, 1985; Markram & Segal, 1990).

It is important to mention that ChAT antibodies for immunocytochemistry staining were one of the first available marker staining, though it was not the first candidate to label cholinergic cells specifically. Early studies showed that acetylcholinesterase (AChE), a reference marker in the Paxinos atlas along DAPI (Paxinos et al., 1980; Franklin & Paxinos, 2019), was not specific to cholinergic neurons but was also expressed in catecholaminergic nuclei and neurons (Armstrong et al., 1983; Butcher & Marchand, 1978).

Another line of research categorized MSDB neurons based on their physiological properties, i.e bursting vs non-bursting subgroups (Lamour et al., 1984). By this time, the role of the MSDB in theta rhythmogenesis was already established through correlative observations (Petsche et al., 1965; Gogolák et al., 1968). This understanding was further supported by lesion studies that specifically targeted the medial, but not the lateral, part of the septum (Wetzel et al., 1978; Mitchell et al., 1982). In vitro patch clamp recordings demonstrated theta-frequency spontaneous firing of MSDB neurons (Segal, 1986). In his study, Segal also reported that neurons with higher input resistance (R_{in}) were more excitable, and fired at a higher rate of spontaneous action potentials (APs) compared to the low R_{in} neurons. The application of GABA to MSDB neurons caused inhibition, while ACh excited the majority of recorded cells. Additionally, ACh increased R_{in}, resulting in greater neuronal excitability. Furthermore, 5-hydroxytryptamine (5-HT, alias serotonin) had an inhibitory effect on the recorded MSDB population. In contrast, other recordings show that 5-HT induces depolarization in a subpopulation of MSDB cells (Alreja, 1996), further highlighting the complexity of this area.

Beyond ACh, other neurotransmitters and neuropeptides were also identified in the MSDB. For example, galanin, which is also secreted by the gastrointestinal system regulating insulin levels (Mitsukawa et al., 2010), is expressed by ~22% of septo-hippocampal projecting neurons (Senut et al., 1989). Senut's study also identified cells that express luteinizing hormone-releasing hormone, calcitonin gene-related peptide, encephalin, dynorphin B, and vasoactive intestinal peptide (VIP). Additionally, neuropeptide Y (NPY), neurotensin and somatostatin also serve as markers in this area (Uhl et al., 1977; Barden et al., 1981; Köhler & Eriksson, 1984; Gaspar et al., 1987). It became clear that the diversity of this small, seemingly disorganized area, makes it difficult to understand its role. Among these transmitters, ACh has become the most extensively studied one.

ACh has a pivotal role in spatial learning and memory, motivated behaviors, theta synchrony and amplitude (Vandecasteele et al., 2014; Dannenberg et al., 2015). Optogenetic targeting of MSDB ChAT+ cells enhances hippocampal theta and low-gamma power across a broad range of stimulation frequencies (3–40 Hz), though without directly mirroring the stimulation frequencies (induced theta range: 3.8–4.6 Hz). This effect persists for several seconds beyond the stimulation offset, suggesting a sustained oscillatory engagement of the MSDB. Furthermore, by focally antagonizing ACh either to the MSDB or to the hippocampus, Dannenberg et al. (2015) distinguished 2 parallel effector pathways: the direct ACh input to HC, and a relayed transmission by cholinergic collaterals in the MSDB. They revealed that ChAT+ neurons decrease and increase the firing rate of HC excitatory and inhibitory cells, respectively, and depolarize PV+ GABAergic cells in the MSDB. These findings are consistent with previous literature, where authors used microinfusion of cholinergic agonist carbachol to MSDB (Lawson & Bland, 1993) or to HC (Konopacki et al., 1987) observing similar effects of ACh "transmission" on theta activity.

Parallel to the studies mentioned above, another branch of MSDB neuroscience focused on the anatomy and role of a different key neurotransmitter-releasing cell type: γ-aminobutyric acid (GABA)ergic cells (Tappaz et al., 1976; Panula et al., 1984). These cells are characterized by the expression of glutamic acid decarboxylase (GAD) as a marker. Over time, extensive research has revealed that GABAergic cells can be further classified based on well-established markers, including parvalbumin (PV), somatostatin (SOM), and calretinin (CR) (Tamamaki et al., 2003).

The PV+ GABAergic cells of the MSDB (Freund, 1989) are theta bursting cells (Simon et al., 2006), shown to play a crucial role in hippocampal theta generation (Hangya et al., 2009). These also express hyperpolarization-activated cyclic nucleotide-gated (HCN) channels, shown to be essential for rhythmic firing (Kocsis & Li, 2004; Morris et al., 2004). These PV+ GABA cells mainly target perisomatic inhibitory PV+ interneurons in the hippocampus (Freund & Antal, 1988). The rhythmic firing of septal PV cells disinhibit the hippocampal principal cells by inhibiting hippocampal PV cells, enabling coherent oscillations across hippocampal circuits (Buzsáki, 2002). In addition to theta, gamma oscillation (20-80 Hz) is also mediated by these MSDB PV neurons (Király et al., 2023).

While PV+ neurons are well-characterized, the roles of other GABAergic subtypes remain less clear. Recent studies have investigated SOM neurons, which inhibit other GABAergic, cholinergic and glutamatergic cell types within the MSDB (Xu et al., 2015). The optogenetic inhibition of septal SOM cells results in increased firing output of MSDB population activity, theta frequency and amplitude in the hippocampus (Espinosa et al., 2022). This effect is proposed through disinhibition of glutamatergic and cholinergic cells, as silencing SOM cells produces similar change in hippocampal theta activity as cholinergic stimulation (Vandecasteele et al., 2014; Dannenberg et al., 2015). On the other hand, enhancing the activity of SOM cells by optogenetic manipulation increases high-calorie food intake and decrease the running of the animal (Xu et al., 2015; Zhu et al., 2017), a set of behaviors that closely linked to MSDB function, as demonstrated by recent findings (Herman et al., 2016; Fuhrmann et al., 2015; Justus et al., 2017; A. Joshi & Somogyi, 2020; A. Joshi et al., 2023). Moreover, SOM neurons were shown to play an important role in appetitive learning paradigms by integrating rewarding food signals, and inhibiting LHb (Shen et al., 2022), a brain region regulationd aversion (Matsumoto & Hikosaka, 2007; G.-W. Zhang, Shen, et al., 2018).

The most recently identified MSDB population consists of glutamatergic cells. Throughout the thesis work, we only consider vesicular glutamate transporter 2 expressing (VGluT2+) excitatory neurons, but it is important to mention that VGluT1, VGluT3, and N-acetyl-aspartyl-glutamate (NAAG) expressing neurons are also present in the MSDB (Sotty et al., 2003; Harkany et al., 2003; Neale et al., 2000). NAAG is a dipeptide acting on NMDA and mGluR3 receptors (Neale et al., 2000). About 26 % of MSDB hippocampal projecting neurons express NAAG (Senut et al., 1990), that prevalently colocalizes with ACh (Forloni et al., 1987). A comprehensive study showed evidence about subset of MSDB neurons being VGluT2+ using mRNA in situ hybridization (Lin et al., 2003). In parallel with this anatomical discovery, studies using in vitro patch recordings confirmed the evidence of existing VGluT2+ cells (Colom et al., 2005; Manseau et al., 2005), applying polymerase chain reaction (PCR) analysis of the intracellular mRNA collected from the patch pipette (Sotty et al., 2003). Conjugating electrophysiology with mRNA identification was essential, as VGluT2 is a challenging molecular marker to detect. While ChAT and GAD are cytoplasmic proteins that produce robust somatic immunostaining, VGluT2 is a synaptic protein localized in the membrane of synaptic vesicles, leading to a very weak signal in somatic immunostaining. Early studies using patch-clamp

recordings of glutamatergic cells revealed that VGluT2+ neurons represent a diverse population with varying electrophysiological properties, including fast-, cluster-, burst-, and slow-firing neurons (Huh et al., 2010). Notably, even the slow-firing subpopulation comprises multiple subclusters (Garrido-Sanabria et al., 2007). More specifically, the first group of VGluT2-positive medial septal neurons exhibit cluster firing pattern with accommodating AP firing. Between those AP clusters, subthreshold oscillation is observable. The second group consists of fast-spiking neurons, showing only little action potential accommodation. Remarkably, some of the fast-spiking glutamatergic neurons express a pronounced sag in response to a hyperpolarizing current injection. This sag, a depolarizing current during hyperpolarization mediated by HCN channels (also known as H-current or I_h), has been demonstrated to influence neuronal excitability and spontaneous rhythmic activity in various neuronal cell types. Blocking this current with a HCN antagonist eliminates sag. Burst-firing glutamatergic neurons show little to no sag, whereas slow-firing neurons exhibit low discharge rates with accommodating APs. These findings highlight the heterogeneity of VGluT2 cells, each with distinct conductances that drive their unique firing patterns. This variety may play a key role in shaping how different neuronal subtypes integrate incoming signals.

In terms of the functional properties of MSDB VGluT2+ cells, several recent studies have convincingly shown what role these cells play in locomotion initiation and maintenance (Fuhrmann et al., 2015; Justus et al., 2017; G.-W. Zhang, Shen, et al., 2018). Fuhrmann et al. (2015) used fiber photometry to monitor the activity of these neurons in the MSDB, and revealed their pre-locomotor tuning before, and correlated cellular activity during locomotion. Optogenetic drive of these neurons resulted in reliable run initiation by applying a long, 20s train of optical pulses at theta related frequencies (3 – 12 Hz), which initiates and sustains locomotion outlasting the stimulus duration in a stimulation frequency dependent manner (higher frequency stimulation results in higher theta frequency and faster locomotion). This long, theta modulated train of pulses also induced hippocampal theta, that effect was abolished by cannula application of fast ionotropic glutamate receptor antagonists, D-AP5 and NBQX, locally into the MSDB prior to stimulation. These results support the hypothesis that VGluT2 cells drive hippocampal theta by MSDB collaterals, but initiate locomotion via their projections outside the MSDB. Although longer (above 10 s) optogenetic activation of these neurons at theta (4 – 12 Hz) or higher frequencies entrains hippocampal theta oscillation (Fuhrmann et al., 2015; Kocsis et al., 2022; J. Robinson et al., 2016),

the effect of a much shorter stimulation (closer to physiological scales of sensory inputs) on MSDB VGluT2 induced run remains to be tested.

In a recent study, the functional activity of VGluT2+ MSDB was shown to form two subpopulations during spatial navigation (Bott et al., 2022). Mice were placed into a 5-arm star-maze, where they had to run from a semi-randomly assigned arm to the target arm to collect reward. Ca^{2+} imaging of VGluT2+ neurons showed a population being active in the preparation before, but silenced during running, whereas another subpopulation was active already shortly before receiving the reward. The activity of these two populations reflected correct choice trials, but only during the early sessions of the task when learning was still occurring, and not during later sessions when the animals were already well-trained. On the contrary, optogenetic silencing of these neurons before and during task engagement impaired memory that was shown by decreased success rate of mice finding the target arm. The authors showed the role of VGluT2 neurons, over locomotion and speed coding, to be involved in higher order cognitive demands, namely in learning. They also hypothesized that those preparatory VGluT2 neurons were mediating goal-driven attention, meaning that mice with higher initial activity tended to be more focused on the task, leading to more correct choices.

In summary, the MSDB is composed of a heterogeneous network of cholinergic, GABAergic, and glutamatergic neurons exhibiting unique properties and functions. To better understand the MSDB functional architecture, it is essential to study not only individual cell types but also the collateral microcircuitry that contributes to intra-MSDB computations and shapes the region's output.

1.1.2 *Interconnection of MSDB cell types*

For the sake of consistency with early 21st century neuroscience (and to simplify conceptualization), we can describe MSDB as being composed of 3 major cell types, cholinergic, GABAergic, and glutamatergic cells. (Tappaz et al., 1976; Panula et al., 1984; Freund & Antal, 1988; Sotty et al., 2003; Colom et al., 2005). To understand the computation that is present in this region to generate its output, we also need to elaborate on the circuitry of the MSDB. Over the past decades, we have gained insights into how individual neurotransmitter treatments affect cellular activity in *in vitro* slices. However, sensitivity to a specific neurotransmitter does not necessarily imply the existence of collateral connections. In general, GABA inhibits, ACh excites

MSDB neurons (Alreja, 1996), while the application of glutamate or kainite (agonist of a subset of ionotropic GluRs), induces GABAAR dependent theta bursting of theta-bursting cells, and field theta in slice preparation (Herz & Gogolák, 1965; Garner et al., 2005), which effect was also observable by the activation of mGluR type I (Lu et al., 2011).

Early studies using electron microscopy to identify synaptic connections have already shown that GABAergic and cholinergic cells form synapses with each other (Leranth & Frotscher, 1989). Later, combined analysis of single-cell and field recordings in the MSDB identified NMDA- and AMPA-dependent glutamatergic synaptic transmission to both cholinergic and GABAergic cells within the region (Manseau et al., 2005). Further investigations with in vitro pair recordings confirmed these findings, revealing that VGluT2+ cells excite GABAergic and cholinergic cells, while GABAergic cells inhibit both glutamatergic and cholinergic neurons (Leão et al., 2015). The role of VGluT2+ cells in driving other cell types through collateral excitation was further supported by optogenetic experiments (J. Robinson et al., 2016), where light-induced depolarization of VGluT2 cells triggered glutamate-mediated postsynaptic potentials in both fast- and slow-firing neurons (putative GABAergic and cholinergic neurons, respectively). These results reinforce the idea that glutamatergic cells drive hippocampal theta by collateral drive of rhythmic GABAergic PV+ neurons (Hajszan et al., 2004). This is also in line with the most recent model, which proposes that tonic VGluT2+ activity is the main driver of the synchronization of rhythmic GABAergic cells (Kocsis et al., 2022). Moreover, this should also imply a similar drive to cholinergic cells. Although this latter connection remains underexplored, overlapping roles of VGluT2+ and ChAT+ populations provide compelling evidence for its existence. For example, chemogenetic activation of ChAT+ or VGluT2+ MSDB neurons induces comparable effects on the state of consciousness in anesthetized rodents (Tai et al., 2014; Xia et al., 2024). Similar parallels have also been observed in learning-related tasks, as discussed earlier.

1.1.3 *MSDB function*

1.1.3.1 Learning, memory, and navigation

The first mention of a brain region being involved in memory dates back to the case of patient HM (Corkin, 1984). Physicians realized that removing both hippocampi induces anterograde amnesia, meaning that the patient remembered all details from his past, but was unable to encode new memories. This case encouraged neuroscientists to investigate the neural networks

and inputs that support HC function. In early studies, EEG recordings revealed a rhythmic activity in the hippocampus, known today as theta oscillations (Green & Arduini, 1954), as technology did not allow single-cell recordings at that time. Subsequent tracing studies identified input regions of the HC, leading to the discovery that stimulation of certain brain areas, especially the MSDB elicited HC theta rhythm (Vertes, 1982). Lesion studies targeting selectively the MSDB confirmed its role in theta generation, as selective damage of MSDB abolished hippocampal theta and impaired memory performance. (Ain et al., 1969; Winson, 1978; Hepler et al., 1985). Furthermore, intraseptal infusion of NMDAR antagonist D-AP5 also impaired memory (Elvander-Tottie et al., 2006). More recent studies have expanded our understanding of MSDB contributions in spatial memory, and investigated its role in e.g. reward-associated, episodic, and social memory.

Canonically, the architecture of memory relies on the MSDB-HC-EC intercommunication. MSDB-generated theta oscillation serves as an important synchronizing framework for principal cells in the medial temporal lobe (MTL), namely in the EC and the HC. Interfering with theta disrupts grid cell activity (J. C. Robinson et al., 2023), which is essential for hippocampal place code. Particularly, disruption of theta prevents the formation of new place fields but leaves pre-existing ones intact (Venditto et al., 2019).

Although it might seem straightforward to assume that MSDB GABAergic projections pace theta oscillations in the hippocampus, juxtacellular recordings combined with subsequent anatomical tracing of theta-bursting MSDB neurons have uncovered a greater complexity in this pathway. The Somogyi Lab identified distinct septo-hippocampal projecting GABAergic subtypes, as low-rhythmic, orchid, Teevra or Komal neurons that differed in projection and physiology (A. Joshi et al., 2017; A. Joshi & Somogyi, 2020; Salib et al., 2019; Unal et al., 2018), further underscoring the complexity of theta generation and it influence on the MTL (Figure 1).

Cholinergic septo-hippocampal projections further complicate MSDB's role in memory. Microdialysis experiments showed that ACh release in the HC increases during learning

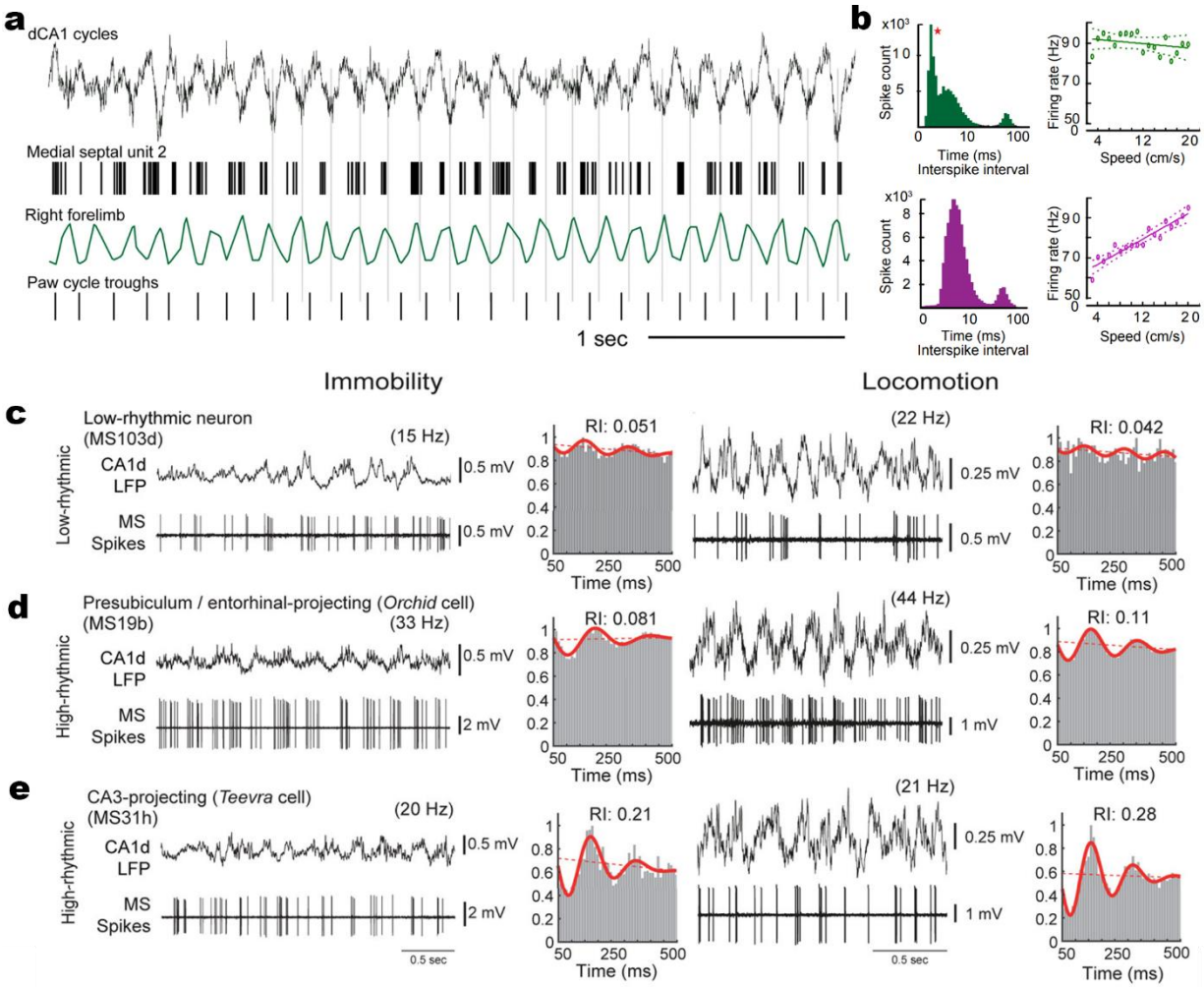

Figure 1. Representative unit activity and rhythmicity of septo-hippocampal GABAergic projecting subpopulations. A, Representative neuron showing tight coupling with stepping rhythm and hippocampal theta. B, (left) Inter-spike interval (ISI) and (right) speed modulation of a representative (top, green) Teevra and (bottom, purple) Komal neuron. C-E: (left) hippocampal oscillation and subsequent MSDB unit firing during immobile periods with autocollerogramm presenting rhythmicity (RI), and (right) similar as (left) but during locomotion. Frequency values in parenthesis show mean firing rate. Adapted from (A) Joshi & Somogyi (2020), (B) Joshi et al. (2017), (C) Salib et al. (2019)

and memory recall (Fadda et al., 2000; Ragozzino et al., 1996; Stancampiano et al., 1999), moreover chemogenetic activation of MSDB ACh cells induces a similar effect (Missault et al., 2022). Conversely, antagonizing ACh in the hippocampus (Mishima et al., 2000), or selective depletion of MSDB ACh neurons impairs memory performance (Berger-Sweeney et al., 2001). Furthermore, individual cell types in hippocampal areas express a diverse array of AChRs and receive direct inputs from MSDB cholinergic fibers. This indicates that, in addition to enhancing theta oscillations, these inputs play a complex neuromodulatory role in hippocampal computations.

Cholinergic activity requires precise timing for this effect. During low ACh activity, hippocampal sharp-wave ripples (SWRs) occur (Buzsáki, 1986), which support memory consolidation during NREM sleep and quiet wakefulness. Disruption of these ripples during sleep impair memory consolidation (Girardeau et al., 2009), and inappropriate activation of MSDB cholinergic neurons (at reward location, but not during locomotion), can inhibit SWRs (Vandecasteele et al., 2014), consequently interfering with memory processing (Jarzebowski et al., 2021).

Beyond spatial memory, social memory, mediated by the ventral subdivision of the HC started gaining the field's attention. Interruption of HC-nucleus accumbens (NAc) impairs discrimination of novel vs familiar conspecifics (Okuyama et al., 2016). SWR related consolidation occurring in the CA2, a classical HC subregion related to social memory (Hitti & Siegelbaum, 2014) was shown to specifically regulate social memory consolidation. MSDB cholinergic neurons showed an increased activity during social interactions. Moreover, activation of these neurons enhances social memory formation, while their focal ACh antagonist infusion to CA2 impaired this function (Pimpinella et al., 2021).

Thus, while the MTL likely contains the core circuitry for memory processing, the MSDB provides essential input regarding synchronization and neuromodulation. As this dissertation does not focus on navigation, I would not dig into the details of this enormous field stated in the title of this subchapter. But it is important to reflect on these findings when we aim to understand the background of some of the roles mentioned below.

1.1.3.2 Appetite

Research over the past decade has uncovered cell-type-specific contributions of MSDB neurons to appetite regulation. Glutamatergic MSDB neurons have been shown to suppress appetite via direct excitatory projections to the paraventricular nucleus (PVN) of the hypothalamus, as chemogenetic and optogenetic activation of MSDB glutamatergic neurons leads to significant reductions in food intake without influencing locomotion or inducing anxiety-like behavior (Sweeney et al., 2017). This anorexigenic effect is mediated by the activation of corticotropin-releasing hormone (CRH) neurons in the PVN. In contrast, MSDB GABAergic neurons modulate appetite through the lateral hypothalamus (LH), they inhibit food intake by suppressing activity in orexin-expressing neurons of the lateral hypothalamus (LH) (Sweeney &

Yang, 2016). In their experiments, chemogenetic activation of MSDB GABAergic neurons decreased food consumption, whereas inhibition resulted in hyperphagia. Finally, the appetite-suppressive effect of ACh, particularly on nicotinic ACh receptors (nAChR), is well known from everyday life. When individuals quit smoking, they often experience weight gain. This phenomenon, however, is not specific to the ACh release of MSDB ChAT+ population (Jo et al., 2002). Ablation or chemogenetic suppression of MSDB cholinergic neurons enhances appetite, while optogenetic activation of the same population decreases food intake (Herman et al., 2016). A more recent study showed that activation of cholinergic neurons suppresses reward-related feeding through ACh transmission in the basolateral amygdala (BLA), suggesting a role of ACh in appetite as a form of motivation drift (Ortiz-Guzman et al., 2024). The hypothesis of motivational drift from hunger to fear-related responses aligns with studies examining how the need of food intake can be overridden by other behaviors (like Maslow's hierarchy of needs), such as social interactions or voluntary exercise (Petzold et al., 2023; Tesmer et al., 2024).

1.1.3.3 Exploration and reward-seeking behavior

When discussing motivation in the context of appetite, it is important to acknowledge that hunger is only one aspect of motivation for taxis. Other types of rewards, such as seeking information about the location of water, pups, or adult conspecifics, should also be considered. Under urethane anesthesia, the rhythmic activity of the posterior hypothalamic supramammilary nucleus (SuM) neurons is emerging phase-locked with hippocampal oscillations (Kocsis & Vertes, 1997). VGluT2+ SuM neurons, which are part of the ascending pathway (Vertes, 1992), project to the MSDB (and also to the HC (Segal & Landis, 1974)), where their activity is tightly coupled with locomotion, and it modulates reward-seeking behavior (Kesner et al., 2021). Application of procaine to this projection pathway suppresses SuM input to the MSDB, reducing the amplitude and frequency of theta rhythmic activity (Kirk & McNaughton, 1991). On the other hand, enhancing SuM activity strengthens hippocampal theta, what is more, synchronizes it with theta oscillation in the medial prefrontal cortex (mPFC) and nucleus reticularis (NR) (Ito et al., 2018). The exact cell type or circuitry accounting for this phenomenon is still not clear, but the activation of the posterior hypothalamic SuM, supposedly through MSDB, induces rhythmical cortical arousal (Starzl et al., 1951), a similarly associated cortical state to locomotive behavior like hippocampal theta oscillation.

In a self-administration test using excitatory drugs like glutamate, GABAAR blocker picrotoxin, or nicotine, rodents learnt lever press (Ikemoto et al., 2004; Ikemoto, 2005; Ikemoto et al., 2006), suggesting the role of the SuM in rewarding behaviors. Recently, Kesner et al. (2021) demonstrated that optogenetic self-stimulation of SuM(VGluT2+) to MSDB projection mediates reinforcement. In this experiment, mice quickly learnt to press the lever associated with the excitation of SuM VGluT2+ neurons, and preferred that lever over the inactive one. In the reversal task, in which the active and inactive levers were swapped, they rapidly adapted to the new lever assignment. This effect aligns with ACh's role in increasing task engagement and attention in learning.

A separate study showed that chemogenetic activation of MS VGluT2+ neurons improved the latency of learning a new rule in a strategy-switch task (Bortz et al., 2022), further emphasizing the importance of the SuM(VGluT2+) to MSDB(VGluT2+) monosynaptic connection (Kesner et al., 2021). Interestingly, SuM(VGluT2+) activity was reduced during sucrose water intake, but inhibition of these neurons did not suppress consumption. This suggests that SuM activity does not directly mediate appetitive behavior, but may be influenced by it, potentially through reciprocal input from the MSDB or via indirect pathways. Finally, using fMRI, they showed subsequent activation of VTA and dopamine release in the striatum, suggesting that SuM's downstream projection influences the activity of VTA, possibly through the SuM-MSDB-VTA axis.

Additional evidence supporting the functional SuM-MSDB-VTA network underlying exploration was provided by the Remy group at the Leibniz Institute for Neurobiology (Mocellin et al., 2024). They showed that MSDB VGluT2+ neurons innervate VGluT2+ and dopamine (DA)ergic VTA populations, and that the activation of this pathway elicits whisking and sniffing (hallmarks of exploratory behavior in mice) prior to locomotion initiation. This pathway did not appear to regulate approaches toward food, objects, or social stimuli, but instead seemed specific to environmental exploration. Notably, since the VTA also projects to the hippocampus, the reciprocal connections within the SuM-MSDB-HC-VTA network form a complex relationship. Conducting future, precise, cell-type-specific studies could help unravel how exploratory behavior is regulated and what aspects of it are transmitted during exploration. Additionally, this pathway might also mediate reward-related learning—potentially even contrasting with aversion—as

midbrain dopamine nuclei have long been recognized for their critical role in learning processes (Schultz et al., 1994; Robbins & Everitt, 1996; Schultz et al., 1997).

1.1.3.4 Nociception and aversion

One of the earliest proposed functions of the MSDB is nociception, as local neurons have been shown to respond to sensory stimuli (Petsche et al., 1962). Early lesion studies of MSDB report reduced latency of escaping from aversive stimuli as heat, shock and sound stimulation, hallmarking hyperreactivity (Brown & Remley, 1971; Hayat & Feldman, 1974; Zin et al., 1977; Mercer & Remley, 1979). This question was recently revisited with a pain threshold test (Fan et al., 2023); the optogenetic excitation of MSDB VGluT2+ ➔ LH projection terminals resulted in lower paw withdrawal latency, indicating reduced pain threshold. In contrast, silencing these terminals had the opposite effect on pain threshold. Interestingly, none of these effects were observed when they were similarly exciting or inhibiting MSDB VGluT2+ ➔ SuM projection terminals in the same study. These results further prove that a distinct projection of the same region has different effects on behavior.

Lateral Habenula (LHb) has a canonical role in aversion or punishment. In human subjects, activity of LHb correlated with the valence of the feedback on outcome prediction task. Specifically, negative feedback following the decision making of the participants increased LHb activity (Ullsperger & von Cramon, 2003). This effect is thought to influence learning through LHb's long-range GABAergic projections to reward-related dopaminergic midbrain areas as VTA or substantia nigra (SN) (Herkenham & Nauta, 1979; Ji & Shepard, 2007). Brief, microsecond long electrical activation of LHb reduces almost 100% of VTA and SN DA neuron activity, while it facilitates the activity of non-DA cell types in the same region, which effect is sensitive to the application of a GABAAR antagonist in the midbrain (Ji & Shepard, 2007).

MSDB VGluT2+ projection to LHb mediates place avoidance behavior (G.-W. Zhang, Shen, et al., 2018). In this study, the authors used a two-compartment place avoidance paradigm, where one compartment was exposed to wind from a fan or to noise, while the other remained neutral. Mice preferred the neutral chamber over the aversive one, but muscimol silencing of MSDB reduced place avoidance of windy/noisy aversive chambers in these animals. Further testing revealed that a subset of MSDB neurons was recruited shortly after the presentation of an air puff or a pulse of noise, indicating that the MSDB codes multisensory aversive stimuli. This

sensory activation was prevented via muscimol silencing of the periaqueductal gray (PAG). In another paradigm of 2 neutral chambers, optogenetic activation of MSDB in one of the chambers induced avoidance of that compartment. More specifically, the selective activation of VGluT2+ MSDB neurons induced avoidance, antagonistically, the selective activation of GABAergic MSDB population promoted preference of the stimulation chamber. Interestingly, the results showed, that MSDB VGluT2+ populations projecting to LHb and to medial preoptic area (mPOA) have distinct behavioral roles, as selective MSDB ➔ POA projection, but not the MSDB ➔ LHb projection induces locomotion, hinting segregate projection pathways of the 2 behaviors of motivation and locomotion. This could be further supported by studies showing that stimulation of MSDB to LH or VTA projections can influence locomotion (An et al., 2021; Mocellin et al., 2024), while MSDB to HC projections are more closely associated with motivation and task engagement, consistent with the LHb projection. Although cross-talk of these behaviors is expected based on collateral computation within the MSDB, the segregation of pathways for motivation and locomotion needs further investigation.

1.1.3.5 Locomotion, navigation, and theta rhythmogenesis

The control of locomotion in mammals relies on a hierarchical organization of neural circuits, integrating descending inputs from the brain with spinal networks that generate rhythmic and coordinated movement patterns. In rodents, this systems-level control of motor initiation, modulation, and adaptation involves key structures, including the basal ganglia (BG), the lateral hypothalamus (LH), the substantia nigra (SN), the cerebellum, the mesencephalic locomotor region (MLR), the reticular formation (RF), and spinal central pattern generators (CPGs) (Shik et al., 1966; Armstrong, 1986; Brudzynski et al., 1993). The current scientific consensus suggests that the basal ganglia (BG) are responsible for selecting the type of locomotor behavior (e.g., walking, galloping, and swimming). In contrast, descending pathways, such as the MLR or other brainstem locomotor centers, execute the selected behavior by activating the CPG through the RF. Supporting evidence indicates that electrical stimulation of these regions induces distinct locomotor modalities (Kiehn & Dougherty, 2013; Mori, 1990). Albeit the literature of locomotion related research is so enormous that could complete another thesis, I will focus on the role of the MSDB and its related circuit in locomotion.

The earliest identified functions of the MSDB is its role in modulating hippocampal theta activity, which underpins learning, memory, and arousal (Green & Arduini, 1954), and its involvement in sensory integration (Petsche et al., 1965). The first study connecting hippocampal theta to voluntary motor behaviors emerged in the late 60's (Vanderwolf, 1969). Vanderwolf (1969) demonstrated that high-effort voluntary movements, such as jumping, locomotion, or rearing, are preceded by hippocampal rhythmic activity. In contrast, fine motor actions, including head or paw movements and the initial phases of grooming, elicited hippocampal theta activity with lower amplitude and a 1-2 Hz reduction in frequency compared to that observed during locomotion. Immobile actions as immobile whisking or chewing led to asynchronous HC activity. These findings were later reinforced by others (Whishaw & Vanderwolf, 1973), and provided early evidence for the involvement of MSDB in locomotion, which was further supported by decreased locomotor activity of rats after selective lesion of the MS, but not the LS (E. H. Y. Lee et al., 1988).

HC and EC theta activity is speed-dependent, with faster running associated with higher theta frequencies, driven by rhythmic burst discharges originating in the MSDB (Petsche et al., 1962, 1965; Gogolák et al., 1968). While stepping frequency is regulated by the CPG in the medulla—a distant region—stepping and theta frequencies remain tightly coupled at higher locomotor speeds (A. Joshi et al., 2017, 2023; A. Joshi & Somogyi, 2020). This points on coordination between descending locomotor pathways and the MSDB. The stimulation of RF is shown to elicit theta rhythmic activity in the MSDB and HC (Petsche et al., 1965; Torii, 1961; Vertes, 1982), further implicating the MSDB as a candidate region through which theta and stepping attain synchronization.

Recent studies highlight the role of MSDB VGluT2 neurons in starting and maintaining movement and locomotion (Fuhrmann et al., 2015; Justus et al., 2017; Mocellin et al., 2024; G.-W. Zhang, Shen, et al., 2018). Using fiber photometry, Fuhrmann et al. (2015), showed that the activity of these cells precedes and aligns with movement. Optogenetic stimulation of MSDB VGluT2+ neurons consistently triggered running, with the animal's velocity and hippocampal theta frequency showing a clear correlation with the stimulation frequency. Precisely, a 12 Hz stimulation of MSDB VGluT2+ population induced locomotion with a higher speed than 9, 6, and 3 Hz. The emergence of HC theta, but not running was reduced by focal MSDB infusion of D-AP5 and NBQX, which was further supported by others (J. Robinson et al., 2016; Mocellin

et al., 2024). This suggests that while MSDB VGluT2 cells influence hippocampal theta within the MSDB (proposedly by their collateral drive of PV+ GABAergic neurons (Kocsis et al., 2022)), their role in initiating movement likely depends on connections outside the area. The study went further and reported that MSDB VGluT2+ neurons form reciprocal connections with brain areas related to locomotion, pupil change and whisking (SuM, LH, median raphe, ventromedial hypothalamus). Out of these, they investigated one projection, namely the optogenetic stimulation of the glutamatergic projecting fibers locally in the HC that influenced pyramidal cell (PC) activity proposedly through feed forward inhibition onto their apical dendrites, proposing the role of this projection in information gating.

The effect of MSDB VGluT2+ population on hippocampal theta was also examined in a parallel study (J. Robinson et al., 2016). The MSDB stimulation of these neurons (but not their axonal projection through the fornix) elicited HC theta tightly following the stimulation frequencies between 4 – 10 Hz, emphasizing the importance of MSDB collateral excitation. This was further confirmed by in vitro MSDB preparation, where optogenetic excitation of VGluT2+ cells triggered depolarizing postsynaptic potentials in local putative GABA- and cholinergic neurons.

This aligns with the broader concept that the MSDB serves as a central hub, linking locomotion with rhythmic activity in the brain. In fact, seminal studies have provided additional insights into the alignment of MSDB activity with stepping (A. Joshi et al., 2023; A. Joshi & Somogyi, 2020). These findings help explain why, although theta oscillation frequency correlates with the animal's speed during active movement (King et al., 1998; Czurkó et al., 1999), this coupling between theta frequency and velocity diminishes when the animal is passively transported (Terrazas et al., 2005; Winter et al., 2015). This synchronization is particularly important in memory formation and retrieval, as one theta cycle is composed by information flow of past, present, and future experiences (A. Joshi et al., 2023). This phenomenon is better understood through phase precession, where the phase of theta-locked rhythmic firing shifts to earlier phases in successive theta cycles as the animal approaches (future) and moves away from (past) the center of the place field (present) (O'Keefe & Recce, 1993; Skaggs et al., 1996). Decoding the animals' position from neural firing of parahippocampal and HC cells confirms this,

further underscoring the complexity and elegance of this system and the crucial role of step-to-theta synchronization (A. Joshi et al., 2023; Vollan et al., 2024).

During locomotion, the brain continuously updates positional information. Successful encoding of past locations helps us navigate, forming a place code that integrates visual flow, vestibular input (acceleration), and self-motion cues (Etienne & Jeffery, 2004). For instance, in the dark, we can often navigate our way to the bathroom without visual cues, relying on self-motion information. Accurately estimating step size is challenging, making proprioceptive information alone insufficient (Terrazas et al., 2005). Visual input is essential to resolve visuo-proprioceptive mismatches, such as discrepancies between stepping patterns and visual flow when they are misaligned (Gothard et al., 1996). Later it was suggested that this conflict of perception is mediated by convergent visual and locomotory inputs integrated by EC (Campbell et al., 2018) and indirectly by the HC. Lesioning or deactivating the MSDB not only eliminates theta activity in the entorhinal cortex (EC) and hippocampus (HC) (Rawlins et al., 1979; Mitchell et al., 1982; Brandon et al., 2011; Koenig et al., 2011), but also disrupts navigation, likely by impairing the transfer of kinesthetic information. Notably, lesions in the EC or MSDB—but not the HC—result in deficits in estimating traveled distance in a linear distance estimation task (Jacob et al., 2017). Virtual reality approach enabled decoupling self-motion and visual information in head-fixed animals, confirming the importance of the EC (Chen et al., 2013). Convincingly, another compelling study also tested the controversies in stepping and visual flow mismatch (Jayakumar et al., 2019). In this study, researchers placed the animals on a circular track under a dome screen, and recorded HC place cells. Modulating the gain of the visual environment so that it gradually follows or lags behind the animal's movement alters the place field representation based on the available visual cues, rather than the animal's internal perception of the distance traveled.

One proposed mechanism for updating location based on self-motion involves EC speed-modulated cells. EC speed cells are mostly fist-spiking inhibitory PV+ neurons projecting to the HC (Ye et al., 2018). They were first studied in an experiment where rats were placed into a controlled cart without a bottom or were let to forage freely (Kropff et al., 2015). It is proposed that EC speed cells integrate speed signals arriving from the MSDB (Justus et al., 2017), and that MSDB inherits that signal from the MLR, more precisely the pedunculopontine nucleus (PPN), as PPN projects to MSDB (Hallanger & Wainer, 1988). Optogenetic activation of PPN neurons

elicited monosynaptic latency firing in the MSDB (~5 ms), and disynaptic-like latency is observable in the EC (~15 ms) (Carvalho et al., 2020). Activation of PPN fibers locally in the MSDB resulted in increased activity of EC speed cells with ~10 ms latency, further validating the functional role of this pathway.

In summary, MSDB is pivotal in orchestrating locomotion and navigation, acting as a central hub that integrates sensory inputs and motor signals to sustain rhythmic activity and continuously update positional information.

1.2 The effect of locomotion on sensory processing

Locomotion is known to influence neural sensory processing by influencing the cortical state and engaging state-dependent mechanisms that prioritize behaviorally relevant stimuli and improve sensory discrimination. These effects are mediated by neural circuit dynamics and arousal-dependent neuromodulation, enabling cortical systems to adapt sensory processing during movement. Experimental data showed how locomotion induces sensory-input biases and their correlation with functional or behavioral outcomes in sensory discrimination and perception across various sensory modalities, particularly vision and audition (Vinck et al., 2015b; G.-W. Zhang, Sun, et al., 2018). This cortical-state change is also represented in pupil diameter (Reimer et al., 2014), which is known to be tightly correlated with cortical NE and ACh levels (Reimer et al., 2016). This reflection of cortical state is so potent that pupil change could solely serve as a readout of cortical activity (Raut et al., 2023). In this context, the locus coeruleus (LC) (primary source of ascending noradrenergic pathways) and the BF (cholinergic nucleus), including the medial septal area (MSDB), are key players in mediating these locomotion-induced changes in cortical activity (Berridge & Waterhouse, 2003; Goard & Dan, 2009).

One of the earliest proposed mechanisms of MSDB is nociception. Old lesion studies of MSDB report reduced latency of escaping from aversive stimuli as heat, shock and sound stimulation, in other words, hyperreactivity (Harvey & Lints, 1965; Brown & Remley, 1971). Recordings from MSDB also show activity change to sensory inputs, not only pain (Hayat & Feldman, 1974). This implies increased arousal, during which HC theta is also present (Green & Arduini, 1954). Additionally, cell-type aspecific MSDB stimulation influences the amplitude of light-flash evoked field potentials in the visual cortex (Lorens & Brown, 1967). These suggest that arousal-related processing could be a relevant mechanism involving MSDB and septo-hippocampal interactions, and could spread to the cortex influencing cortical state and attention (Harris & Thiele, 2011).

We learn better when we pay attention; therefore, it is hard to distinguish between learning and attention. A recent study highlighted MSDB's role in auditory fear conditioning (FC) paradigm (G.-W. Zhang, Sun, et al., 2018). The authors describe a multi-relay pathway from the cochlea to the MSDB through the PPN and the PAG, which pathway transfers auditory related information selective to disturbingly high dB noise, but not pure tones. This auditory response was

prominent in the EC, output region of the MSDB, but sensitive to AMPAR antagonist DNQX. Moreover, silencing MSDB with lidocaine diminished this response. Building up a FC paradigm using disturbing noise conditioning stimulus revealed the importance of MSDB in auditory learning. In line with the literature, this proves the importance of MSDB in learning. This effect may be similar to the gain-modulation of the primary visual cortex (V1) discussed below (Fu et al., 2014; McGinley et al., 2015).

A central aspect of arousal is locomotion-induced gain modulation of sensory responses (Eldar et al., 2013). In the V1, locomotion enhances stimulus encoding by reducing noise correlations and improving temporal reliability of neural population activity (Niell & Stryker, 2010; Vinck et al., 2015b; Dadarlat & Stryker, 2017). In particular, visual stimuli presented during active locomotion lead to long-lasting potentiation in V1 (several days), a process that is NMDA receptor-dependent (Kaneko et al., 2017). This potentiation is reduced in stationary mice compared to the runners. Although this effect on V1 is proposed to be mediated by afferents from the MLR, literature on attention and gain control involving MSDB investigations identify direct ACh input to cortical VIP+ cells (Fu et al., 2014). In this study, VIP+ cells (inhibitory neurons inhibiting other GABAergic neurons) were shown to have a potent tuning of locomotion in the visual, auditory and barrel cortices; but antagonizing nAChRs locally diminishes speed tuning. Furthermore, optogenetic activation of these neurons enhances V1 visual response in still standing animals, while the ablation of VIP+ cells reduced the effect of locomotion on the cortical response. This bidirectional investigation serves as evidence of the MSDB effect on multi-sensory integration during locomotion through cholinergic transmission.

One aspect of locomotion is luminescence independent pupil dilation, a canonical hallmark of the sympathetic system. A dilated pupil enables a higher load of visual input, supporting better visual discrimination and learning. Pupil change also occurs in stationary animals during cognitive processing and task engagement (Beatty, 1982; Wang & Munoz, 2015), thus it is used as a readout of arousal (Hess & Polt, 1964; Bradshaw, 1967; Vinck et al., 2015b). Furthermore, as pupil change predicts LC dynamics and LC electrical stimulation dilates pupil (S. Joshi et al., 2016), they also serve as an indirect measure of LC activity (Iriki et al., 1996). These small fluctuations in pulse diameter during quiet wakefulness are also referred to as microarousal episodes, and reflect cortex wide change in NE and ACh activity (Reimer et al., 2016). In their

study, authors imaged cortical NEergic and cholinergic axonal activity, arising from LC and BF, respectively, and compared their results with velocity and pupil diameter. Upon locomotion initiation, cortical NE activity peaks and slowly decays during acceleration to a steady-state locomotion level, maintaining higher activity than baseline (no run). Cholinergic neurons show constantly high activity throughout movement. During microarousal episodes, transient peaks in neuromodulatory signals precede pupil dilation, with NE signals leading by approximately 1 s and ACh signals following at a lag of about 0.5 seconds before pupil dilation (Figure 2).

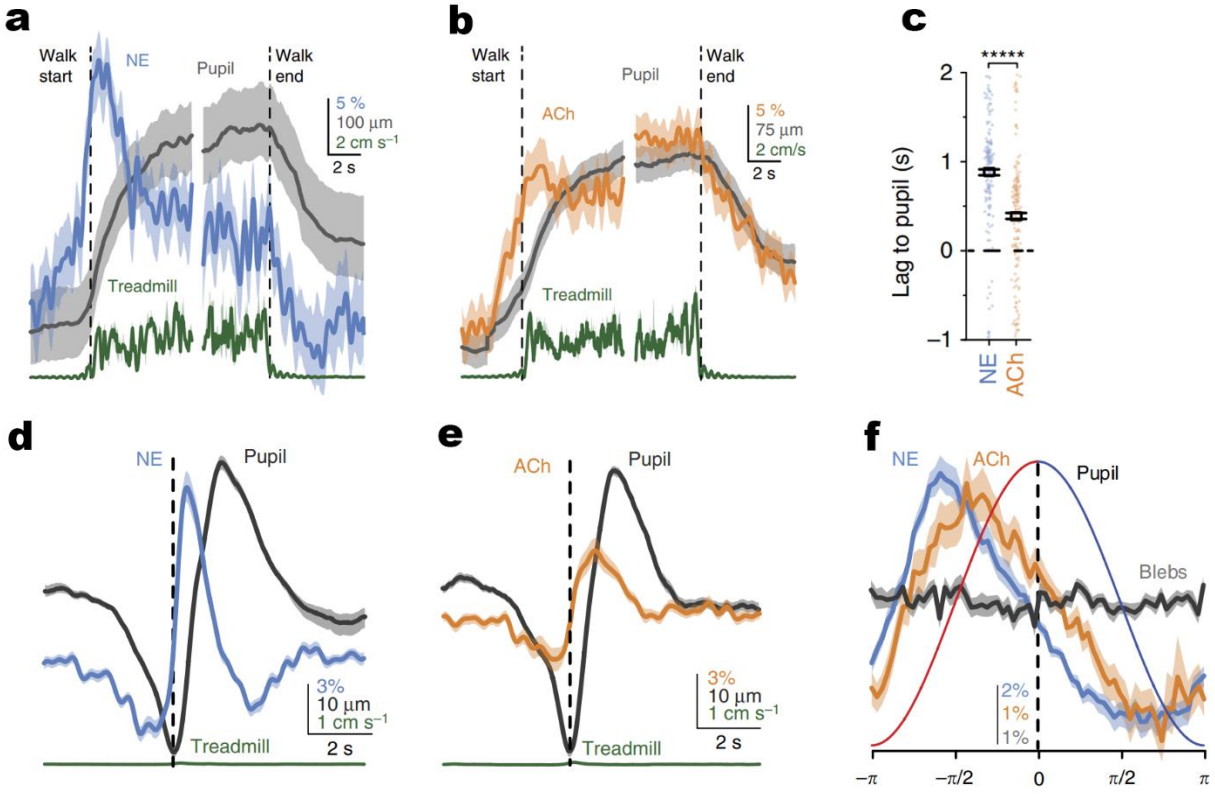

Figure 2. Imaged Ca^{2+} activity of neuromodulatory synaptic terminals in the cortex. A, Average NE signal (blue) in comparison with pupil (grey), and velocity (green) of the animal during locomotion. B, Similar to A, but with averaged ACh terminal imaged Ca^{2+} activity (orange). C, Temporal sequence of both neuromodulatory signals. D, Average NE signal (blue) in comparison with pupil (grey) in stationary pupil fluctuation during microarousal episodes. E, Similar to A, but with averaged ACh signal. F, Phase relationship of the two signals further explaining the dynamics between neuromodulatory signals and pupil. Adapted from Reimer et al., (2016)

The LC is known to be one of the main source of ascending noradrenergic pathways, sending axonal projections to the MSDB, which in turn influences cortical activity (Herz & Gogolák, 1965; Pickel et al., 1974; Segal, 1976). In this latter study from Segal, he showed that short electrical stimulation of the LC resulted in long latency (30-100 ms), long duration (100 –

300 ms) increases of MSDB population firing. Application of a longer, 1 s LC stimulation persistently modulated MSDB by maintaining an increase of population firing that lasted for several seconds. It is reasonable to speculate that this long-lasting activity may be mediated by persistent firing neurons in the MSDB, but this idea remains to be tested.

The LH has a proposed role in locomotion initiation. Using Ca^{2+} imaging, Karnani et al. (2020) pointed to the orexinergic (ORX) LH population being recruited shortly before, and during locomotor activity. They tested 3 means of locomotion initiations: voluntary movement initiation, and locomotion triggered by optogenetic activation of ORX neurons or by sensory stimulation of the animal. The activity change preceded locomotion onset for all three cases with about 1 – 3 s, with inverse relationship between optogenetic stimulation frequency and run latency from stimulation onset. A similar long latency was observed with sensory stimuli (like air puff, LED flash and different odors), where the stimulus onset activated most of the ORX neurons. However, locomotion was initiated only 1 – 3 s after the sensory stimuli, shortly before the Ca^{2+} signal reached its peak (Karnani et al., 2020), suggesting a preparatory period of LH activity before the animal starts running. Interestingly, motor preparatory activity is also present in the SN and BG, but the latency of locomotion compared to increased neural firing is rather on the sub-second timescale (Cui et al., 2013; da Silva et al., 2018). Another series of studies identifying LH projections and afferents revealed that this brain region is, like MSDB, considered as a sub-cortical hub due to its interconnections with almost the entire brain (Peyron et al., 1998). A retrograde labeling study investigated the LH neurons projecting to MSDB and to the spinal cord, and showed an overlapping population of those projecting neurons (Bittencourt & Elias, 1998). Moreover, activation of MSDB VGluT2+ terminals in the LH leads to a state transition of the animal from sleep to wakefulness (An et al., 2021), further suggesting MSDB role in locomotion.

The LH sends ORX projections to the LC, with LH ORX neurons being activated during locomotion, regardless of the underlying cause or reason for movement initiation (Karnani et al., 2020). These neurons also influence pupil size via the LC (Grujic et al., 2023). Optogenetic inhibition of LC norepinephrine (NE)-ergic neurons or systemic administration of an ORX antagonist suppresses the effect of LH ORXergic activation on pupil size. However, it remains unclear whether the LC receives direct input from MSDB VGluT2+ cells or if this input is mediated indirectly through the LH.

An et al. (2021) revealed that MSDB VGluT2+ innervates the LH, and the optogenetic activation of this projection in the LH transitioned the animal's behavior state from sleeping to wake, or active. This observation is in line with Yang Dan's hypothesis (tested in the SN (Liu et al., 2020)) that there are discrete behavioral states that are sequentially transitioning into one another, namely locomotion ⇔ movement ⇔ quiet wakefulness ⇔ slow wave sleep ➔ movement, which is represented widely throughout the brain in the form of sleep promoting and wake promoting neurons. Related to this, one can wonder about An et al. (2021) may have induced locomotion following MSDB VGluT2+ -LH pathway activation. However, they did not include speed analysis in their study. Anesthesia studies, targeting wake-promoting glutamatergic populations that transition rodents from deep anesthesia to wakefulness support this hypothesis (Tai et al., 2014; Xia et al., 2024).

1.3 Whisking

Whisking is another important aspect of locomotion, and it serves as a sensory input for rodents and other mammals helping with navigation and exploration, especially in darkness, providing essential tactile information for safe movement (Niederschuh et al., 2015). Stationary whisking has similar cortex-wide effect regarding synchronicity and state influence as locomotion, ie. amplifying sensory modalities (Crochet & Petersen, 2006; Reimer et al., 2014). Aroused cortical state is the hallmark of MSDB cholinergic activity. The barrel cortex, like the visual and auditory cortices discussed earlier, receives cholinergic input (Eggermann et al., 2014). Given this cholinergic drive, and considering the role of the barrel cortex in processing sensory input from whiskers, it is reasonable to suspect that MSDB is involved in the neural representation of whisking, but this idea remained to be tested.

This aligns with recent findings by Mocellin et al. (2024), who observed facial motion preceding locomotion as an expression of exploration when VTA terminals of the MSDB VGluT2+ population were stimulated. This observation is consistent with existing literature identifying whisking as a preparatory act for locomotion (Sofroniew et al., 2014). However, it remains an open question whether the projecting fibers indirectly induce whisking by activating postsynaptic executive cells or if the MSDB population itself directly represents whisking activity. Interestingly, studies investigating coupling between whisking and other rhythmic phenomena (like sniffing, stepping, or theta) reported contradictory results. Studies measuring 4 – 12 Hz whisking frequency postulated general synchronicity between these modalities (Ranade et al., 2013; Chakrabarti et al., 2022). Whereas others showed the absence of this type of systemic synchronization, and reported faster whisking in the 10 – 30 Hz range (Niederschuh et al., 2015). This contradiction is potentially due to distinct whisking patterns present during locomotory whisking and exploratory whisking (Berg & Kleinfeld, 2003), but the mechanisms underlying these phenomena are underexplored.

Compared to rhythmicity, positional modulation of the vibrissa is more thoroughly studied. Whiskers are pointing towards objects, and their position is modulated during turning. To test whether and how mice naturally rely on whisking in narrow corridors, Sofroniew et al. (2014) built a head-fixed, closed-loop tactile VR system where they placed two small walls on both sides of the animal at the level of the vibrissae while the mouse was running on a spherical ball.

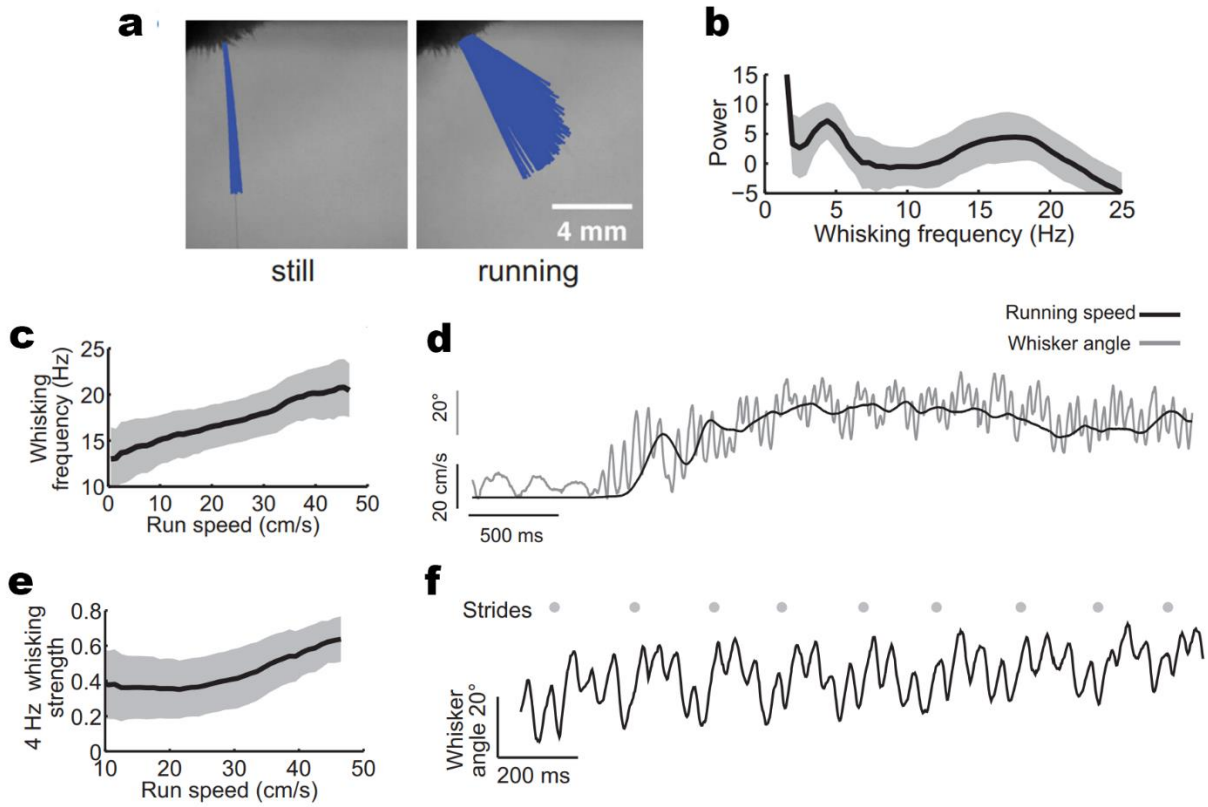

Figure 3. Parameters of whisking. A, Top view of whisking behavior during stationary and running periods. B, The power spectrum of the oscillating whisking forms 2 distinct peaks around 4 and 17 Hz. C, Mean whisking frequency in relation with locomotor velocity. D, Representative traces of simultaneous whisking (grey) and running (black) superimposed. Note the preparatory whisking before run initiation. E. Mean speed tuning of the stepping akin lower band whisking oscillation. F, Representative whisking trace in relation with strides. Adapted from Sofroniew et al., (2014)

Adjusting the distance of these walls with respect to the animal, but keeping the wall-to-wall distance constant (modelling a slight turn in the burrow) made animals take turns, positioning themselves again to the center of the “corridor” even in complete darkness (Sofroniew et al., 2014). Additionally, during turning or adjusting the locomotion angle relative to the head's fixed axis, the whiskers appeared to 'steer' the animal in the turning direction. Specifically, the whiskers on the turning side were more retracted compared to those on the contralateral side. Furthermore, the study showed that whisking preceded and maintained during locomotion (Figure 3), and correlated with locomotion velocity. They also report 2 peak frequencies on the whisking power spectrum around 4 and 17 Hz, with the slower frequency coupled with stepping. Breathing also shares a similar low frequency range with whisking (Ranade et al., 2013). A stepping-breathing coupling is reported in other mammals and even in birds, where breathing is coupled with wing stroke (Bramble & Carrier, 1983).

Although the role of whisking in navigation and sensory processing has been extensively studied, further research is required to uncover the precise neural mechanisms connecting whisking, movement, and cortical states, particularly in relation to the MSDB and its associated pathways.

1.4 Persistent firing

The classical model of neural firing incorporates spatio-temporal summation of dendritic inputs integrated at the soma. When the input reaches a threshold, the neuron generates an AP, and returns to its resting state. In contrast, persistent firing (PF) is a characteristic sustained, even seconds long change in neural activity discharge that outlasts the stimulus offset. This prolonged activation particularly fits with cognitive processes, when a specific input is needed to be present for behaviorally relevant time scales, like in working memory (Fuster, 1973; Funahashi et al., 1989), the head direction system (Yoshida & Hasselmo, 2009), in plasticity and learning (Knauer et al., 2013) sensory input to motor command transformation (Di Prisco et al., 2000), and motor planning in delayed response task (N. Li et al., 2016). Additionally, PF has also been observed in defensive behaviors, highlighting its role in maintaining relevant neural states beyond the immediate stimulus (Kennedy et al., 2020). These behaviors share one aspect, a certain neural population maintains its activity to execute prolonged actions. Pupil microdilations (Petty et al., 2021), and short whisking are hallmarks of micro arousal episodes, i.e. prolonged bursts of attention segmenting quiescence. However, whether this process is also governed by PF mechanism remained to be investigated.

1.4.1 *Mechanism of Persistent Firing*

PF can be influenced by both the intrinsic properties of neurons and network dynamics, with network effects typically playing a role in its duration by mediating termination through synaptic inhibition (Anderson & Strowbridge, 2014). The intrinsic mechanisms often involve depolarizing cation currents. More specifically, certain neurons employ persistently active Na^+ channels, which differ from regular voltage-gated Na^+ channels by maintaining Na^+ current and thus depolarization for a longer duration (Yamada-Hanff & Bean, 2013). In other regions, Ca^{2+}-dependent mechanisms contribute to PF with certain voltage-gated Ca^{2+} channels, like L- and T-type channels (Otsuka et al., 2001; Hughes et al., 1999; O'Malley et al., 2020). These mechanisms have been demonstrated in vitro without requiring pharmacological agents, though certain ligands like carbachol (a muscarinic ACh receptor agonist) may help in expressing these firing patterns. Carbachol-induced persistent firing is mediated via calcium-activated nonselective cation currents (I_{CAN}), and the test of these mechanisms usually requires muscarinic ACh receptor (mAChRs) activation (Haj-Dahmane & Andrade, 1996; Rahman & Berger, 2011).

For instance, Egorov et al. (2002) provided a detailed insight into PF mechanism at the cellular level using in vitro recordings from EC layer V neurons. During recordings, the GABA- and glutamatergic synaptic transmission was antagonized, and carbachol was applied to the bath. Neurons were depolarized by brief current injections, and their response was observed. Following the depolarization of neurons by brief current injections, they showed long lasting Ca^{2+} plateau potentials triggering a sustained train of AP firing that persists even after the current injection offset. This persistent firing was graded, meaning the firing rate correlated with the strength of the initial stimulus, and mediated by mAChR mediated I_{CAN}. Others have shown that besides mAChRs (Haj-Dahmane & Andrade, 1996), the most investigated mediators of I_{CAN} are type I mGluRs (O'Malley et al., 2020), and transient receptor potential (TRP) channels, like TRPC4/5 (Z. Zhang et al., 2011), TRPM4 (O'Malley et al., 2020) and TRPM5 (Lei et al., 2014).

In addition to intrinsic properties, PF can also arise from network dynamics, with recurrent excitatory synaptic connections playing a key role in maintaining activity over time. Studies on cortical microcircuits have shown that recurrent excitation generates and sustains activity even after external stimulation has disappeared. Balanced inhibitory inputs stabilized and prevented the system from runaway (Wang, 2001).

1.4.2 *Function*

One of the earliest observations of PF came from electrophysiological recordings in the dorsolateral prefrontal cortex (dlPFC) of monkeys performing delayed response tasks. Neurons exhibited elevated and sustained activity during the delay period, maintaining memory of the cues even after the initial stimulus was removed. This activity was maintained until the monkey made the decision or focused on the screen, but disengagement from the task led to the termination of PF, which is coherent with the above discussed role of ACh on attention (Himmelheber et al., 2000).

Kennedy et al. (2020) explored the role of PF in defensive behavior in the ventromedial hypothalamus (VMH). Firstly, they tested rat odor, which elicited long-lasting neural firing in the VMH, correlating with the duration of freezing. Similar to rat odor, optogenetic activation of VMH neurons also elicited PF and defensive behaviors that persisted well beyond the stimulation offset. Different subpopulations of VMH neurons were selectively activated by specific types of threats. For example, some neurons responded to predator odors, while others reacted to visual or auditory

stimuli. Importantly, overlapping, yet distinct subsets of neurons encoded different threats, maintaining stimulus-specific representation during persistent activity. Pharmacological abolishment of local synaptic connections prevented PF, and avoidant behavior, which supported their claim that recurrent excitatory-inhibitory interactions could underlie these phenomena. It is not with certainty to conclude whether the authors excluded the artificial effect of the pharmacological dissection of sensory pathways in the thalamus (whisking is also represented in VMH), which could also explain this effect.

1.5 MSDB to HPC projection

The hippocampus is a medial temporal lobe structure that is involved in episodic memory and spatial navigation (O'Keefe & Dostrovsky, 1971). A significant amount of research provided evidence that there are major differences in the dorsoventral axis of the hippocampus, regarding their connectivity (Swanson & Cowan, 1977; Cenquizca & Swanson, 2007), molecular profiles (Fanselow & Dong, 2010). As for their functions, while the dHC is involved in accurate coding of spatial location guiding navigation, vHC is known to have a pivotal role in social (Okuyama et al., 2016) and emotional (Henke, 1990) behavioral responses, and context recognition. The picture, however, should be more complex, as other comparative studies fail to distinguish these roles thought to be specific. For example, both poles of the HC are involved in odor recognition tasks based on their activation by cue odors (Biane et al., 2023), but dHC lesion impairs odor recognition in working memory task (Kesner et al., 2021), suggesting complex computations along the dorsoventral HC axis.

Studies have shown that the above-mentioned functionality differences at least partially could originate from the information coding specificity between the dHC and vHC cells (Jung et al., 1994). It is well established that dHC place cells exhibit narrow place fields, characterized by tightly tuned firing patterns that create a sparse, location-specific code, thereby encoding relatively high spatial information. In contrast, vHC place cells have significantly broader place fields, indicating less precise spatial coding (Kjelstrup et al., 2008). This distinction exemplifies the numerous functional differences between these regions.

Another line of research suggested that the molecular profile and the projection map differences should underlie these functional differences. For example, while the gene expression of the dHC correlates with cortical structures gene expression playing roles in navigation, the vHC genes correlate more with the gene expression of emotion and stress related areas (Fanselow & Dong, 2010). In addition, there are differences in the efferent projections of these structures, the dHC project to parahippocampal areas and to LS, while the vHC forms dense connectivity with the amygdala and hypothalamic endocrine nuclei (Swanson & Cowan, 1977).

The MSDB provides extensive cholinergic, GABAergic, and glutamatergic projections to the HC (Freund & Antal, 1988; Sotty et al., 2003). These projections play distinct roles in regulating HC activity, with cholinergic neurons influencing learning and memory

processes through tonic neuromodulation, which modulates HC synchrony. Notably, selective ablation of cholinergic cells results in lower amplitude but unchanged frequency theta oscillations, suggesting that the cholinergic input plays a role in modulating theta rhythm (M. G. Lee et al., 1994). Cholinergic cells, furthermore, could play a role in motivation shift, when the animal is hungry (Ortiz-Guzman et al., 2024). Ghrelin (gastrointestinal hormone secreted in hunger) mediated increase of neural activity in the vHC was observed (Wee et al., 2024). GABAergic neurons are crucial due to their rhythmic burst firing, they are critical in entraining hippocampal theta rhythms (Hangya et al., 2009). Meanwhile, glutamatergic projections, mediating hippocampal theta, likely play a role through gating EC input via activation of oriens lacunosum-moleculare (OLM) interneurons (Fuhrmann et al., 2015). However, there may be other, yet-to-be-identified functions of these projections. Reciprocally, HC also projects back to the MS through pathways primarily involving the subiculum and entorhinal cortex (Tóth & Freund, 1992). These interactions contribute to the dynamic interplay between regions, potentially allowing bidirectional modulation of rhythms and information flow.

The projection bias between these 3 cell types may also contribute to distinguishable theta rhythmic activities of the two poles of the HC. In the dHC, the prominent type I theta, associated with locomotion and navigation, is resistant to HC infusion of mAChR antagonist atropine, and oscillates in the 7 – 12 Hz range. On the other end, type II theta, a 4 – 8 Hz oscillation during quiet wakefulness, anxiety and small movements is atropine sensitive (Green & Arduini, 1954; Kramis et al., 1975; Sainsbury et al., 1987; Kocsis & Kaminski, 2006; Wells et al., 2013). A study showed that the HC synchronizes with the mPFC, a downstream anxiety related cortical region in open field test and on elevated plus maze (Adhikari et al., 2010). Theta-frequency activity in the vHC, but not dHC was highly correlated at baseline, and this correlation increased in both anxiogenic environments. Optogenetic excitation of a specific hippocampal interneuron population expressing the nAChR α2 subunit resulted in increased type II theta power in both the dHC and vHC, although this effect was more pronounced in the ventral hippocampus (Mikulovic et al., 2018). These findings provide additional evidence of the functional divergence between the dHC and vHC, potentially influenced by differences in their respective MSDB cholinergic inputs.

Considering the critical role of the MSDB in hippocampal theta activity and its status as a major input source to the HC, it is essential to investigate whether septo-hippocampal

projections converge or diverge along the dorsoventral axis of the HC. A recent study revealed significant variability in the input projections to the dHC and vHC (Tao et al., 2021). Here the authors used rabies viral construct and tracked the retrograde synaptic partners of hippocampal neurons. They injected the tracer to Thy1-cre animals to the dHC or to the vHC, and showed that for example the olfactory areas send strong projection to the vHC but not to the dHC. In the contrary, they observed the opposite when they analyzed the isocortical afferents. Additionally, the study identified differences in projections from the MSDB to the dHC and vHC, specifically noting that a greater number of cells in the DB project to the vHC. However, questions remain regarding the neurotransmitter profiles of these projections, their similarities and differences along the dorsoventral hippocampal axis, and whether individual MSDB neurons simultaneously project to both regions.

In addition to the neurotransmitter profile of septo-hippocampal projecting neurons, their further molecular details may enable them to fulfill specific roles (Kuhn et al., 2024). These subdivisions have already been discussed above regarding the GABAergic cells (PV+, SOM+, CR+). Recently, among cholinergic neurons, their expression of calbindin (CB) alias D28K, a vitamin-D dependent Ca^{2+} binding protein, further divides this population (X. Li et al., 2022; J.-L. Wu et al., 2024). Along the expression profile of various ion channels, and their morphology underlying their electrophysiological characteristics, their projection preference also distinguished them. Specifically, the CB+ cholinergic subpopulation mainly targeted the vHC, while CB- neurons the dHC. Additional mRNA profiling revealed that CB+, but not CB- neurons express specific apoptotic markers, which may explain the cholinergic cell loss in Alzheimer's disease (Schliebs & Arendt, 2011). This thesis aims to further provide a detailed quantification of MSDB cell population projections along the dorsoventral hippocampal axis and discuss the potential functional implications of these anatomical differences.

2. The thesis

This thesis explores the medial septum-diagonal band of Broca (MSDB), with a focus on its cellular mechanisms, circuit dynamics, and its role in locomotion, sensory integration, and hippocampal connectivity. Fuhrmann et al. (2015) demonstrated that a 1-second theta-frequency stimulation induces persistent running; however, the underlying cellular and network mechanisms remain unclear. To address this, we utilized Neuropixels technology, enabling large-scale recordings and a detailed examination of the MSDB network and its relationship with locomotion-related behavioral variables.

The overarching goal of this thesis is to uncover how specific neural populations and pathways within the MSDB contribute to distinct behavioral and physiological processes. The specific objectives are:

1. To investigate how three aspects of animal movement—whisking, pupil dilation, and locomotor behavior—are synchronized by a specific brain region and neural populations

2. To identify the role of persistent firing neurons in the MSDB

3. To neurochemically characterize and quantify septo-hippocampal projections to dorsal and ventral hippocampal subfields.

3. Materials and methods

3.1 Electrophysiological recordings of the MSDB and activating VGluT2 cells

3.1.1 *Transgenic mice*

In vivo experiments were performed in adult, 10–14 week old homozygous VGluT2-cre mice (B6J.129S6(FVB)-Slc17a6$^{tm2(cre)Lowl}$/MwarJ) of both sexes (The Jackson Laboratory, Bar Harbor, ME USA). Mice were group-housed before, and single-housed after the surgery under 12-hour inverted dark and light cycle. All experiments were performed in the dark phase of the cycle with food and water ad libitum. All experimental procedures were approved by the local authorities of Saxony-Anhalt and performed in accordance with LIN regulations in agreement with the European Committee's Council Directive.

3.1.2 *Surgery*

Stereotactic surgery was performed under deep isoflurane anesthesia (Vetflurane 1000 mg/g, Virbac, Carros, France) in a stereotactic frame (MA-6N head-holder, GM4 anesthesia mask, Narishige, Tokyo, Japan) under the guidance of stereomicroscope (M80, Leica Microsystems GmbH, Wetzlar, Germany), and mice were kept at 30°C with a heating pad (Rodent Warmer X2, Stoelting Co, Wood Dale, IL, USA) throughout the surgery. After scalp removal, the skull was prepared, dried, a checkerboard pattern was carved into the bone, and phosphoric acid gel (37.5 %, Gel Enchant, Kerr, Kloten, Switzerland) was applied to increase the adhesion surface. A thin layer of Primer and Adhesive (Optibond, Kerr, Kloten, Switzerland) were applied to the skull avoiding the areas where the drill will have been used. A small craniotomy was drilled (Q Basic ST drill, Schick GmbH, Schemmerhofen, Germany; H71.104.003 drill bit, Komet Dental - Gebr. Brasseler GmbH & Co. KG, Lemgo, Germany) above the medial septum (+1.0 mm anterior and 0 mm lateral, relative to bregma), and the sinus was carefully pushed away by the 34G beveled needle of a Hamilton syringe (WPI, Sarasota, FL, USA), with its opening pointing to the midline, and channelrhodopsin (pAAV2.1-EF1a-double floxed ChR2-EYFP-WPR (H134R)) or opsin free virus (pAAV2.1-EF1a-double floxed EYFP-WPR (H134R) (Addgene, Watertown, MA, USA)) of 400 nl was injected into each of two loci of the medial septum (4.5 mm and 4.0 mm ventral, relative to bregma) with 100 nl/min speed using motorized manipulators (Mini 23-XR motors, SM-7 remote control pad, SM-10 control box, Luigs & Neumann GmbH, Ratingen, Germany) and micropump (UMP3 pump, Micro4 pump control, WPI, Sarasota, FL, USA). After injection, a 1

mm diameter circle (centered at AP: 1.0 mm, ML: 0.7 mm relative to bregma) was drawn and slightly carved into the bone to mark the craniotomy sight, and a small metal bar was placed above the posterior part of the skull for the acute head-fixed experiments (Luigs-Neumann, Ratingen, Germany). To prepare reference and ground electrode outposts, 3 craniotomies were made on the occipital bone, and into each craniotomy, a blunt ending golden pin connected silver wire was immersed epidural above the cerebellum. The skull was covered up with UV-curable dental cement (Gradia Direct Flo, GC Corporation, Tokyo, Japan), except above the carved window, that was covered by Kwik-sil (WPI, Sarasota, FL, USA) until the preparation for the acute experiment. After the surgery, animals were single-housed with a home cage treadmill to ensure their activity during the experiment. Animals were allowed to recover for 2 weeks before the habituation.

3.1.3 *Recording preparation*

After the mice were handled and habituated to head fixation, they were trained on the treadmill until they become good runners (meaning that they covered at least 20 m in 10 min). Before the experiment, mice went under isoflurane anesthesia, and the pre marked 1 mm craniotomy and subsequent duratomy was made. We made sure that the exposed brain tissue is always covered with saline, while a non-operating (dummy) Neuropixels 1.0 probe (IMEC, Leuven, Belgium) was immersed into the tissue to ensure penetration. After this test, the tissue was covered with 1% low melting point agarose (dissolved in saline) (Agarose low EEO, PanReac AppliChem, Darmstadt, Germany), and Kwik-sil, and mice were allowed to rest overnight, or at least 6 h before the acute probe immersion.

3.1.4 *Recording*

Before fixing the mice to the treadmill (length: 360 cm, width: 7 cm, color: black, no cue), the Neuropixels 1.0 probe (IMEC, Leuven, Belgium) combined with optical lambda fiber (Optogenix, Lecce, Italy) with 2.5 mm active length was gently painted with DiI (1 mM, Vybrant, Invitrogen, Thermo Fisher Scientific, Waltham, MA, USA) to later recover the site of recording. The combined probe (Fig 7a) was than immersed slowly into the brain (<5μm/s) with 10° angle until reaching the 5500 μm from brain surface. The probe was held for at least 15 min to stabilize the tissue, and to reach sufficient signal-to-noise ratio. The recording consisted 5 different protocols, where the 473 nm diode laser (LuxX473-80, Omicron-Laserage Laserprodukte GmbH, Rodgau-Dudenhofen, Germany) was controlled by custom written code (Igor Pro 7, WaveMetrics,

Portland, USA). We used 1) 1 s continuous wave stimulation with 2 min inter-stimulation intervals (IStI), 10 stimulations, 2) 500 ms cw stimulation with 20 s IStI, 5 or 10 stimulations, 3) 100 ms cw stimulation with 20 s IStI, 5 or 10 stimulations, 4) 5 ms cw stimulation with 20 s IStI, 5 or 10 stimulations, and 5) 10 s long stimulation at 8 Hz with 1 ms pulse width. Only protocol 1 and 5 were analyzed in this study.

Electrophysiological data was acquired through the Neuropixels on board amplifier, transferred by a tether cable, and sampled at 30 kHz through an acquisition module (PXIe-1071, National Instrument, Austin, TX, USA), and by an interface module (MXI-Express x8, PXIe-8381, National Instrument) was further transferred to the acquisition computer (Z4, HP Inc., Palo Alto, CA, USA), controlled by Open Ephys software (v 0.6.4, Open Ephys Inc., Atlanta, GA, USA). One infrared lamp (LIU780A, Thorlabs Inc., Newton, NJ, USA) and two side cameras (acA2040-90umNIR, Basler, Ahrensburg, Germany) were used to monitor the animals' face and body, and the face camera signal was further analysed to acquire pupil signal (DeepLabCut 2.3.5, Mathis et al., 2018, Nath, Mathis et al., 2019), and camera motion energy (custom written code, Python). The speed of the animal was monitored by a rotation sensor built in the treadmill (Luigs-Neumann, Ratingen, Germany).

3.1.5 *Spike sorting*

After the recordings, we used Kilosort 3 (Pachitariu et al., 2024) to preprocess and sort the spikes, and subsequently phy software for manual curation (https://github.com/cortex-lab/phy). Good units were selected based on template waveform, refractory period validation, and amplitude distribution throughout the recording. Units were merged and split manually by the guidance of firing rate maps, waveform, anatomical location, and template principal component charts. The spike times for the good units were extracted to python for further analyses with Npyx package (Beau et al., 2021).

3.1.6 *Data analysis*

3.1.6.1 Software

Data analysis was performed using custom-written scripts in Python v3.6.10, with the packages Numpy v1.19.2, Scipy v1.5.2, Neo v0.7.1, Elephant v0.6.2 and Matplotlib v3.3.2.

3.1.6.2 Spiking activity

Persistent activity was defined as significantly increased firing rate in the time interval 1–3 s after the stimulus offset (i.e. 2–4 s after the stimulus onset), compared to baseline calculated over 2 s before the stimulus onset. Only units showing persistent activity at least 50% in response to the 1 s stimulations (5 out of 10 stimulations) were considered persistent firing units. Persistent activity length was calculated by binning the spike trains to 200 ms bins, and a 2 s window before the stimulation was statistically tested against the 2 s window from stimulation onset. Then this latter 2 s window was shifted with 200 ms, and p-values were continuously collected. When the list of p-values increased above 0.05, the last AP from that time point was considered as the end of persistent firing.

Optotagged units were identified with protocol 5), a train of 1 ms laser pulses at 8 Hz. Units that showed response at least 10% of the stimulation within 5 ms were considered optotagged.

For identifying theta-rhythmic and bursting neurons, we adapted the method from (Kocsis et al., 2022). First, the autocorrelation function was calculated at a 1 ms resolution, smoothened by a 20 ms wide moving window and normalized to have an integral equal to 1. To assess whether the neuron is theta-rhythmic and/or bursting, we calculated two measures: the rhythmicity index (RI) and the burst index (BI).

Theta-rhythmic neurons were characterized by their auto-correlation function where it shows significant modulation in the theta-frequency range. The RI is based on the comparison between the amplitude at the peak and at the trough of the autocorrelation function. To calculate the peak value, we first concatenated segments of the autocorrelation function in the lag intervals (110 ms, 150 ms) and (240 ms, 280 ms), where theta peaks are expected and denoted this signal ac_{peak}. For the trough values, we similarly concatenated the lag intervals centered in between the expected peak position, i.e. (45 ms, 85 ms) and (155 ms, 195 ms) to obtain ac_{trough}. Then the RI is calculated as

$$\mathrm{RI} = \frac{ac_{peak} - ac_{trough}}{max(|ac_{peak}|, |ac_{trough}|)} .$$

Cells with RI > 0.3 during periods of voluntary locomotion were marked as theta-rhythmic.

For Burst units, we calculated burst indices (BI). Values in the lag interval (15 ms, 40 ms) of the autocorrelation function, denoted as ac_{theta}, were compared with values in an extended interval (15 ms, 80 ms) denoted as ac_{ext}. The BI was calculated as

$$\mathrm{BI} = \frac{mean(ac_{theta}) - mean(ac_{ext})}{max(max(ac_{ext}), min(ac_{ext}))}.$$

Cells with BI > 0.3 were considered bursting.

3.1.6.3 Generalized linear model

To investigate the unit coding of individual or conjunctive behaviors, we used a Generalized Linear Model (GLM) to infer unit activity based on the min-max normalized behavioral variables (CME, speed, pupil diameter). First, we grouped the behavioral variables as well as the spiking data into 20 second long windows centered around each voluntary run initiation, resampled the signals to an equal same sample rate, and finally binned the signals into bins of 250 ms. A GLM for Poisson-distributed observables was then trained on 80% of the time windows for each animal consisting of the behavioral variables as predictors and the binned spiking as outcome variable using the statsmodels Python library (v 0.14.3). We then ran prediction of unit activity based on the remaining 20% of time windows and computed the R2 scores between the real and inferred data. To validate if the correlation is significant over chance, we bootstrapped the behavioral data by first dividing the behavioral data into blocks of 19 data points and randomly permuting the blocks, and second by circular shifting the time series by a given offset. The procedure was repeated 100 times, and units with the original R2 scores higher than 95% of the bootstrapped R2 scores were considered significantly predicting unit activity from the behaviors. Conjunctive coding was annotated to units having significant activity predictions by at least 2 behavioral variables.

3.1.7 *In Vitro Experimental Procedures*

3.1.7.1 Slice preparation

For MEA recordings of spontaneous and light-induced action potentials, with isofluran, we anesthetized adult (22–48 week old) VGluT2-cre mice that went under surgery 26–60 day before the experiment, and 400 µm thick coronal MSDB slices were cut in ice-cold high sucrose artificial cerebrospinal fluid (ACSF) (mM): 85 NaCl, 75 sucrose, 2.5 KCl, 25 glucose,

1.25 NaH_2PO_4, 4 $MgCl_2$, 0.5 $CaCl_2$, and 24 $NaHCO_3$; using Leica VT1200S vibratome. After cutting, slices were transferred to an interface chamber (Warner Instruments, Hamden, USA) containing standard ACSF (Maier et al., 2009) for recovery (mM): 125 NaCl, 3 KCl, 26 $NaHCO_3$, 2.6 $CaCl_2$, 1.3 $MgCl_2$, 1.25 NaH_2PO_4, and 15 glucose, oxygenated with 95% O_2 and 5% CO_2. MSDB slices were kept inside the interface chamber on lens cleaning tissue (Grade 105, Whatman, Maidenstone, England) allowing optimal oxygenation due to a laminar flow of preheated (35°C) ACSF above and underneath the slices for at least 30 minutes of incubation until they were used for the experiment, when the slices were transferred to the recording chamber for data acquisition.

3.1.7.2 Microelectrode Array (MEA) recordings

Extracellular waveforms in the MSDB slices in VGluT2-cre mice were recorded with a MEA2100-System (Multi Channel Systems, Reutlingen, Germany, RRID:SCR_014809) on 60pMEA100/30iR-Ti MEAs with round titanium nitride electrodes, as described in Sosulina et al. (2021). In detail, the MS slices were positioned onto a 6 × 10 matrix of electrodes, with a spacing of 100 µm and an electrode diameter of 30 µm. ACSF temperature was adjusted to 35°C using heatable PH01 perfusion cannulas together with a TC01 controlling unit (Multi Channel Systems, Reutlingen, Germany). The position of the slice was stabilized by applying of a constant negative pressure of 25–30 mBar. Data were acquired with Multi Channel Experimenter (V 2.18.0.21200, Multi Channel Systems, Reutlingen, Germany) at 25 kHz sampling rate with an MEA2100-lite-Interface Board.

3.1.7.3 Optogenetic stimulation in MSDB brain slices

Brain slices of VGluT2-cre mice expressing channelrhodopsin in the MSDB were used for optogenetic experiments. Optogenetic stimulation in slices was performed with a light fiber coupled 473 nm diode laser (LuxX473-80, Omicron-Laserage). The light fiber tip was placed at a distance of ≤ 5 mm to the slice. We used a custom-written Igor script stimulation protocol forwarded to the multielectrode array (MEA) board to synchronize the recording with the stimulation. The 30-min-long stimulation protocol consisted of 5 minutes of baseline period before and after the stimulation for sanity control of the condition of the slice, in between 10 pulses of 1 s continuous laser stimulation with 2 min inter-stimulation intervals was applied. In pharmacological experiments, ACSF bath solution was changed after the 5th repetition of the stimulus to blocker cocktail containing ACSF solution serving as an inner control for our in vitro

experiments (μM): 10 NBQX, 50 D-AP5, 10 SR-95531, 1 CGP52432, 10 Atropin, 0.2 MLA, 1 MCPG.

For Ca^{2+} recordings, we used our standard ACSF solution (see above), but to adjust extracellular calcium concentration ($[Ca^{2+}]_o$) different concentration of $CaCl_2$ was added, low $[Ca^{2+}]_o$ contained 0 mM, mid $[Ca^{2+}]_o$ contained 1.3 mM, and high $[Ca^{2+}]_o$ contained 2.6 mM of $CaCl_2$. ACSF with distinct $[Ca^{2+}]_o$ levels were changed after the 5th repetition of the stimulus, and conditions followed each other semi-randomly for better comparison. In EYFP experiments the 10 repetition protocol was applied without any change of the standard ACSF bath solution.

3.1.7.4 Analysis of MEA experiments

After data collection, slices were transferred overnight to 4% paraformaldehyde (PFA) solution, and were mounted for confocal tile-scan imaging (SP8, Leica, Germany). Only slices with EYFP expression were then used for data analysis. Recordings were exported to HDF5 format and were analyzed with Python. Data were preprocessed using 300–6000 Hz band-pass filter, and common median reference using Spikeinterface package (Buccino et al., 2020). Spikes were sorted with Tridesclous 2 sorter, and manually curated. Spike times combined with stimulation times were further analyzed.

3.1.7.5 Statistical testing

In the cases with clearly defined pairs of values (e.g. pre- and post-stimulus value of the mean firing rate), the two-sided Wilcoxon's signed-rank test was used. In all other cases, the non-parametric two-sided Mann–Whitney U-test was applied, as the data were not normally distributed.

3.2 Dorso-ventral projection difference of septohippocampal neurons

3.2.1 *Animals*

All mice were bred and raised in the animal facility at the Leibniz Institute for Neurobiology (LIN), Magdeburg, Germany. A total of 8–10 weeks old adult C57BL/6J and VGluT2cre/TdT double heterozygous (B6J.129S6(FVB)-Slc17a6$^{tm2(cre)Lowl}$/J × B6.Cg-Gt(ROSA)26Sor$^{tm9(CAG-tdTomato)Hze}$/J) mice were used in this study. The mice were kept in a 12 h light/dark cycle with food and water ad libitum. All experimental procedures are in accordance with the LIN and government regulations, and were approved by the committee in charge of ethics.

3.2.2 *Surgery and Virus Injection*

dHC (A-P: -1.5 mm; M-L: -1.1 mm; D-V: -1.7 mm and -1.6 mm); vHC (A-P: -3.2 mm; M-L: -4.0 mm; D-V: -4.4 mm and -4.2 mm). Two Hamilton syringes were filled with retrograde adeno associated viruses pAAV-hSyn-EGFP (1.5 × 1012 genomic copies per ml) and pAAV-CAG-tdTomato (1.32 × 1012 genomic copies per ml), and 250 nl were injected into the each D-V coordinates of the dHC and vHC, respectively with a speed of 100 nl/min. For some of the experiments (n = 6), we switched the two constructs, and injected TdT expressing virus to the dHC, and GFP expressing to the vHC to control for the different promoters. This dataset was pooled with the others as they showed similar results. For VGluT2cre /TdT animals only pAAV-hSyn-EGFP was injected either to the dHC or the vHC. Mice were anaesthetized and perfused 4 weeks after surgery with 4% paraformaldehyde (PFA) in phosphate-buffered saline (PBS), and the brain tissue was stored in the same solution at 4°C overnight, and placed in 0.01 M PBS until sectioning. Brains were embedded in 3.5 % agarose (Low EEO Agarose, AppliChem Panrea) and 40 µm thick coronal sections were made using vibratome (VT1000 S, Leica, Germany).

3.2.3 *Immunohistochemistry*

On each brain, three distinct immunohistochemistry staining were performed, and every third slice of the MSDB was selected for each of the protocols, namely no immunostained, ChAT, CaMKII, GAD67, and PV stainings.

Primary antibodies were used against ChAT (rabbit polyclonal anti-ChAT, Millipore, AB143, 1:250), GAD67 (mouse polyclonal anti-GAD67, Millipore, mab5406, 1:500), PV (rabbit polyclonal anti-PV, Abcam, AB11427 1:1000), CaMKII (rabbit polyclonal anti-CaMKII alpha/beta/delta, Invitrogen, ThermoFisher Scientific, PA5-99558) after blocking and permeabilization of the tissue wit 0.3% Triton X, and 5% normal goat serum for ChAT and CaMKII protocols. GAD67 and PV slices were blocked in 0.01M Tris buffer solution with 10% normal goat serum. Primary antibodies were incubated over 3 nights at 4°C, and after PBS wash steps, they were incubated with secondary antibodies (donkey polyclonal anti-rabbit Alexa Fluor 405, Abcam, ab 175649, 1:1000; Goat polyclonal anti-rabbit Cy5, Jackson ImmunoResearch, 111-175-144, 1:400; Donkey polyclonal Anti-Mouse Alexa Fluor 647, Invitrogen, ThermoFisher Scientific, A31571, 1:200) for 2 h on room temperature. Sections were mounted using Mowiol® 4-88 medium (Carl Roth Gmbh & Co. Kg).

3.2.4 *Imaging*

Coronal sections were imaged using confocal laser scanning microscope (SP8 and SP8-3X, Leica, Germany). MSDB cells were manually counted using ImageJ software, and animals with detectable microbeads or spread of labeling at the injection site were analysed.

3.2.5 *Analysis*

Analysis was done by custom written Python code. MSDB was divided into 4 areas, and their size were taken for calculating the volume of the tissue to calculate cell density. Paired ratio (PR) was calculated for each animal by dividing the total cell count of dHC or vHC projecting neurons with the total amount of projecting cells. For PR of immunolabeled neurons, the number of projecting neurons for the given staining was divided by the total number of projecting neurons labeled for that given staining. PR is indicated with connected datapoints. Percentage of cells was used as a measure of immunopositivity ratio of a given projection; therefore, it was calculated dividing dHC or vHC projecting immunolabeled neurons by the number of dHC or vHC projecting neurons, respectively. The two measures represent different relationships in the dataset; therefore, we used both. For Bregma position analysis, we noted the Bregma estimate for all slices, which were binned into 5 bins.

3.2.6 *Statistics*

Datasets were checked for normal distribution using Shapiro–Wilk normality test, PRs were tested using paired t-test, while cell densities and percentages of immunolabeling were tested with Student's t-test. For Bregma location comparison, t-test with Bonferroni correction was applied. Data is written in the form of mean ± SEM, or median(IQR) for box plots.

4. Results

4.1 VGluT2 population of Medial Septum Diagonal band of Broca complex (MSDB), the conductor of the locomotory orchestra

4.1.1 *Prolonged 8 Hz stimulation induced locomotion with high success rate*

Building on previous studies that demonstrated MSDB VGluT2-dependent run initiation requires activation lasting over 10 seconds and that run initiation is delayed by several seconds following stimulation onset (Fuhrmann et al., 2015; Kocsis et al., 2022), we designed our experimental protocol to examine the effects of shorter, more physiologically relevant activation durations. In order to test how the length of the stimulus affects locomotion induction in head-fixed mice running on a treadmill, we injected AAV1-EF1a-DIO-ChR-EYFP or an appropriate control construct (AAV1-EF1a-DIO-EYFP) into the MSDB of VGluT2::Cre mice, and implanted an optical fiber to deliver 473 nm laser light. In parallel, we investigated the effect of this activation on other locomotion-related modalities, including the face movement and pupil change using Camera Motion Energy (CME) analysis and pupillometry, respectively (Fig 4a). Two types of stimulus protocols were applied: a previously-used 10s long stimulation at 8 Hz frequency, related to theta oscillation frequency (Fuhrmann et al., 2015) or 1s square pulses with 2 min inter-stimulation period (Fig 4b). When compared to the control animals, 8 Hz prolonged stimulation

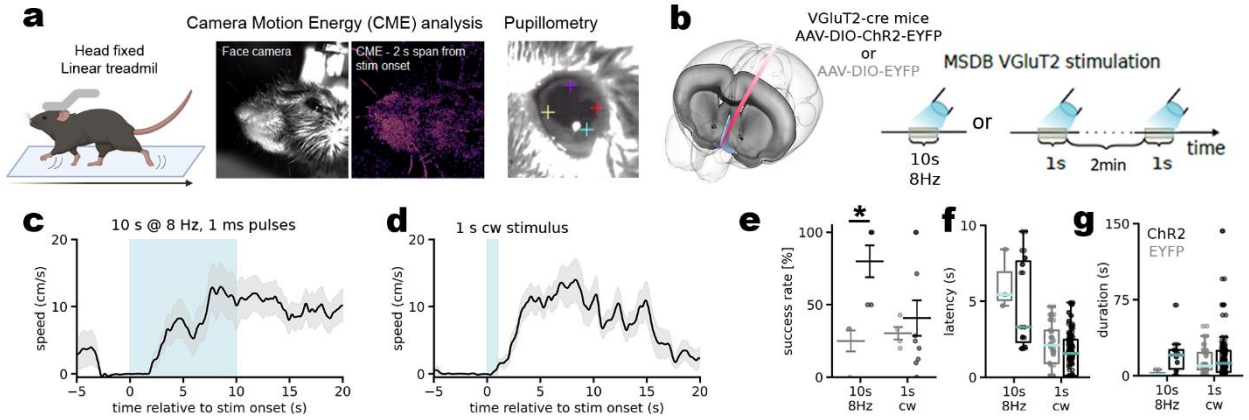

Figure 4, Short, 1 s stimulation of MSDB VGluT2 neurons elicit locomotion. A, Experimental setup and behavior analysis, (left) running of the animal was tracked on a linear treadmill, (middle) Camera Motion Energy signal is analyzed from the face camera recordings, example heatmap of 2 s CME shown, (right) pupillometry with DeepLabCut. B, (left) Placement of the electrode combined optic fiber to the MSDB of ChR2 or control virus injected animals, (right) stimulation protocols. C, Average speed during and around 10s optical stimulation of VGluT2 neurons at 8 Hz, D, same as in C with 1s continuous wave optical stimulation. E, Success rate of the stimulation protocols. F, Latency of run initiation from stimulation onset comparing the protocols and the ChR2 with control. G, Duration of elicited running.

induced locomotion with significantly higher success rate (EYFP control: 25.00 ± 7.22 %, ChR2: 80.00 ± 10.95 %, U=0.0, p=0.016, Mann-Whitney U-test, median(IQR)) tendentiously longer duration (EYFP: 1.25(0.64-2.87) s, ChR2: 20.49(6.82-25.52) s, U=9.0, p=0.142), and with comparable latency (EYFP: 5.45 (5.08-6.93) s, ChR2: 3.30 (2.31-7.64) s, U=22.0, p=0.456) (Fig 4c-g). In contrast, a transient 1s stimulation resulted in the success rate that was not different than chance level (EYFP: 30.30 ± 4.34 %, ChR2: 40.83 ± 12.27 %, U=20.0, p=0.816), as well as no difference in latency (EYFP: 2.12(0.93-3.10) s, ChR2: 1.58(0.10-2.49) s, U=1141.0, p=0.106) and duration (EYFP: 9.75(6.11-22.73) s, ChR2:12.32(3.77-24.74) s, U=904.0, p=0.793) of locomotion (Figure 4e-g).

4.1.2 *Photoexcitation of MSDB VGluT2 neurons elicits facial movement (CME), pupil dilation and locomotion*

Animals exhibit preparatory behaviors, such as facial movements, prior to locomotion initiation, potentially related to exploration (Mocellin et al., 2024). Additionally, pupil changes are observed during natural running. Therefore, we tested whether the 1-second stimulation protocol influenced these behaviors as well. In contrast to running, CME and pupil were both reliably elicited by 1s MSDB VGluT2 stimulation (CME success rate EYFP: 46(25-69) %, ChR2: 83(80-100) %, U=2.5, p=0.018; pupil amplitude change EYFP: 0.06(0.01-0.13) a.u., ChR2: 0.26(0.12-0.32) a.u., U=181.0, $p=1.620*10^{-4}$) (Fig 5a-c) with a conserved behaviorally relevant difference in their latencies (latency of CME: 0.17(0.12-0.30) s, pupil: 1.20(1.00-1.45) s, run: 2.18(1.73-2.95), H=79.967, $p=4.319*10^{-18}$, Kruskal-Wallis test; post-hoc Dunn-test with Bonferroni correction: CME vs. run: $p=4.706*10^{-17}$, CME vs. pupil: $p=3.743*10^{-10}$, pupil vs. run: $p=1.189*10^{-3}$) (Fig 5d), although the duration of the three measured behaviors did not differ from each other (duration of CME: 18.26(12.07-30.30) s, pupil: 10.07(6.87-18.90) s, run: 9.46(1.81-15.58) s, H=5.758, p= 0.056) (Fig 5e), suggesting that these behaviors may be simultaneously modulated by VGluT2 population. To investigate why the same stimulation induces CME and pupil changes yet sometimes fails to trigger running, we analyzed CME and pupil signals during successful (CMEr/PUPr) and unsuccessful (CMEnr/PUPnr) run initiations (Fig 5f-h). In particular, the magnitude of CME and pupil change was predictive to locomotion initiation success, higher

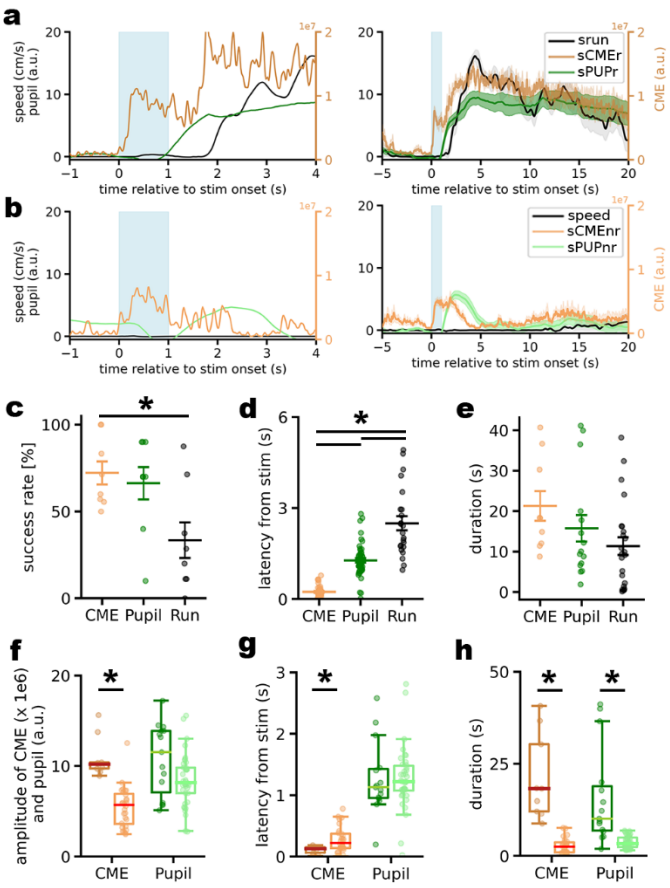

Figure 5, 1 s stimulation of MSDB VGluT2 neurons elicits CME and pupil dilation. A, (left) Representative trace of successful run initiation, (right) average run initiations of all experiments. B, same as in A, but for non-successful run initiation. C-E, success rate, latency and duration of the 3 behaviors. F-H, Comparison of CME magnitude and pupil amplitude, latency, and duration between successful (darker toned color) and non-successful (lighter toned color) run initiation traces.

magnitudes were detected on successful compared to non-successful run initiation trials (magnitude of CMEr: 10.22(9.71-10.40)*10^6 a.u., CMEnr: 5.69(3.58-6.91)*10^6 a.u., U=245.0, p=2.730*10^{-5}; amplitude of PUPr: 11.54(7.09-13.89) a.u., PUPnr: 8.18(6.99-9.81) a.u., U=385.0, p=0.049) (Fig 5f). Additionally, the successful trials initiated CME more promptly compared to no-run trials (latency of CMEr: 0.13(0.06-0.15) s., CMEnr: 0.22(0.14-0.37) s, U=63.0, p=0.027; latency of PUPr: 1.13(0.95-1.42) s, PUPnr: 1.22(1.07-1.48) s, U=251.0, p=0.508) (Fig 5g). As expected, the duration of CMEr and PUPr were more prolonged compared to CMEnr and PUPnr (duration of CMEr: 18.26(12.07-30.30) s., CMEnr: 2.48(0.94-3.67) s, U=243.0, p=3.723*10^{-5}; duration of PUPr: 10.07(6.87-18.90) s, PUPnr: 3.33(2.40-4.94) s, U=517.0, p=4.855*10^{-6}) (Fig 5h).

4.1.3 *Comparision of voluntary and stimulated behaviors*

Next, we compared the voluntary (v) and stimulated (s) behaviors differentiating whether those were followed by run initiation or not (srun, vrun, sCMEr/nr, vCMEr/nr, sPUPr/nr, vPUPr/nr), and analyzed their relationship. No difference in locomotion speed and running duration was observed when the animals were running voluntarily, compared to the induced locomotion (average speed of srun: 9.69(5.01-11.74) cm/s, vrun: 9.48(4.75-14.19) cm/s, U=1257.0, p=0.579; average duration of srun: 9.46(1.81-15.58) s, vrun: 10.47(2.62-22.93) s, U=1244.0, p=0.530) (Fig 6a,b). However, the latency of CMEr and PUPr relative to the onset of

locomotion differed between stimulated and voluntary behaviors. The median value of vPUPr lagged behind the onset of run initiation, highlighting the significance of the naturally occurring preparatory period in which pupil dilation onset is synchronized with run initiation during voluntary behavior (latency previous to run onset: sCMEr: 2.16(1.71-2.45) s, vCMEr: 1.57(0.91-3.05) s, U=706.0, p=0.302; sPUPr: 0.66(0.08-1.53) s, vPUPr: -0.15(-0.56-0.51) s, U=757.0, p=0.015). The CME precedes run initiation in both conditions, but the pupil change onset could happen either before or after the run onset (Fig 6c). We observed no difference in magnitude between sCMEr and vCMEr; however, the magnitude of sCMEnr was significantly higher than that of vCMEnr (magnitude of sCMEr: 10.22(9.71-10.40)*10^6 a.u., vCMEr: 10.28(8.84-11.54)*10^6 a.u., U=613.0, p=0.814; sCMEnr: 5.69(3.58-6.91)*10^6 a.u., vCMEnr: 4.23(3.06-5.36)*10^6 a.u., U=29921.0, p=0.004). Similarly, the stimulation also induced higher amplitude of pupil change than the voluntary behavior both with and without subsequent run initiation (amplitude of sPUPr: 11.54(7.09-13.89) a.u., vPUPr: 7.71(5.93-9.77) a.u., U=741.0, p=0.024; sPUPnr: 8.18(6.99-9.81) a.u., vPUPnr: 4.58(3.72-5.72) a.u., U=12528.0, p=2.150*10-13) (Fig 6f). The duration of sCMEnr vs vCMEnr, and sPUPnr vs vPUPnr were significantly different (duration of sCMEnr: 2.48(0.94-3.67) s, vCMEnr: 0.62(0.27-1.09) s, U=36748.5, p=8.351*10-8; sPUPnr: 3.33(2.40-4.94) s, vPUPnr: 1.63(1.29-2.26) s, U=12456.5, p=4.505*10-13) (Fig 6g). However, the duration of these behaviors following successful run initiation did not differ, consistent with the observed similarity in the durations of srun and vrun (duration of sCMEr: 18.26(12.07-30.30) s, vCMEr: 14.34(8.64-27.94) s, U= 693.5, p=0.355; sPUPr: 10.07(6.87-18.90) s, vPUPr: 11.70(3.93-25.21) s, U=568.0, p=0.757) (Fig 6g). This provides evidence that stimulating MSDB VGluT2 neurons recruits a population of neurons that directly or indirectly connects whisking, running, and pupil changes—three key modalities of locomotor behavior. Finally, lagged cross-correlation analysis of voluntary behaviors revealed strong correlations between these modalities (Fig. 6h), with CME preceding running and pupil dilation occurring after both CME and running (Fig. 6i, j). Interestingly, while the correlation between running and pupil changes is a well-established phenomenon, the maximum cross-correlation latencies for run vs. pupil were longer compared to those for CME vs. pupil. This indicates a closer temporal association between CME and the other behavioral variables. This analysis also revealed an alternative sequence of the three behaviors when voluntarily elicited compared to their order during stimulation. During stimulation, the

sequence sCMEr-sPUPr-srun is observed, whereas in voluntary behavior, the order vCMEr-vrun-vPUPr occurs more frequently (Fig. 6i, j).

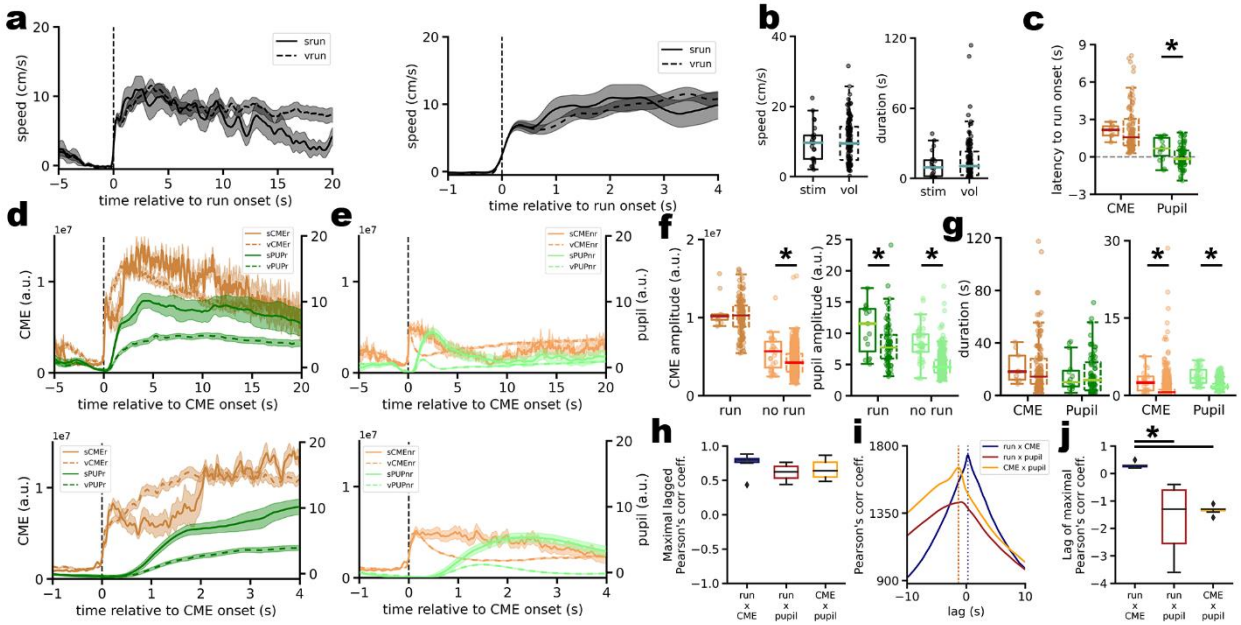

Figure 6, Comparison of voluntary and stimulated run, CME, and pupil signals. A, Average voluntary and stimulated run traces throughout all experiments. B, Comparison of speed and duration of voluntary and stimulated running bouts. C, Latency of CME and pupil compared to stimulated (solid) and voluntary (dashed) run onset. D, (top) Average traces of vCMEr, sCMEr, vPUPr, sPUPr around CME onset, (bottom) the same traces on different time-scale. E, (top) Average traces of vCMEnr, sCMEnr, vPUPnr, sPUPnr around CME onset, (bottom) the same traces on different time-scale. F, (left) CME amplitude of sCMEr, vCMEr, sCMEnr, and vCMEnr, (right) pupil amplitude of sPUPr, vPUPr, sPUPnr, and vPUPnr. For legend use D and E. G, Similar to F but with comparison of duration. H, Boxplot of maximum of lagged cross-correlation coefficients of the experiments. I, Average lagged cross-correlation of the 3 behaviors through all experiments. J, Box plot of the lag of the maximum cross-correlation coefficients of the 3 behaviors compared.

Upon stimulation, pupil dilation precedes locomotion, although the PUP signal further increases during running. This is reflected in the biphasic rise of pupil diameter observed in srun, in contrast to the monoexponential rise seen in vrun (Fig. 6d). These findings suggest that both whisking and locomotion contribute to pupil dilation, with a tighter synchronization during voluntary locomotion initiation. Stimulation likely alters the behavioral sequence by decoupling preparatory whisking from run initiation, thereby modifying the natural coordination of these behaviors

4.1.4 *Neurophysiological correlation of MSDB activity and locomotion-related behaviour*

To examine the neurophysiological correlates of the behavioral variables induced by MSDB VGluT2 stimulation, we conducted Neuropixels (NPX) recordings in VGluT2-ChR and control animals (Fig. 7).

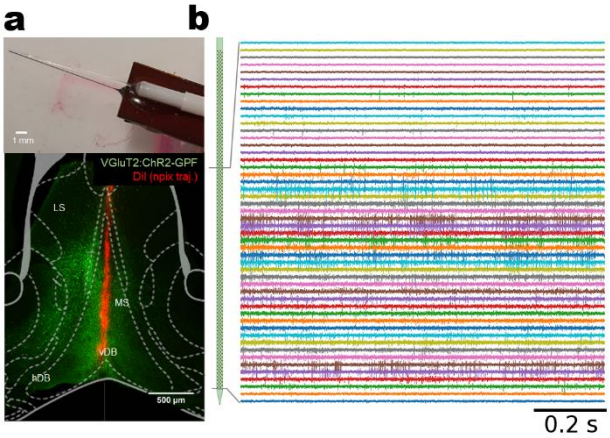

Figure 7, Design of NPX recordings. A, (top) Self-designed optrode of a tapered optic fiber attached to the NPX probe, (bottom) trajectory of NPX probe of a representative experiment. B, representative recording cut-out of the shank placed in MSDB. The size of the schematic probe is matched with the histology micrograph.

Initially, we recorded few or no directly optically driven cells along the probe during the first experiments. We hypothesized that this was due to the distance between the implanted optic fiber and the acutely inserted NPX probe, as blue light penetration in tissue is limited (Hu et al., 2020). Since the MSDB is a deep brain structure, even small deviations from optimal angles could lead to distant implantations, resulting in excitation of a neuronal population different from the one being recorded. To ensure activation of MSDB VGluT2 neurons along the entire MSDB axis, we employed tapered optical fibers (Pisanello et al., 2017), which distribute light not only at the apex but also laterally along the fiber length. By attaching the optical fiber to the NPX probe, we aimed to achieve light activation throughout the length of the NPX electrode shank (Fig. 7a). Before inserting our custom-made optrode, we coated the NPX shank with the membrane-binding dye DiI, enabling post-experiment reconstruction of the recording sites. This approach allowed us to record hundreds of units per animal across the depth of the MSDB (Fig. 7b) (138.9 ± 17.4 units per animal, n = 8). This setup facilitated the investigation of network recruitment in relation to changes in speed, CME, and pupil size, while also enabling comparison of network activity between stimulated and voluntary behaviors. Using this method, we recorded unit activity, sorted the spikes with Kilosort3 (Pachitariu et al., 2024), and curated the data using Phy software. We then identified MSDB cell types through optical tagging (putative VGluT2 neurons, referred to as optotagged or opto), literature references (e.g.,

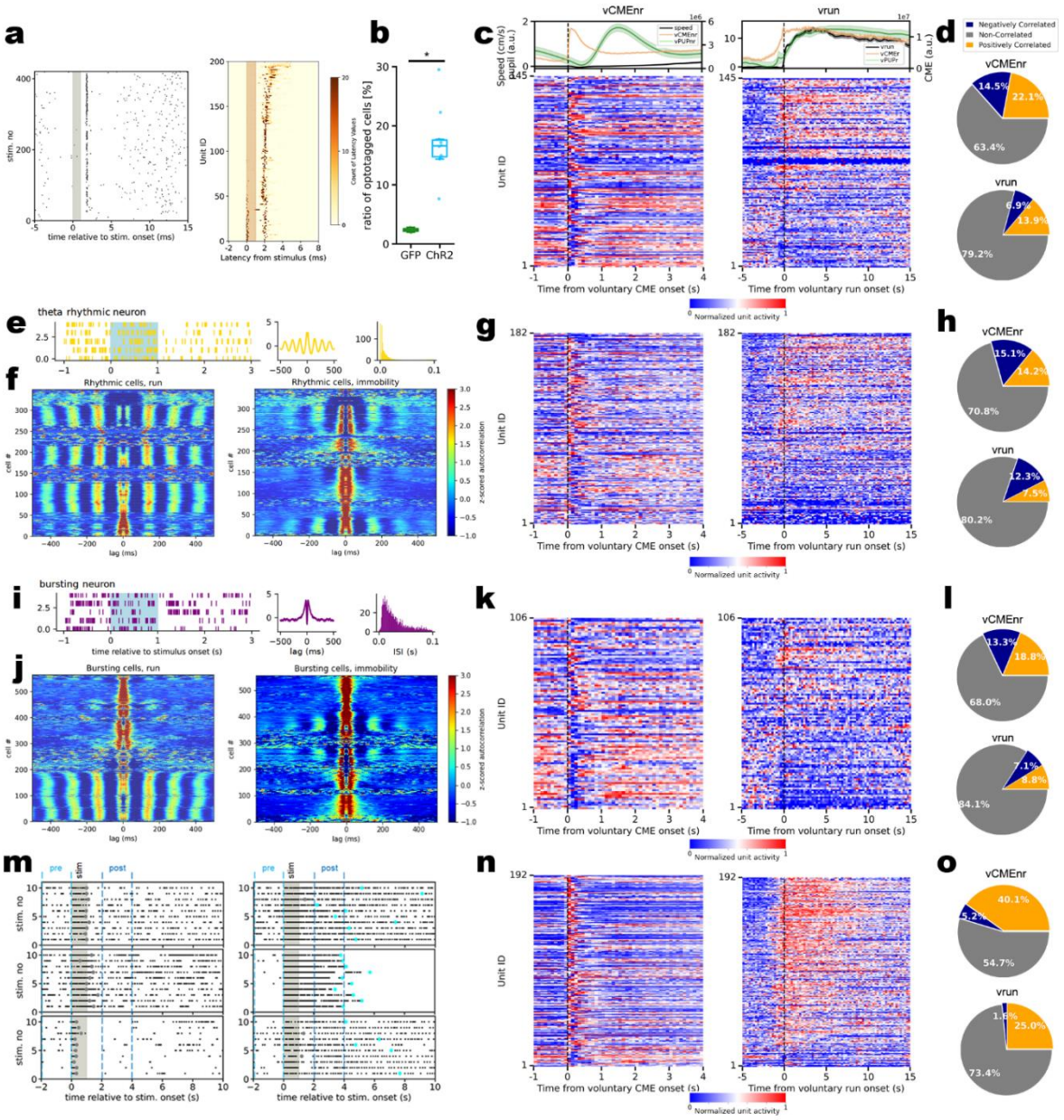

Figure 8, Cell type characterization. A, (left) Raster plot of a representative optotagged unit throughout a train of 1 ms stimulation, with (gray) stimulation, and (black squares) action potentials. (right) Color mapped representation of the response reliability and latency of all optotagged units. B, Ratio of optotagged units. C, (top, left) Average run, CME and pupil signals around vCMEnr onsets. (top, right) Average run, CME and pupil signals around vrun onsets, with (bottom) normalized activity of optotagged units. D, Pie chart of positively and negatively correlated units of optotagged group with (top) vCMEnr, and (bottom) vrun. E, (left) Raster plot of 5 stimulations, (middle) autocorrelogram, (right) ISI histogram of a representative theta rhythmic unit. F, Heatmap of z-scored autocorrelation of all theta rhythmic units during (left) running and (right) immobility. G, Similar as in C, but with theta rhythmic units. H, Similar as in D, but with Theta units. I-L, Similar as in E-H, but with Burst units. M, Raster plots of 3 representative (left) regular firing, and (right) PF units around 1 s long stimulations. Round markers show the length of elevated firing (gray) shorter or (cyan) longer than 2 s. N,O, Similar as in C-D, with PF units.

theta cells, bursting cells), and firing duration following 1-second stimulation (e.g., persistent firing cells) (Fig. 8-9).

4.1.5 *Cell type characterization*

Using 1 ms light stimulation, we first optotagged MSDB VGluT2 population. In detail, we analyzed the latency of unit responses and the probability of spike occurrence upon stimulation. Units that met our criteria—latency (<5 ms) and probability (>10%)—were classified as optotagged (see Methods; Fig. 8a). The proportion of optotagged cells across animals was approximately 17%, consistent with previously reported estimates of VGluT2 neuron prevalence in the MSDB (Colom et al., 2005) (ratio of optotagged cells in EYFP controls: 2.38(2.17-2.59) %, in ChR2 animals: 16.59(14.75-17.58) %, U=0.0, p=0.030) (Fig 8b). Optotagged VGluT2 neurons displayed a heterogeneous relationship with voluntary CME and running, comprising upregulated, downregulated and non-regulated cell populations (Fig 8c,d). Previous studies have reported the existence of theta rhythmic and theta bursting neurons in MSDB (Kocsis & Li, 2004; Simon et al., 2006). Using the classification approach as previously described (Kocsis et al., 2022), we identified both subpopulations of theta rhythmic and bursting neurons, which also showed heterogeneous relationship with movement-related variables (Fig 8e-l). Notably, we identified cells, that upon optogenetic activation of MSDB VGluT2 neurons showed maintained persistent firing (PF) for several seconds after the stimulus offset, similar to those reported by others in cortical and other subcortical regions (Yoshida et al., 2008; Kennedy et al., 2020). We applied strict criteria to classify a unit as PF, requiring it to exhibit elevated activity for more than one second following stimulation offset in at least 50% of the trials, regardless of whether the animal was already active (Fig. 8m-o). In this thesis, we further analyze network activity based on these categories, treating them as inclusive groups with overlapping classifications (e.g., some optotagged units may also fall into the PF, theta, and/or burst categories, among others) (Fig 9).

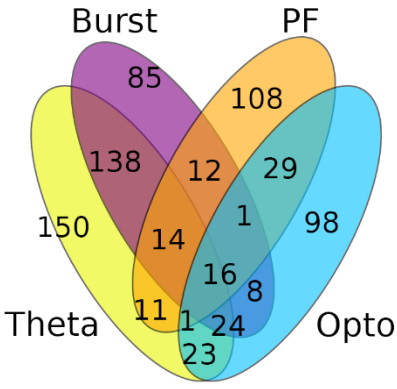

Figure 9, The occurrence of the identified cell types illustrated in a Venn diagram.

4.1.6 *Evaluation of PF phenotype*

During analysis of neural firing data, we identified a subpopulation of neurons (192/1269 units), that displayed PF following the offset of the stimulation, lasting for several seconds, that distinguished them from regularly firing neurons (Fig 10a,b). These neurons increased their firing rates both during successful and non-successful run initiation trials, ie. regardless whether the animal started running or not after the stimulation (firing rate before stimulation (-2-0 s): 20.50(8.50-45.00) 1/s, after stimulation (2-4 s): 45.50(21.00-72.50), U=54464.0, p=4.300*10^{-25}) (Fig 10c). Approximately 20% of our recorded cells elicited PF at least 50% of the stimulations (for detailed criteria see Methods) in ChR2 animals. Due to our strict criteria we did not identify any PF cells in control animals (ratio of PF cells in EYFP experiments: 0.00(0.00-0.00) %, in ChR2 animals: 19.17(8.10-25.02) %, U=0.0, p=0.049) (Fig 10d).

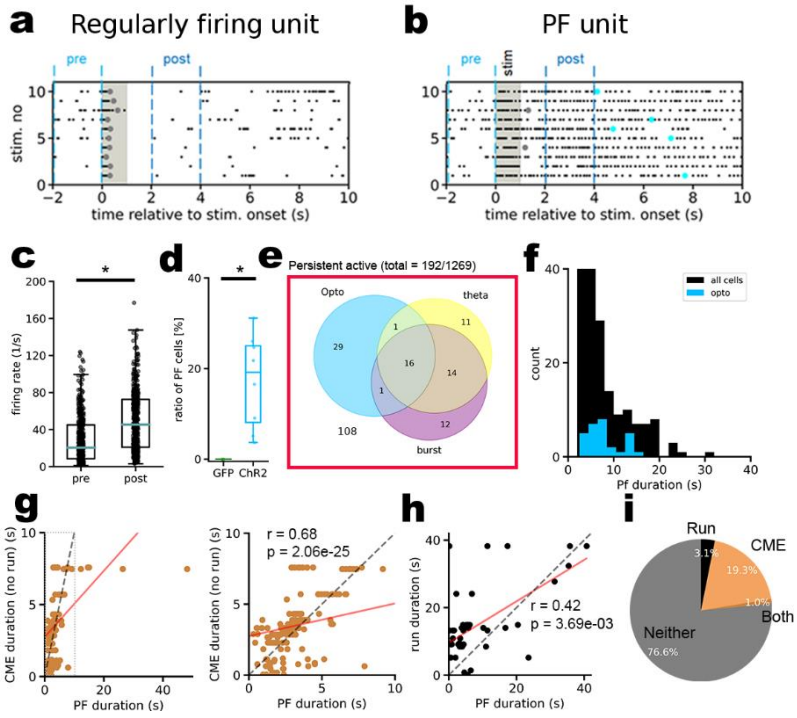

Figure 10, PF duration is correlated with CME and running. A, Raster plot of 10 stimulation sweeps of a representative unit showing regular firing. B, A representative units showing persistent firing (PF). C, Comparison of firing rate of PF units before (pre) and 1s after the (post) stimulation. D, Ratio of PF cells compared to GFP control. E, Venn-diagram of the cell type of the categorized PF units, and the number of non-categorized PF units outside the diagram. F, Distribution of all the PF durations compared to optotagged PF durations. G, (left) Correlation of PF length with CME duration, and (right) the same on different x-axis scale with (red) linear fit, and (dashed gray) a diagonal line. H, Correlation of PF length and run duration. I, Percentage of PF units showing correlation between PF length and CME and/or run duration.

The PF population represented a heterogeneous group of units, with approximately half of the population classified into at least one of the previously defined cell type categories (optotagged, theta rhythmic, bursting; Fig. 10e). Most PF durations were under 10 seconds, although sustained firing was observed for up to 30 seconds following stimulation (Fig. 10f). To investigate whether the distribution of PF durations correlated with running behavior (if present during a given trial) or CME duration, we analyzed the data further. We found that 23.4% of all

PF neurons were tuned to either CME or running (Fig. 10g, h). Specifically, 19.3% of PF units showed a significant correlation between firing duration and CME duration (Spearman's r = 0.683, $p = 2.056 \times 10^{-25}$), while 3.1% were correlated with run duration (Spearman's r = 0.420, $p = 3.685 \times 10^{-3}$).These results suggest that PF duration may contribute to the mechanisms underlying sustained whisking and/or running following a single pulse of stimulation.

Given the correlation between PF and CME and/or running, we sought to determine whether PF is generated intrinsically within the MSDB or driven by behavior or external inputs from other brain regions. To decouple the network from behavior, we used an acute MSDB slice preparation from VGluT2-Cre mice expressing Cre-dependent ChR2 (n = 11 animals) and included an opsin-free variant of the virus as a control (n = 3 animals). The slices were incubated in an interface chamber and placed onto a perforated 6 x 10 microelectrode array (MEA) chip (Fig. 11a). We applied a protocol consisting of 1-second continuous optical stimulation with 2-minute inter-stimulation intervals (IStI), repeated 10 times. Midway through the protocol, we introduced

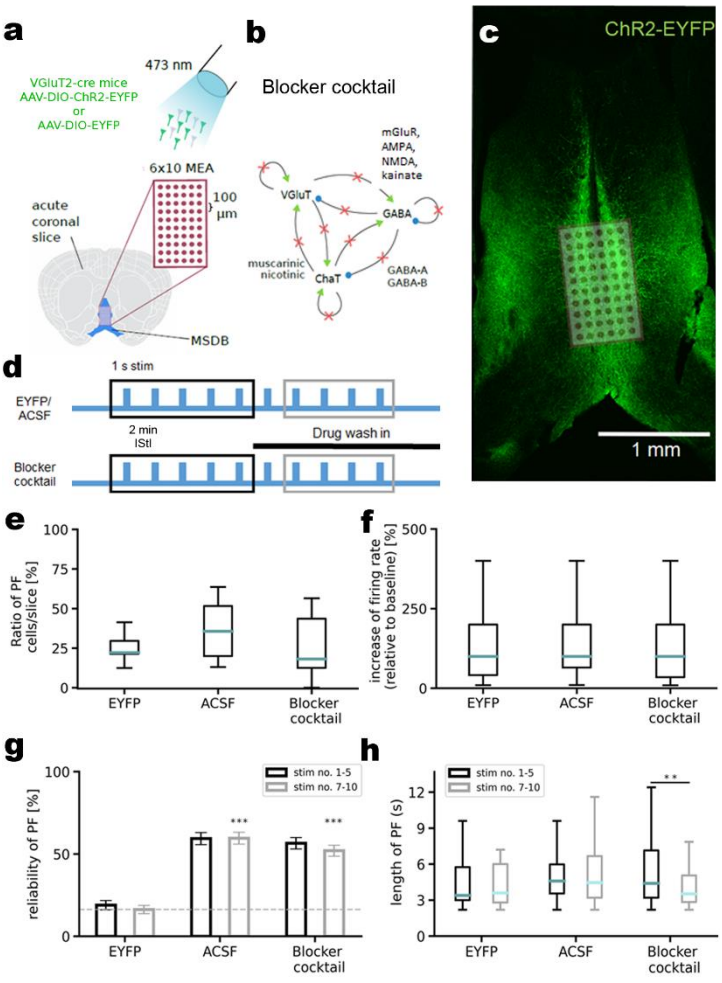

Figure 11, In vitro PF is modified, but not blocked by dissecting MSDB micronetwork. A, Experimental design of in vitro slice preparation with Cre-dependent ChR2 expression, 6 x 10 MEA grid. B, Schematic of the mechanistic effect of the applied blocker cocktail. C, Placement of ChR2 expressing MSDB slice preparation on the MEA grid. D, stimulation protocol. E, Ratio of detected PF units in recorded slices over different conditions. F, Photostimulation-induced firing rate change (2 s post-stimulation compared to 2 s pre-stimulation) of PF units were similar between conditions. G, Reliability of PF elicitation, successfully elicited PF trials over all trials in different conditions at the first half (black) and second half (gray) of the experiment. Dashed line shows the proportion of randomly detected persistent firing by the algorithm in opsin free EYFP slices that was significantly lower than ChR2 expressing slices recorded in ACSF or blocker cocktail. H, The length of persistent firing decreased with drug application (Blocker cocktail, gray), compared to drug-free baseline (Blocker cocktail, black).

a bath-applied blocker cocktail to examine network dynamics (Fig. 11b, d). In agreement with our in vivo findings, MSDB neurons exhibited increased firing rates during the 1-second stimulation, which remained elevated for several seconds after the stimulus offset. This persistent activity was observed even when the MSDB microcircuit was isolated from behavior, suggesting an intrinsic origin within the MSDB network. To further examine the role of collateral connections on PF, we tested the effect of a general synaptic blocker cocktail, that antagonized the main neurotransmitter receptors of the MSDB, namely mGluRs, iGluRs, GABAA, GABAB, and mAChR, and nAChR (Fig 11b). Our protocol made it possible to directly compare the same MSDB slice between ACSF and drug cocktail bath, as we compared persistent activity during the 1st-5th stimulation with the 7th-10th stimulation and excluded the 6th stimulation from the analysis to avoid data with incomplete effect of the antagonists. To control for slice degradation that could have potentially occurred during our 30 min protocol, we recorded slices without drug wash in (ACSF only). Persistent activity was observed in several units across all conditions at least once out of all trials (EYFP: 22.22(21.43-29.63) % PF units over all recorded units, n = 217 cells, 12 slices, 3 animals; ACSF: 35.71(20.02-51.67) %, n = 318 cells, 11 slices, 11 animals; Blocker cocktail: 18.19(12.60-43.64) %, n = 364 cells, 10 slices, 8 animals; EYFP vs ACSF: U = 32.00, p = 0.20; ACSF vs Blocker cocktail: U = 73.50, p = 0.20; EYFP vs Blocker cocktail: U = 53.00, p = 0.54; Mann-Whitney U-test, two-sided, median(Q1-Q3)) (Figure 11e). The increase of firing frequency upon photostimulation (2-4 s, post stim) compared to baseline (-2-0 s, pre stim) did not vary over conditions (EYFP: 100.00(41.18-200.00) %, n = 55 cells; ACSF: 100.00(64.88-200.00) %, n = 90 cells; Blocker cocktail: 100.00(34.58-200.00) %, n = 100 cells; EYFP vs ACSF: U = 1515.0, p = 0.42; ACSF vs Blocker cocktail: U = 6810.5, p = 0.15; EYFP vs Blocker cocktail: U = 2569.5, p = 0.84; Mann-Whitney U-test, two-sided, median(Q1-Q3)) (Figure 11f). Thus, we included all units and tested for PF at around every stimulation, and calculated reliability as the ratio of successful persistent activation over all the attempts to differentiate false positive detection from reliable PF units. We observed no change in the reliability of persistent activity elicitation between the first and second half of the protocol in any experimental condition (EYFP 1-5th: 18.93 ± 2.79 %, 7-10th: 16.27 ± 2.51 %, n = 217 cells, 12 slices, 3 animals, U = 4950.5, p = 0.99; ACSF 1-5.: 59.37 ± 3.70 %, 7-10: 59.61 ± 3.58 %, n = 318 cells, 11 slices, 11 animals, U = 4950.5, p = 0.83; Blocker cocktail 1-5.: 56.51 ± 3.45 %, 7-10: 52.00 ± 3.35 %, n = 364 cells, 10 slices, 8 animals, U = 4950.5, p = 0.37; Mann-Whitney U-test, two-sided, mean ± sem), suggesting that blocker

cocktail did not alter the probability of PF elicitation. Reliability in the ChR2 experiments was significantly above chance level, as evidenced by the clear difference in reliability between the ChR2 experiments and the opsin-free control experiments. (EYFP 7-10.: 16.27 ± 2.51 %, ACSF 7-10: 59.61 ± 3.58 %, U = 528.5, p = 5.35e-11; Blocker cocktail 7-10: 52.00 ± 3.35 %, U = 728.0, p = 1.73e-09) (Figure 11g). The length of PF was maintained throughout the protocol (ACSF 1-5.: 4.60(3.55-5.98) s, 7-10: 4.47(3.20-6.67) s, U= 2783.0, p = 0.70), and was sensitive to blocker cocktail, which considerably shortened PF duration after photoexcitation (Blocker cocktail 1-5.: 4.40(3.20-7.14) s; 7-10: 3.52(2.84-5.05) s, U= 4453.5, p = 8.74e-03) (Figure 11h).

Given that the observed phenomenon of PF appears to be an intrinsic property of MSDB neurons, we investigated its dependence on Ca^{2+} by testing various external Ca^{2+} concentrations ($[Ca^{2+}]_o$). In our experiments we used nearly 0 mM $[Ca^{2+}]_o$ (lowCa), close to physiological (midCa; 1.3 mM $[Ca^{2+}]_o$), and our standard ACSF (highCa; 2.6 mM $[Ca^{2+}]_o$), and changed the solution during data acquisition after the 5th optic pulse, similarly to our blocker cocktail experiments (Fig 12a). We observed PF in all three conditions (Fig 12b,c), and the lower $[Ca^{2+}]_o$ elongated the duration according to the maximum absolute difference between the

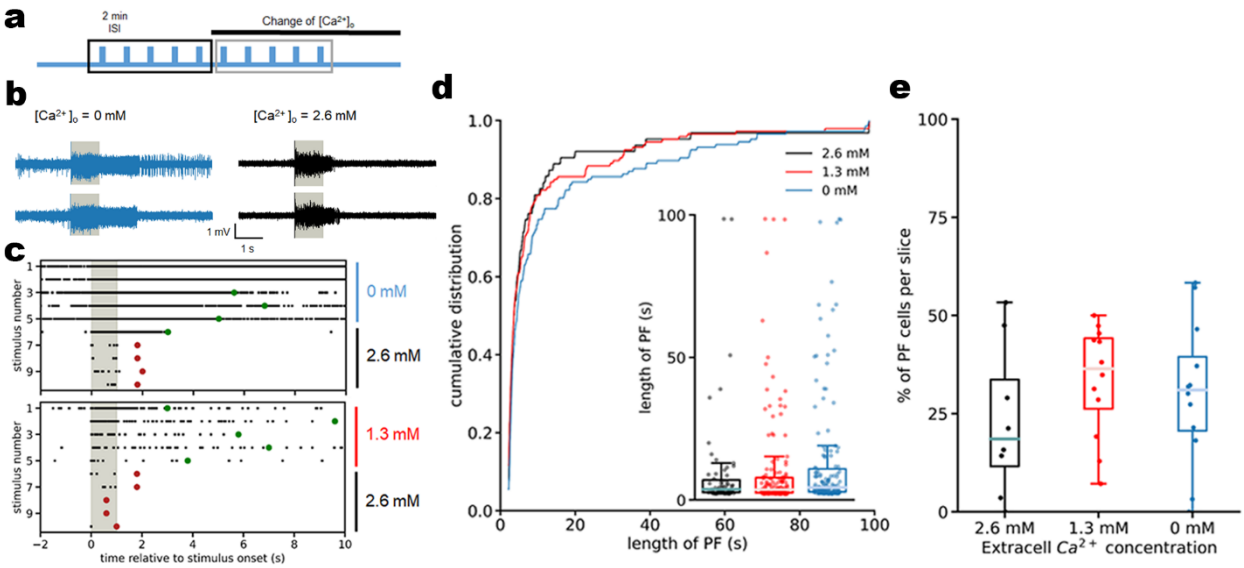

Figure 12, In vitro PF is sensitive to extracellular Ca^{2+} concentration. A, Experimental protocol. B, Raw multi-unit traces of a representative MEA electrode site at peri-stimulation time (stimulation: gray bar) in (left) lowCa conditions (blue), and (right) the same electrode after the change of $[Ca^{2+}]_o$ to highCa (black). C, (top) Raster plot of a representative sorted single unit plotted peri-stimulation with 10 repetitions. The detected length of PF is marked with circles (dark green: >2 s; dark red: <2 s). Bath ACSF $[Ca^{2+}]_o$ is marked on the right side. (bottom) Another experiment similar to (top), with $[Ca^{2+}]_o$ change from midCa (red) to highCa. D, Cumulative distribution of PF length, with (inset) boxplot of the individual length values. E, Boxplot of the proportion of PF units over all recorded units per slice in different $[Ca^{2+}]_o$ conditions.

cumulative distribution functions of PF lengths (Figure 12d) (lowCa vs midCa: $p = 8.42*10^{-15}$, statistics = 0.26; midCa vs highCa: $p = 1.67*10^{-30}$, statistic = 0.37; lowCa vs highCa: $p = 1.57*10^{-28}$, statistic = 0.36; Two-sample Kolmogorov–Smirnov test) and slightly but not significantly increased the abundance of the PF cells in the slices (lowCa: 31.02(20.62-39.49) %; midCa: 36.49(26.22-44.18) %; highCa: 18.53(11.61-33.65) % of cells/slice; lowCa vs midCa: U = 62.00, p = 0.58; midCa vs highCa: U = 34.00, p = 0.31; lowCa vs highCa: U = 61.50, p = 0.32; Mann-Whitney U-test, two-sided, median(Q1-Q3)) (Figure 12e). In summary, we successfully elicited PF in slice preparations decoupled from behavior, where the application of synaptic blockers in the MSDB did not eliminate persistent activity but instead modulated it. These findings suggest that the intrinsic biophysical properties of MSDB neurons underpin the emergence of persistent activity, which is further shaped by network dynamics.

4.1.7 *Distinct recruitment of MSDB cell types during vrun vs vCMEnr*

Next, we investigated the MSDB network activity during behavior. In each experiment, we identified subsets of neurons that were positively tuned during both srun and vrun compared to the no-run baseline (Fig 13a). We then identified unitary CME and run events, both voluntary and stimulated, and averaged and normalized the activity of units to compare with the averaged behavioral data across all animals (Fig. 13b-e). To quantify changes, we calculated activity change scores for all units based on values derived from normalized activity histograms. In total, we saw positively and negatively vCMEnr and vrun correlated units in all cell types, with PF cells showing the highest proportion of positive, and lowest proportion of negative modulation (Fig 13b). Interestingly, if we compare the heatmaps of all unit activity during voluntary and stimulated behaviors, we observed that prolonged activation of the MSDB during sCMEnr compared to vCMEnr was represented in longer duration CME and pupil dilation - related signals (Fig 13d). The heatmap approach, based on normalized values, does not provide precise information about changes in firing rates between voluntary and stimulated behaviors. Therefore, we conducted further analysis to investigate network modulation under these conditions (Fig 13f,g). Overall, we observed a correlation between the firing rate changes of vCMEnr and sCMEnr ($R^2 = 0.38$, m = 0.61, b = 0.17), but this correlation was notably weaker compared to that of vrun and srun ($R^2 = 0.60$, m = 0.73, b = 0.80).

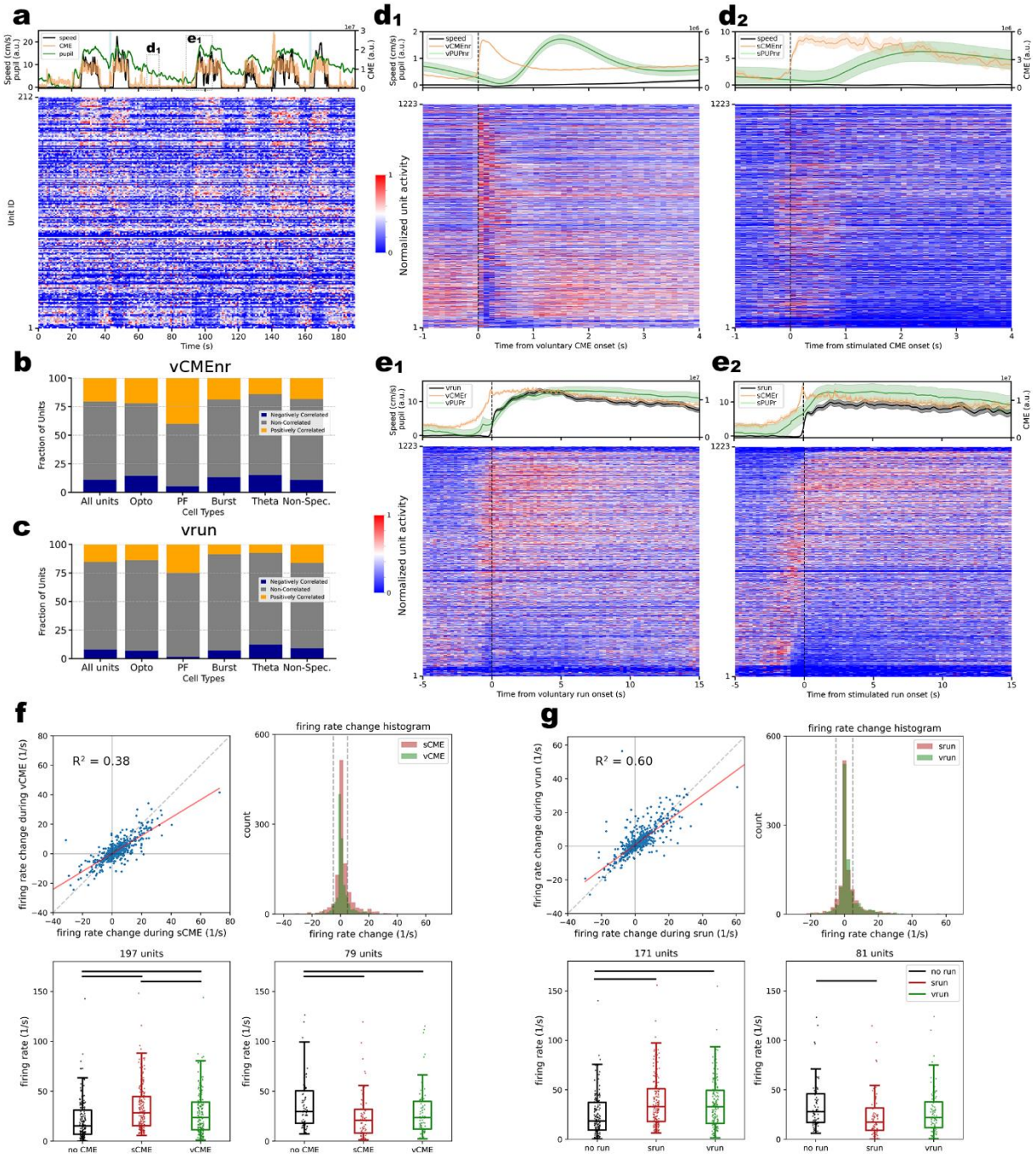

Figure 13, Recruitment of MSDB neuronal subgroups in voluntary and stimulated behaviors. A, Snippet of a representative experiment with (top) run, CME and pupil plotted and (bottom) subsequent normalized neural activity. The light blue lines on the top represent 1s stimulation. B, Cumulative bar plot of the ratio of MSDB cell types positively tuned, negatively tuned, or non-modulated during vCMEnr bouts. C, Similar as in B, but during vrun. D1, (top) Average run, CME and pupil signals around vCMEnr onsets, and (bottom) the subsequent averaged, normalized neural activity of all units. D2, Similar to D1 around sCMEnr. E, Similar to D, but with E1 vrun, E2 srun. F, (top, left) Firing rate change of recorded units during stimulated CME vs voluntary CME, (top, right) distribution of firing rate changes of units voluntary compared to stimulated CMEs, with (gray dashed lines) indication of 5 Hz firing rate threshold. (bottom, left) Boxplot of firing rate of positively correlated units, and (bottom, right) boxplot of firing rate of negatively correlated units. G, Similar to F, but during srun and vrun.

This indicates that network modulation varied significantly during CME but remained consistent during locomotion maintenance. (Fig 13f,g; top left). We compared the distribution of the firing rate change, and identified upregulated (CME: n = 197 units, run: n = 171) and downregulated (CME: n = 79 units, run: n = 81) units based on at least 5 Hz firing rate change of either positive or negative direction, respectively (Fig 13f,g; top right). The firing rate of both positively and negatively correlated units were different between CMEnr and no CME condition (positively correlated unit firing rate during no CME: 15.31 (6.86 - 31.27) Hz, sCMEnr: 28.43 (15.61 - 44.68) Hz, vCMEnr: 23.68 (11.46 - 39.08) Hz, no CME vs. vCMEnr U = 14800.0, p = $4.632*10^{-5}$, no CME vs. sCMEnr U = 11838.0, p = $2.170*10^{-11}$; negatively correlated unit firing rate during no CME: 29.78 (17.78 - 50.45) Hz, sCMEnr: 20.85 (8.07 - 31.80) Hz, vCMEnr 23.55 (12.11 - 39.86) Hz, no CME vs. vCMEnr U = 3782.0, p = 0.022, no CME vs. sCMEnr U = 4154.0, p = $3.278*10^{-4}$, Fig 13f; bottom). Consistent with our observations from the heatmaps (Fig. 13d) and the weaker correlation (Fig. 13f, top left), we measured a greater firing rate change during sCMEnr compared to vCMEnr. This difference reflects the variation in firing rates of positively modulated units between the sCMEnr and vCMEnr conditions (positively modulated units vCMEnr vs. sCMEnr U=22347.0, p = 0.002), although the negatively modulated units firing rate did not differ in the two conditions (negatively modulated units vCMEnr vs. sCMEnr U=2643.0, p = 0.097).

Similarly to CME, we observed that the firing rates of both positively and negatively correlated units differed between running and no-running conditions (positively correlated unit firing rate during no run: 18.50 (9.42 - 37.17) Hz, srun: 32.89 (18.08 - 50.98) Hz, vrun: 32.82 (15.97 - 49.46) Hz, no run vs. vrun U = 10456.0, p = $5.246*10^{-6}$, no run vs. srun U = 9523.0, p = $2.472*10^{-8}$; negatively correlated unit firing rate during no run: no run: 27.97 (16.99 - 46.09) Hz, srun: 17.22 (9.05 - 31.54) Hz, vrun: 21.98 (11.73 - 37.84) Hz, no run vs. vrun U = 3836.0, p = 0.063, no run vs. srun U = 4382.0, p = $2.260*10^{-4}$). Notably, the firing rate of both positively and negatively modulated units between srun and vrun condition did not differ (positively modulated units vrun vs. srun U = 15399.0, p = 0.395, negatively modulated units vrun vs. srun U=2756.0, p = 0.079), i.e. this population comparably increased their firing rate in vrun vs srun (Fig. 4F, lower panels). This suggests that during stimulation, the network may be overstimulated when eliciting only CME. In contrast, running appears to involve similar modulation whether initiated voluntarily

or through stimulation, likely because, once locomotion begins, the MSDB network is primarily engaged by the act of running itself.

We then compared the modulation of individual cell types during voluntary behaviors, vCMEnr and vrun. Across conditions, all cell types exhibited similar activity changes during vCMEnr and vrun, consistent with the overall population-level differences described earlier (Fig. 14a). However, when comparing across cell types, the burst, opto, and all units groups demonstrated highly similar modulation patterns during both behaviors (Fig. 14b, c). Theta cells showed the strongest negative modulation in both conditions, with significant differences compared to the aforementioned groups during vrun but not vCMEnr. In contrast, PF cells were predominantly excited during these behaviors, displaying distinct distributions compared to all other cell categories.

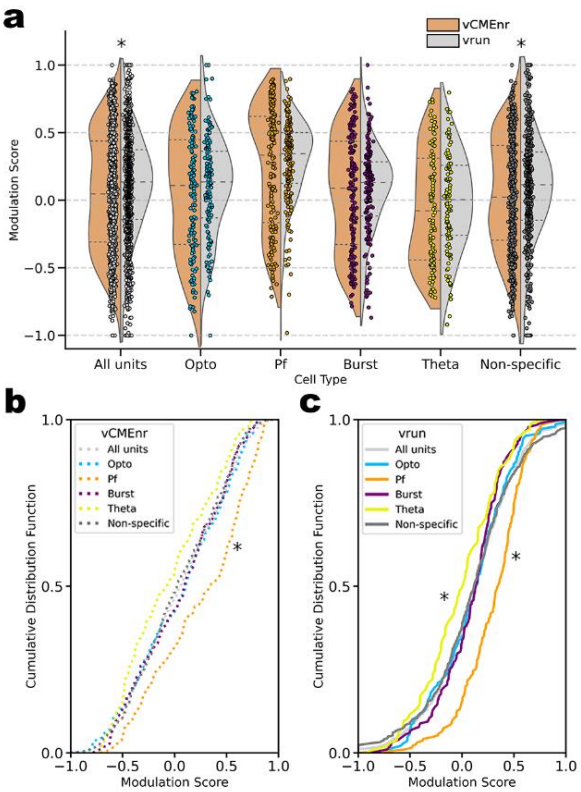

Figure 14, PF cells are the most involved cell types during voluntary CME and running. A, Firing rate change representing modulation score distribution plots of all cell types during vCMEnr and vrun with (dashed lines within the distribution plots) median (sparser dashed line in the middle) and interquartile range(denser dashed line on the sides). B, Cumulative distribution of the modulation scores of identified cell types during vCMEnr. C, Similar as in B, gut with during vrun.

4.1.8 *Tight coupling between CME and MSDB activity*

To further explain why the stimulation has a different effect on CME and run behaviors, we investigated the timing precision of neuronal activity using lagged cross-correlation analysis. Briefly, we downsampled the behavior signals to 250 ms data points and correlated those to the normalized unit activity histogram with same binning. Subsequently, all cross correlation values during shifting one signal over the unit activity were collected and analyzed (Fig 15). Visual representation of these cross-correlation values revealed the a small subset of MSDB units were tightly correlated with vCMEnr bouts, which peaked around -250 ms time lag (Fig 15a,b). This observation is in line with the previously mentioned stimulation latency of sCMEnr (Fig 5d). The proportions of units across individual cell types were similar but consistently low across groups.

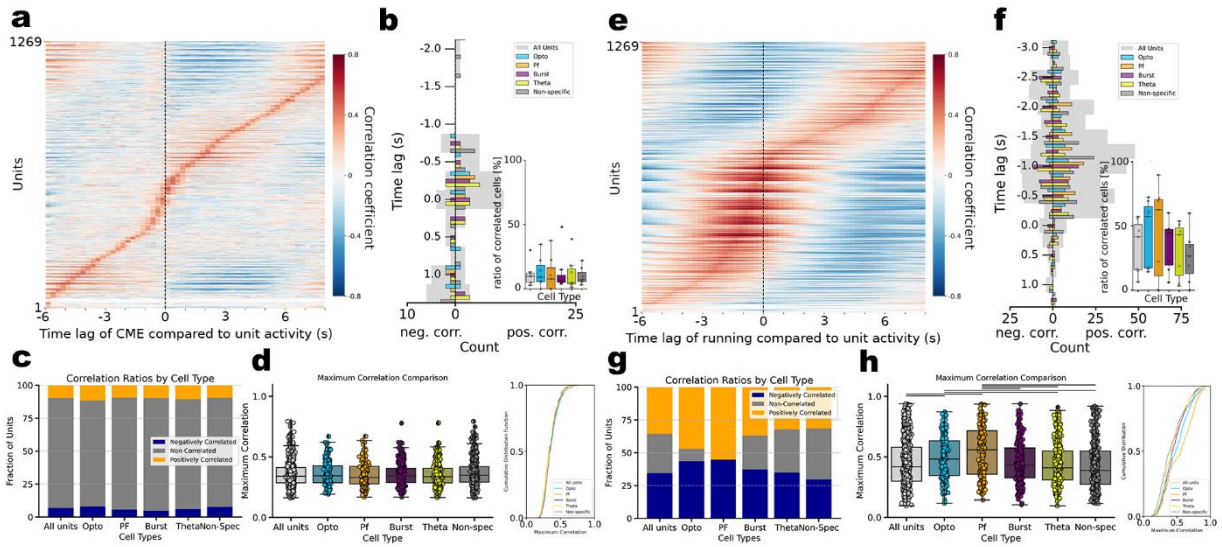

Figure 15, CME is lagged behind MSDB unit activity on a subsecond scale. A, Lagged cross-correlation heatmap of activity of all units with vCMEnr signal. B, Distribution of the lag of maximum positive and negative correlation of all cell types, (inset) ratio of positively correlated cells over the total number of units of the given cell type. C, Cumulative barplot of the fractions of CME lag-correlated units of each cell type. D, (left) Maximum correlation coefficient values of each cell type, and (right) their cumulative distribution. E-H, Similar as in A-D, but lagged correlation is analyzed between MSDB activity and running.

Notably, the activity of all cell types preceded vCMEnr by approximately 250 ms (Fig. 15b, c).The overall maximum correlation coefficients, similarly to the time analysis, showed no difference in between the groups (median(IQR) correlation coefficient values for all units: 0.34(0.29-0.41), Opto: 0.34(0.29-0.43), Pf: 0.33(0.28-0.42), Burst: 0.34(0.29-0.41), Theta: 0.34(0.29-0.41), Non-specific: 0.35(0.29-0.42), H = 6.515, p = 0.481, Kruskal-Wallis ranked test) (Fig 15d). On the contrary, majority of the units were recruited during running, and showed correlated activity with this behavior (Fig 15e-g). MSDB activity seems to precede vrun with about 1-1.5 s, which value is also representative (Fig 15f), but not identical to those we measured for srun run initiation latencies (Fig 5d). We also noticed, that almost the entire MSDB network is correlated with running signal, either positively, or negatively, out of which optotagged, confirming the findings from Fuhrmann et al. (2015), and PF cells activity showed the highest degree of correlation with vrun (median(IQR) correlation coefficient values for all units: 0.42(0.30-0.58), Opto: 0.48(0.35-0.63), Pf: 0.56(0.36-0.72), Burst: 0.43(0.33-0.57), Theta: 0.41(0.31-0.55), Non-specific: 0.39(0.27-0.55), H = 65.610, p = $1.134*10^{-11}$, Kruskal-Wallis ranked test) (Fig 15h). This suggests, that CME is not only elicited by activation of photosensitive, putatively VGluT2+ cells, but the activity of these, and other cells in the MSDB predicts vCMEnr. This method lacks the sensitivity

to detect distinct activation patterns of MSDB units during vCMEnr, which may account for the low number of cross-correlated units observed in this study.

To explore the diverse phenotypes of MSDB responses around vCMEnr, we examined the population and identified neurons exhibiting either positive or negative tuning during CME (Fig 16). Out of these, part of the population sustained their activity matching the length of averaged vCMEnr, which we named positive or negative sustained modulated units (303/1243 and 234/1243 units, respectively). Among these, a smaller subset of neurons exhibited positive or negative peaks (168/1243 and 114/1243 units, respectively). Interestingly, the latter group typically displayed theta-bursting activity that abruptly ceased in parallel with CME occurrence (Fig. 16d). Collectively, these findings highlight the heterogeneous recruitment of MSDB cell types closely associated with CME.

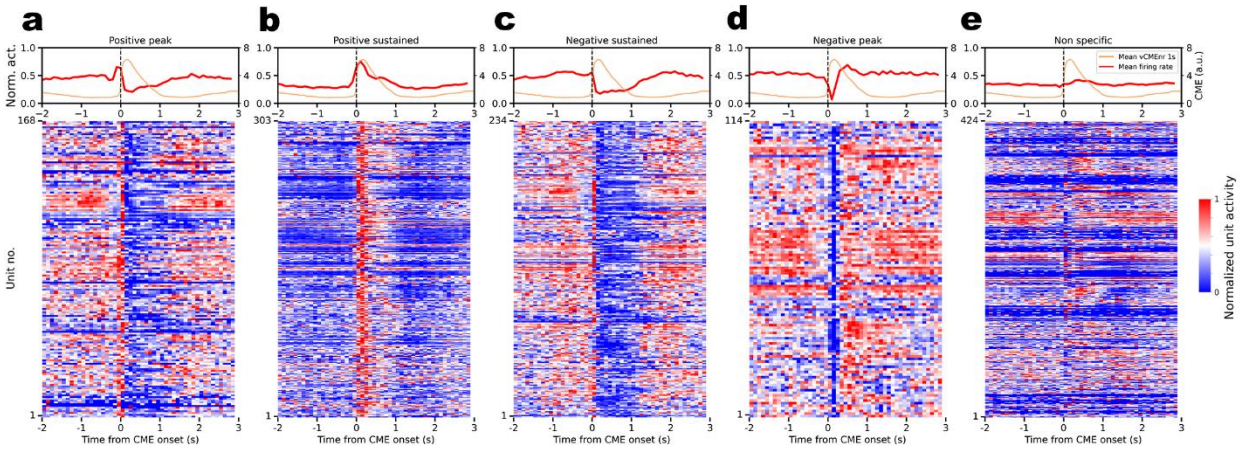

Figure 16, CME modulated MSDB units respond differently to vCMEnr. A-E, (top) Averaged (red) normalized unit activity, and (orange) 0.5-1s long vCMEnr through all experiments. (bottom) Heatmap of individual units in the presented activity phenotype groups.

4.1.9 *Pupil microdilation length is linked with preceding CME*

Following initial observations suggesting a potential relationship between CME and pupil signals (Fig. 6c-j), we further examined the strength of their coupling. To achieve this, we first binned vCMEnr bouts by their duration and collected the signals of all three behaviors accordingly, and calculated the average of each signals in each duration bin. Notably, the shortest vCMEnr was followed by the shortest and smallest amplitude pupil change, which gradually increased with the increased lengths vCMEnr duration bins (Fig 17a). Measuring the duration of all vCMEnr and subsequent vPUPnr signals revealed strong correlation (Person's r=0.35,

p=2.062*10^{-55}) (Fig 17b). Upon binning cell activity into similar bins as the 3 behaviors showed that MSDB population is indeed involved in CME activity. Average normalized activity histograms of positive sustained units, shown before (Fig 16b), was remarkably mirrored by vCMEnr (Fig 17c).

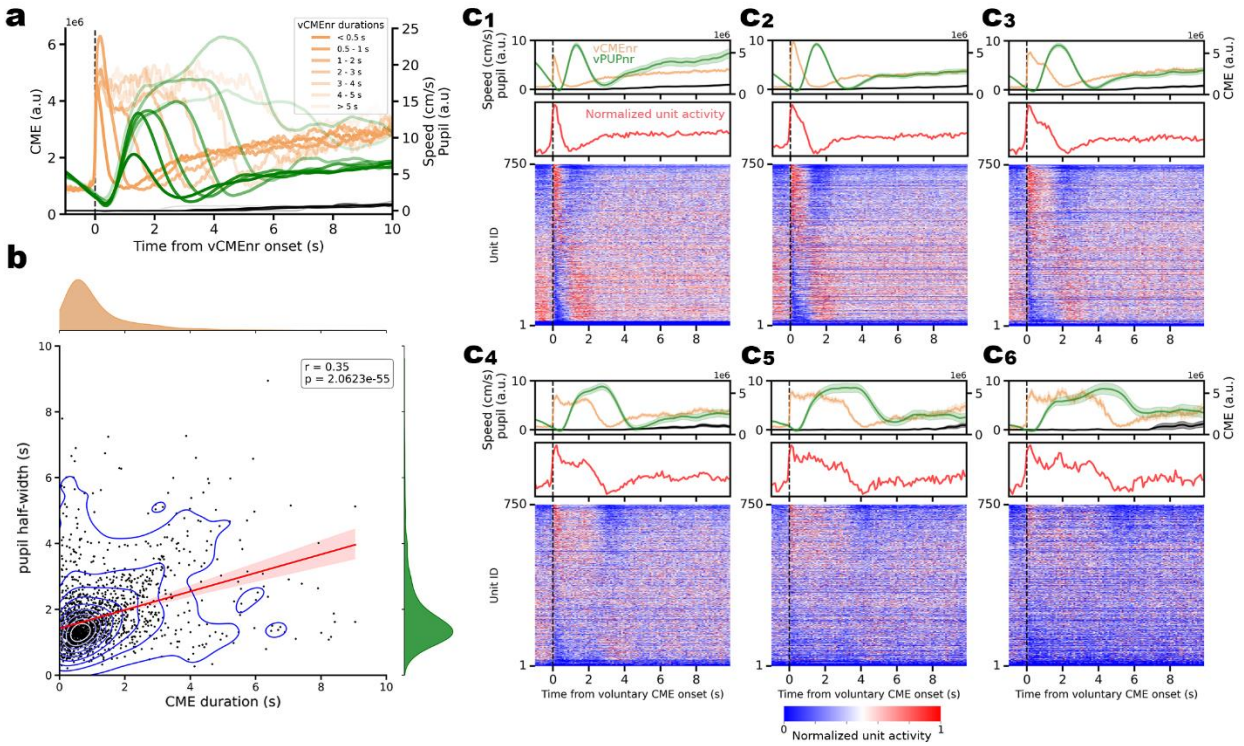

Figure 17, Length of CME, pupil sustained MSDB unit activity is tightly correlated. A, Binned averaged vCMEnr and corresponding vPUPnr signal showing linked modulation. B, Spearman correlation of CME duration and the half-width of the subsequent pupil dilations, with (red) regression line, and (blue) kernel density estimate plot lines. (on the sides) Distribution of the CME (orange), and pupil (green) durations. C, (top rows) Average run, CME and pupil signals around binned vCMEnr onsets, with (middle rows) averaged acitivity of the top third (250 units) of the (bottom rows) average normalized activity heatmaps. C1-C6, vCMEnr duration bins of 0-0.5 s, 0.5-1 s, 1-2 s, 2-3 s, 3-4 s, 4-5 s bins respectively.

4.1.10 *Lagged coupling between MSDB network modulation and pupil.*

We next analysed the network during pupil dilation. In general, we reliably elicited pupil dilation by our stimulation compared to opsin-free control experiments (Fig 18a). The overall correlation of cell types firing to pupil size was relatively uniform (Fig 17c). However, when we shifted the unit activity to the pupil signal using the lag-correlation (see Methods), we observed a high fraction of correlated units (Fig 18b), as well as higher correlation strength for optotagged and PF cell firing compared to other cell types, with the burst cells being the most independent (median(IQR) correlation coefficient values for all units: 0.35(0.29-0.43), Opto: 0.38(0.32-0.47),

Pf: 0.42(0.34-0.51), Burst: 0.33(0.28-0.40), Theta: 0.33(0.28-0.40), Non-specific: 0.34(0.29-0.42), H = 132.042, p = $2.352*10^{-25}$, Kruskal-Wallis ranked test) (Fig 18c). As the 3 behaviors are correlated (Fig 6h), we next compared two types of pupil dilation, namely vPUPr vs vPUPnr (Fig 18d). We observed that the peak correlation of the units predominantly occurred 1–2 seconds prior to pupil dilation (Fig. 18e, f), aligning with the previously noted time lag between CME and pupil signals (Fig. 6j). Majority of the optotagged and PF units were correlated in this 1-2 s time-scale (Fig 18f). A fraction of pupil correlated cells, similar to the example (Fig 18d), showed no or little activity during quiescence, but fired sparse (1AP/cycle) theta rhythmic, highly correlated with the

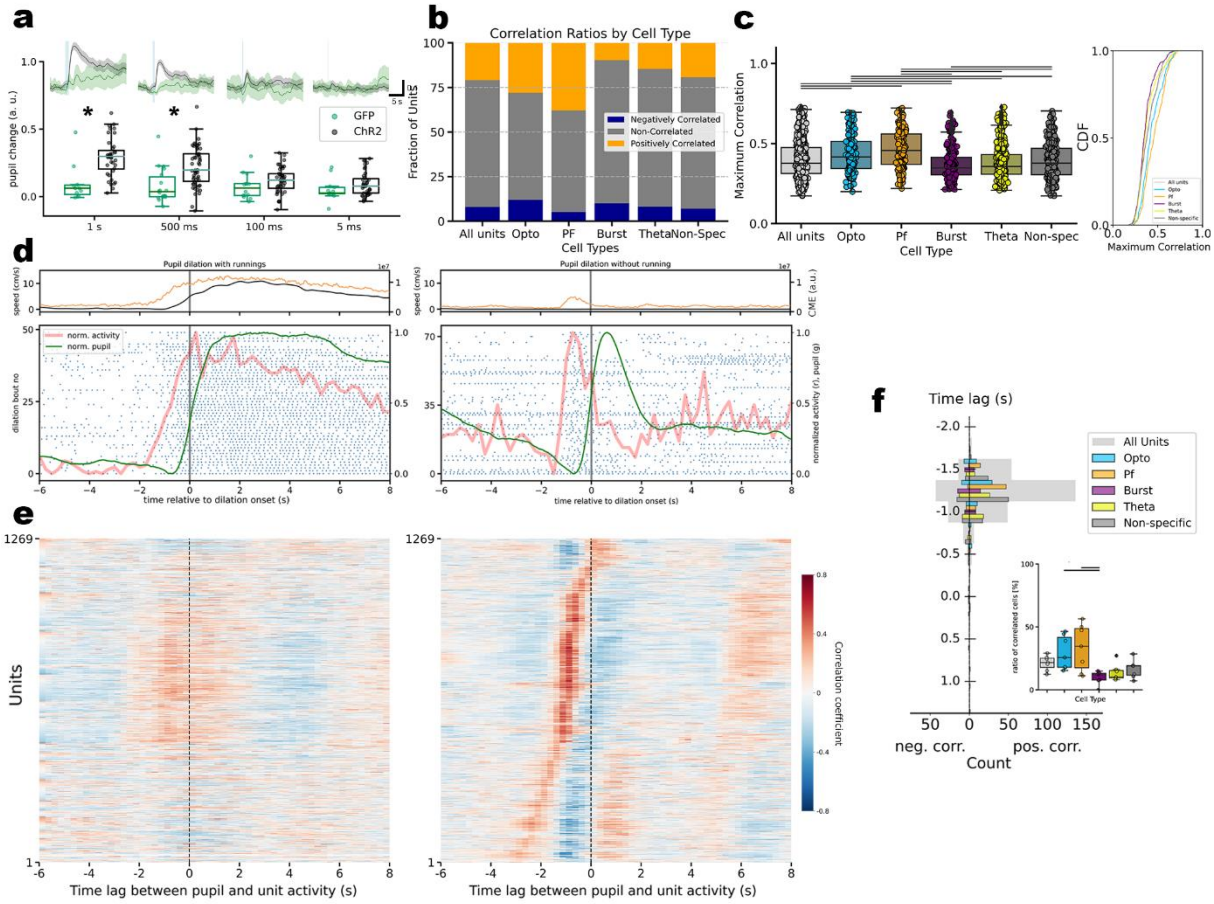

Figure 18, Pupil dilation signal tightly follows MSDB activity. A, Stimulation of MSDB VGluT2 cells induce pupil dilation even with shorter stimulation durations. (top) Average pupil traces after various lengths of stimulation of ChR2 animals compared to EYFP control, (bottom) box plot of pupil change. B, Cumulative barplot of the fractions of vPUPnr lag-correlated units of each cell type. C, (left) Maximum correlation coefficient values of each cell type, and (right) their cumulative distribution. D, Raster plots, averaged run, CME and pupil signals, and average activity histogram of a representative unit centered around (left) vPUPr onset, and (right) vPUPnr onset. E, Lagged cross-correlation heatmap of all units during to (left) vPUPr onset and to (right) vPUPnr onset. F, Distribution of the lag of maximum positive and negative correlation of all cell types, (inset) ratio of positively correlated cells over the total number of units of the given cell type.

oncoming pupil signal. These units may represent the cholinergic cells. However, we cannot be certain about it, as we could not isolate the cholinergic population in our experiment. The current data suggests that pupil dilation is a secondary behavior that follows CME, which could involve the different degrees of complexity of the downstream pathways.

4.1.11 *GLM confirms cell-type involvement in specific behaviors*

Finally, we trained a GLM to infer cellular activity based on behavioral data and compared the results with a conservative analysis method for conjunctive coding. This approach involved identifying the percentage of run-correlated cells that were also correlated with CME and pupil signals, along with their permutations. In the GLM, we incorporated run initiation episodes and subsampled the three behaviors to match the number of bins corresponding to the binned firing rates of the neurons. The GLM was then trained to predict cellular firing based on the training dataset (Fig 19a). The analysis suggested that CME alone had the strongest ability to infer cellular firing when considering individual behavioral effects. However, when all three behaviors were analyzed together, they produced the highest proportion of correctly encoded cells, surpassing the predictive capability of CME alone (Fig. 19b). The conservative conjunctive coding method further showed that most run-modulated cells were also involved in CME coding, although the reverse relationship was slightly less pronounced. A large percent of the cells engaged during running showed conjunctive coding with other behaviors. A majority of these units co-correlated with CME, and only a smaller fraction co-correlated with pupil (fraction of run and CME positively correlated units among run positively correlated units: 0.48 ± 0.08, run and pupil: 0.16 ± 0.03, paired t-test t=3.032, and p = 0.019; fraction of run and CME negatively correlated units among run negatively correlated units: 0.77 ± 0.07, run and pupil: 0.21 ± 0.07, paired t-test t=3.990, and p = 0.005) (Fig 19c; left). Vice versa, a proportion of the units being positively modulated during CME showed conjunctive coding with other behavioral variables, with majority of these units co-correlated with run, and only a fraction of them co-correlated with pupil (CME and run: 0.45 ± 0.08, CME and pupil: 0.08 ± 0.05, t=3.248, and p = 0.014) (Fig 19c; middle). Furthermore, the

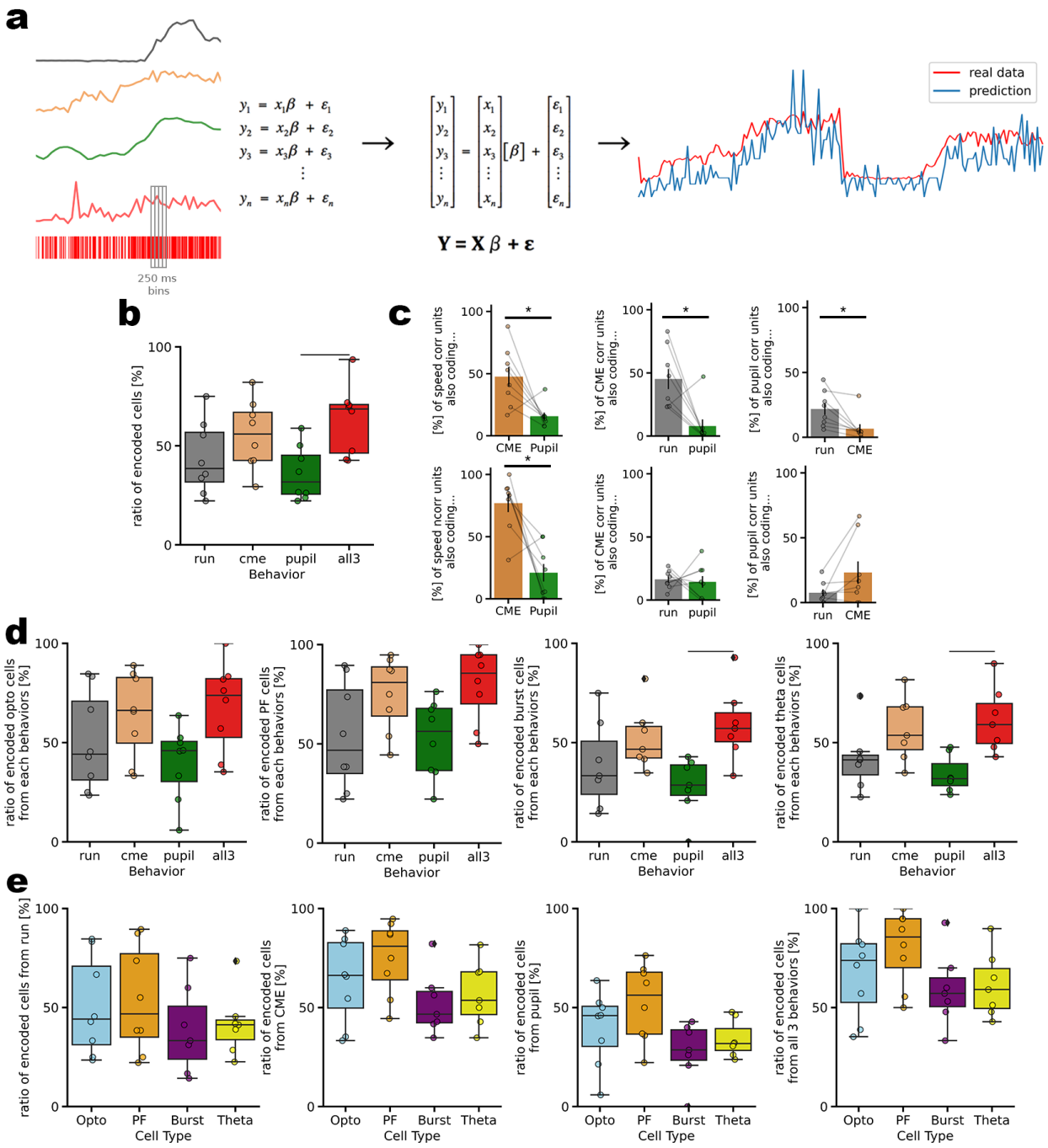

Figure 19, GLM predicts the firing of units from CME with the highest ratio. A, (left) Input of the GLM (black, run; orange, CME; green, pupil; red, unit firing), (middle) schematic of GLM, (right) prediction of the firing of a representative neuron using all the 3 behavioral variables. B, Ratio of significantly encoded cells by each behavioral signal and all 3 combined. C, (top) Conjunctive coding of positively (left) speed, (middle) CME, (right) pupil modulated units with the other 2 behavior, (bottom) similarly with negatively modulated units. 100 % is always the total number of modulated units by the reference behavior. D, Similar to B, but for individual cell types (from left to right: optotagged units, PF units, Burst units, Theta units). E, Fraction of encoded cells of a given cell type by the behaviors (from left to right: encoding from run signal, CME signal, pupil signal, or all the 3 signals combined).

minority of positively pupil tuned cells being co-tuned with running (pupil and run: 0.22 ± 0.05, pupil and CME: 0.07 ± 0.03, paired t-test t=3.049, and p = 0.019), while tendentiously higher proportion of negatively pupil modulated units were negatively co-tuned with CME (pupil and run: 0.08 ± 0.03, pupil and CME: 0.23 ± 0.09, t=-1.925, and p = 0.096). Difference in the proportion of negatively conjunctive coding neurons was not observed (CME and run: 0.16 ± 0.02, CME and pupil: 0.14 ± 0.05, t=0.271, and p = 0.794) (Fig 19c; right). From the 3 behaviors, pupil change was the least correlated among speed and CME coding units, but pupil-run conjunctive coding units were larger in number compared to pupil-CME coding ones. This reflects the lag between the pupil and the CME, but the synchronization of pupil with running. The GLM analysis reinforces our findings, providing further evidence that PF units are the cell type most strongly correlated with the examined behaviors. Notably, PF cellular firing was inferred with the highest accuracy from the CME signal (Fig. 19d, e). These results underscore that, among all behaviors, CME is the most prominently represented within the MSDB network.

4.1.12 *Recruitment of PF and theta bursting cells could predict the success of run initiation.*

To investigate MSDB network effect on the success of 1 s stimulation run initiation, we compared successful (run) and non-successful (no run) run initiation trials. Out of all cell types, PF units were modulated differently during run and no run trials (Fig 20a), although they elicited a longer lasting activation in both cases (Fig 20b). As the PF population is heterogeneous (Fig 8), we hypothesized that the recruitment of putatively excitatory PF cells (i.e the optotagged, and the non-characterized, putative cholinergic ones) would shift the E/I balance in the MSDB network. We tested this by analyzing the modulation of individual cell types during successful (run) versus unsuccessful (norun) trials. This was achieved by subtracting the cellular firing rate changes between the two cases and calculating the area under the curve of the resulting difference trace. This calculation yielded a success score ranging from positive values (indicating greater activity during runs), to zero (no activity difference), to negative values (greater activity during no-runs). For further analysis, we focused on the top and bottom 5% of these scores. To test E/I balance, we analyzed the overlapping population of Theta and Burst cells (i.e theta-bursting cells), which are the putative GABAergic ones. This subgroup showed distinguishable recruitment during run vs no

run, namely the bottom 5% of the theta-bursting cells were recruited during non-successful, and were inhibited during successful run trials (Fig 20c-e), suggesting a feedback mechanism of the inhibitory cells, supporting the hypothesis of shifted E/I balance. Taken altogether, our data suggest that the primary recruitment of PF units and the secondary recruitment of rhythmic cells are modulating run initiation.

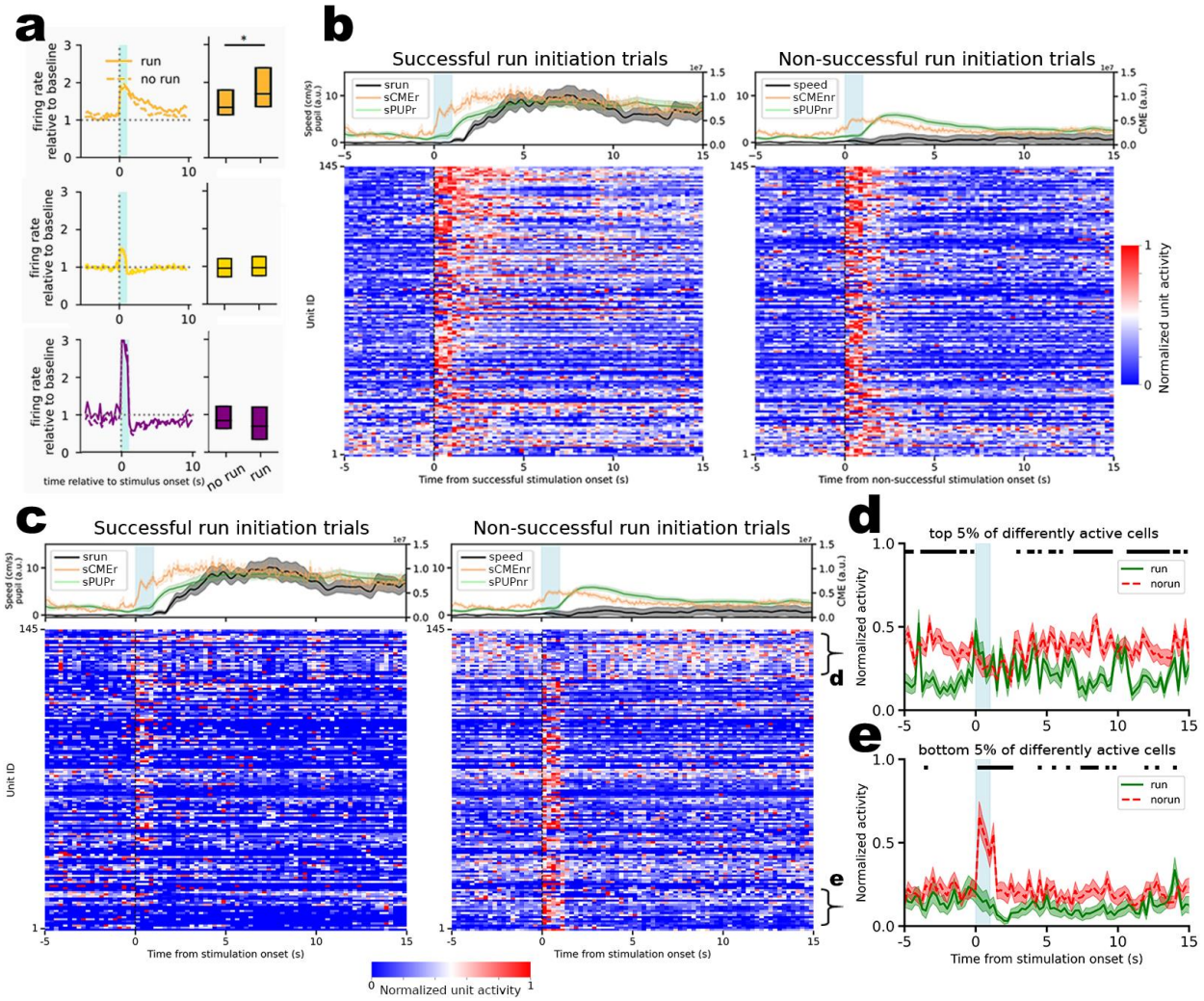

Figure 20, PF and theta-bursting unit recruitment is distinguishable between successful and non-successful run initiation. A, (left) Firing rate histogram around the 1 s stimulus of (top) PF, (middle) Theta, and (bottom) Burst units, upon successful (solid line), and non-successful (dashed line) run initiations. B, (top) Average run, CME and pupil signals around stimulation onset of (left) successful, and (right) non-successful run initiations, and (bottom) the subsequent averaged, normalized neural activity of PF units. C, similar to B, but with normalized neural activity of theta-bursting units. Brackets on the right represent the top and bottom 5% of differently active (success-dependent) units. D, Averaged activity histograms of the top 5% of those units presented on C around stimulation in separated to cases when run initiation was successful (green), or not (red). Black squares on the top shows where the activity histograms are significantly different. E, Similar to D, but presenting the bottom 5% of differently modulated theta-burst units.

In summary, this study marks the first exploration of the MSDB neural network through large-scale neural recordings combined with targeted activation of a specific cell population, while establishing its precise temporal relationship with behavioral variables associated with locomotion. Our findings reveal that along running, MSDB network is also engaged during whisking. Furthermore, we characterized PF MSDB neurons and showed that they are engaged in CME and running. Optogenetic activation of MSDB VGluT2+ cells engages other MSDB cell types. However, an important unresolved question remains: how the molecular and biophysical profiles of MSDB neurons relate to their projection patterns. As noted in the introduction, the septo-hippocampal pathway is one of the most extensively studied, yet the role of septal input along the dorsoventral axis has largely been overlooked. To address this gap, we aimed to gain a deeper understanding of the diversity within this pathway, as detailed in the following sections.

4.2 Molecular identification of dorso-ventral hippocampus projecting MSDB neurons

The MSDB plays a crucial role in both cognitive and emotional processes, and this duality may be explained by its diverse inputs. Similarly, the HC is also involved in these processes, with distinct functional differences between its dorsal and ventral regions. Traditionally, the dHC is associated with spatial navigation and the precision of spatial coding, while the vHC is more closely linked to valence coding. The second part of my PhD work aims to lay a solid foundation for future investigations into whether distinct septo-hippocampal projection patterns fulfill different functional roles. To systematically test the projection of the three major MSDB cell types (GABAergic, cholinergic and glutamatergic) along the dorsoventral HC axis, we retrogradely labeled septo-hippocampal projecting neurons from the dHC and vHC of C57BL/6J

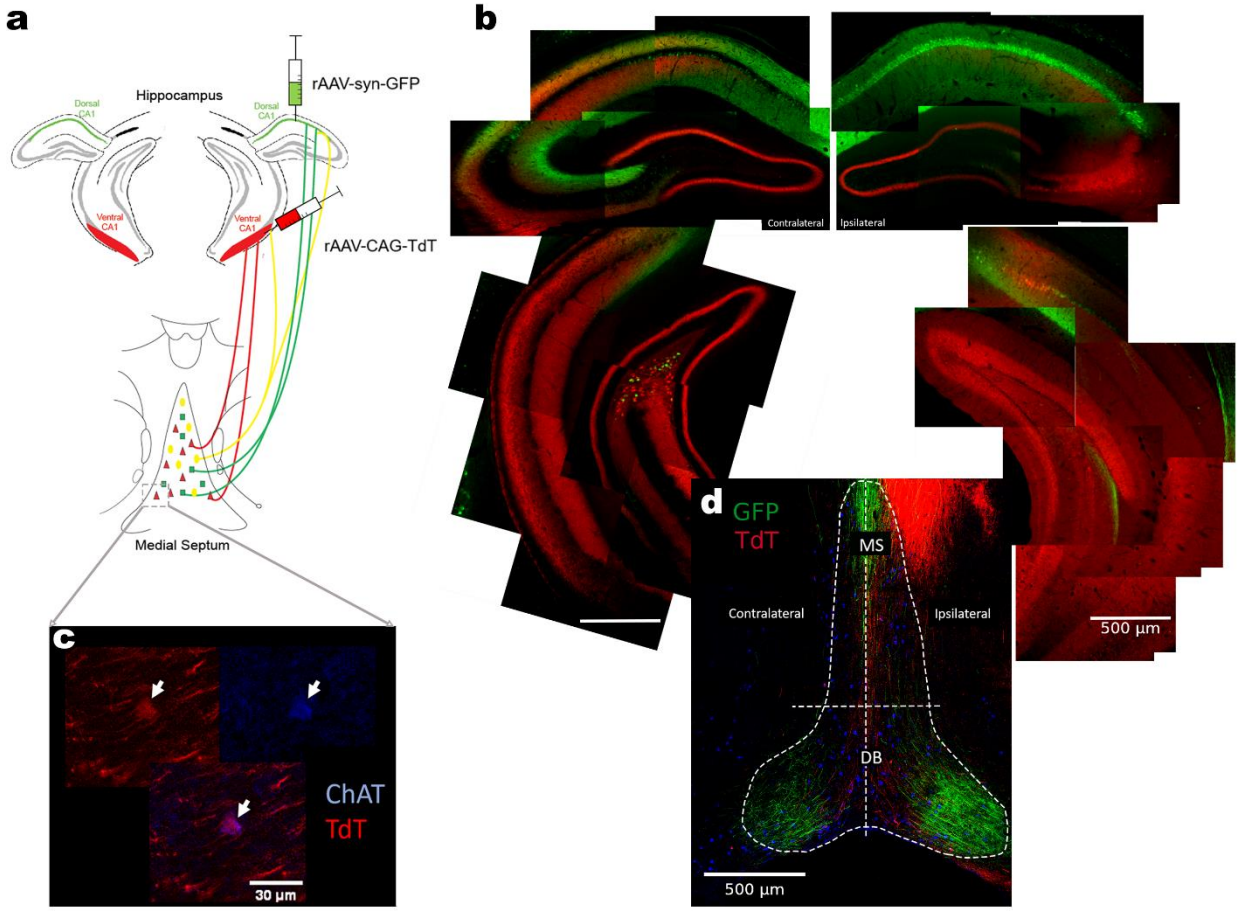

Figure 21, Experimental design of the characterization of septohippocampal cells projecting along the dorvso-ventral hippocampal axis. A, Schematic of the virus injection to dorsan and ventral hippocampus, and the MSDB. B, Stitched micrographs taken 4 weeks post-injection with (left) the contra- and (right) ipsilateral side. C, Confocal micrograph of a ChAT+ vHC projecting neuron introducing the colocalization quantification. D, subregions of the MSDB that we used to analyse the localization of septo-hippocampal projecting neurons.

mice by injecting rAAV-hSyn-EGFP, and rAAV-CAG-tdTomato of the unilateral HC poles, respectively (Fig 21). After 4 weeks of incubation time, mice were perfused, and immunohistochemistry was performed on coronal MSDB slices, and projecting neurons with or without neurochemical marker expression were quantified.

4.2.1 *Majority of MSDB neurons project to the ipsilateral vHC*

First, we counted the GFP or TdT labelled dHC and vHC projecting neurons, and defined their paired ratio (PR), by investigating the ratio of each projections (dorsal or ventral) over all projecting neuron. With this method, we normalize for the variation of cell counts within

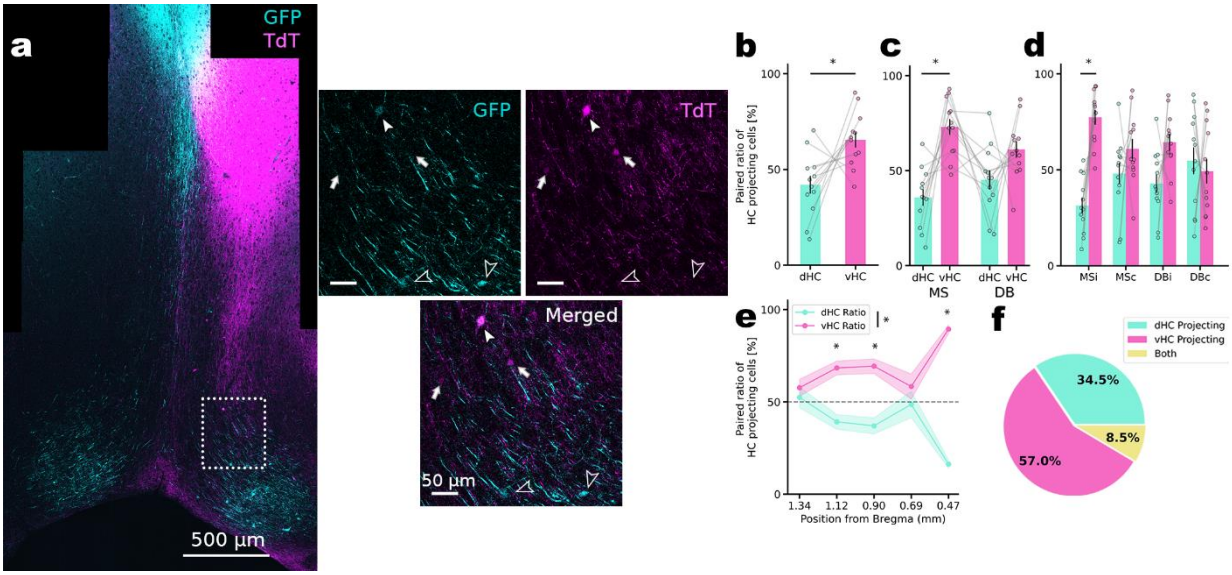

Figure 22, MSDB shows projection bias towards the vHC. A, (left) Confocal micrograph of the MSDB with retrograde labeling of (cyan) dHC, and (magenta) vHC projections. (right) Magnified images of the 2 channels and the merged micrograph of the area represented by the dashed rectangle on the left showing dHC projecting (empty arrowheads), vHC projecting (arrows), and double labeled (full arrowhead) neurons. B, Paired ratio of the projecting neurons representing dHC or vHC projecting cells ratio among all projections. Individual connected datapoints represent individual animals. C, Same as in B, but with dividing MSDB to MS and DB. D, Similar as in B and C, but further subdividing MSDB to ipsi and contralateral hemispheres regarding the unilateral injection site. E, PR of dHC vs vHC along bregma positions (the higher number the more anterior). Pie chart representation of the ratio of dorsally, ventrally, or double-projecting neurons of all experiments.

individual animals. In general, we detected the expression of both fluorophores in the MSDB (Fig 22a), and vHC projecting cells comprised a higher ratio of all projecting cells (PR of dHC: 41.99 ± 4.63 %, vHC: 65.46 ± 4.02 %, t = -2.617, p = 0.024, n = 12 mice; *paired t-test*, *mean* ± *SEM*) (Fig 22b). Furthermore, we divided MSDB into 4 parts: ipsilateral MS (MSi; side of the HC injection), contralateral MS (MSc), ipsilateral DB (DBi), and contralateral DB (DBc). A higher ratio of vHC projecting cells was observable in the MS, but not in the DB (PR of dHC MS: 35.81

± 4.31 %, vHC MS: 72.97 ± 4.17 %, dHC DB: 45.22 ± 4.97 %, vHC DB: 61.13 ± 4.30 %; dHC MS vs vHC MS t = -4.270, adjusted p = 0.008, n = 12 mice; *paired t-test with Bonferroni correction, mean ± SEM*) (Fig 22c), and most of these projecting neurons originated from the MSi, showing marked lateralization PR of MSi dHC: 31.41 ± 4.03, MSi vHC: 77.36 ± 3.91, MSc dHC: 48.08 ± 5.54 %, MSc vHC: 60.92 ± 5.13 %, DBi dHC: 42.77 ± 4.81 %, DBi vHC: 64.37 ± 4.43 %, DBc dHC: 54.71 ± 7.05 %, DBc vHC: 49.22 ± 6.46 %; MSi dHC vs MSi vHC, t = -5.657, adj. p = $5.889*10^{-4}$) (Fig 22d). We collected coronal sections along the anteroposterior axis of the MSDB, which in general showed higher ratio of vHC projecting cells, and at certain coordinates the ratio of dHC vs vHC projecting neurons were significantly different (PR over bins: Bregma 1.34 mm dHC: 52.47 ± 6.88 %, vHC: 57.68 ± 5.64 %; 1.12 mm dHC: 39.22 ± 4.22 %, vHC: 68.42 ± 3.91 %, t = -3.678, adj. p = 0.025; 0.9 mm: 37.02 ± 4.57 %, 69.35 ± 4.16 %, t = -3.762, adj. p = 0.022; 0.69: 48.66 ± 7.82 %, 58.34 ± 7.49 %; 0.47 mm: 16.30 ± 4.38 %, 89.39 ± 4.50 %, t = -8.872, adj. p = 0.021; n = 12 mice; *paired t-test with Bonferroni correction, mean ± SEM*) (Fig 22e). We also tested the hypothesis, of whether the ratio of dHC and vHC projecting neurons are equal, by testing whether the calculated PRs are deviant from 50 %. Both dHC and vHC showed significant deviation from 50 %, supporting our observation of significant projection bias of MSDB population towards vHC (dHC PR vs 50%: t = -2.888, p = 0.006; vHC PR vs 50%: t = 5.915, p = $3.616*10^{-7}$; *one-sample t-test*). We also identified, that 8.5 % percent of all projecting neurons were double positive for the two tracers (Fig 22f). This suggest, that although there is a projection bias along the dorso-ventral HC axis, there are some neurons projecting to both regions. We observed that all the neurochemical markers tested labeled some double-projecting neurons. However, due to their relatively small numbers, we could not draw definitive conclusions based on their prevalence. This finding merely confirms their existence, and as a result, we did not pursue further analysis. Taken together, our data demonstrate the presence of MSDB neurons projecting to both the dorsal and ventral hippocampal poles. Additionally, the findings suggest that more MSDB cells project stronger to the vHC than to the dHC, with MS-projecting neurons preferentially sending ipsilateral afferents to the vHC.

4.2.2 *Majority of GABAergic MSDB neurons project to vHC*

To investigate GABAergic projecting neurons, we labeled MSDB slices with antibodies against the isoform 67 of glutamic acid decarboxylase (GAD67). We chose this marker over the GAD65 isoform, as it was a more reliable marker of GABAergic cells, according to the literature (Castañeda et al., 2005), and our tests arrived to the same conclusion. One of the most studied subpopulation of GABAergic MSDB neurons are expressing PV (Freund, 1989), therefore we also investigated this marker (Fig 23a). The ratio of GABAergic vHC projecting neurons over all GABAergic projecting neurons was higher compared to the dHC (dHC: 39.47(22.54-47.06) % vs vHC: 73.77(65.69-78.95) %; t = -3.273, p = 0.011, n = 9; *paired t-test, median(IQR)*) (Fig 23b). On the contrary, the subpopulation of these cells, the PV+ neurons, that are important pacemaker cells of both poles of the hippocampus interestingly did not show difference in their PR (dHC: 29.67(10.78-31.58) % vs vHC: 39.38(34.07-40.79) %; t = -1.537, p = 0.163, n = 9) (Fig 23b). Slight majority of both dHC and vHC projecting neurons where positive to GAD67 (percentage

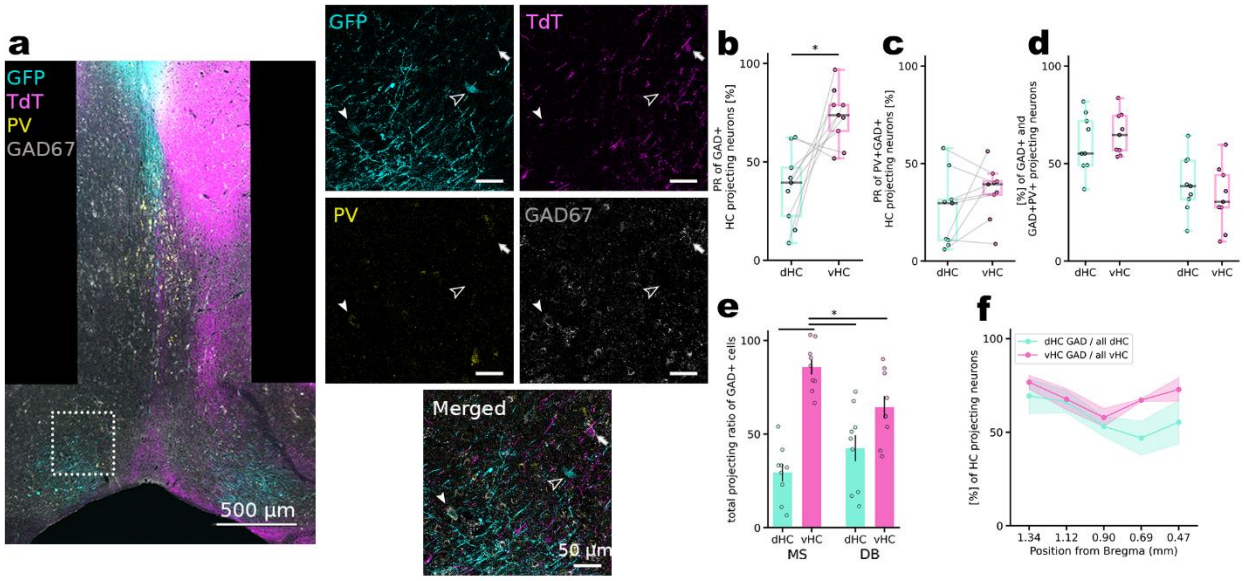

Figure 23, MSDB GAD67+, but not GAD67+PV+ shows projection bias towards the vHC. A, (left) Confocal micrograph of the MSDB with retrograde labeling of (cyan) dHC, and (magenta) vHC projections, and additional immunohistochemistry against (yellow) PV, and (gray) GAD67. (right) Magnified images of the 4 channels and the merged micrograph of the area represented by the dashed rectangle on the left. It shows a GAD+PV+ dHC projecting (full arrowhead), a GAD-PV- dHC projecting (empty arrowhead), and a GAD+PV- vHC projecting (arrow) neuron in the DB. B, Paired ratio of the projecting neurons representing GAD+ dHC or GAD+ vHC projecting cells ratio among all GAD+ projections. Individual connected datapoints represent individual animals. C, Same as in B, but with GAD+PV+ dHC or GAD+ PV+ vHC projecting ratio among all GAD+ projections. D, Percentage of (left) GAD or (right) GAD and PV immunoreactivity of the retrogradely labeled neurons. E, Same as in B, but with dividing MSDB into MS and DB. F, Percentage of GAD+ dHC or GAD+ vHC along bregma positions (the higher number shows the more anterior position).

of GAD+ dHC neurons: 55.17(49.18-71.83) %, vHC: 64.71(56.86-74.44) %; t = -0.822, p = 0.435), and about half of this population was composed of PV+ neurons (percentage of GAD+PV+ dHC neurons: 38.46(31.82-51.52) %, vHC: 30.39(27.51-44.12) %; t = 1.082, p = 0.311, n = 9) (Fig 23d). We found no differences in the overall percentage of GABA- or PV-expressing neurons projecting to the dHC and vHC. This suggests that although the proportion of neurons projecting to the dHC is smaller compared to those projecting to the vHC (Fig. 22), their immunoreactivity for GAD67 and PV is proportionate. Being in line with the general projection results, the MS innervated the vHC with much higher ratio than the dHC, and this innervation bias was also significantly increased compared to the ratio DB located projecting neurons (PR of dHC MS: 32.14(23.08-33.33) %, vHC MS: 86.54(78.33-92.86) %, dHC DB: 47.62(19.05-53.62) %, vHC DB: 59.52(53.85-82.54) %; dHC MS vs vHC MS t = -6.846, adjusted p = 0.001; dHC DB vs vHC MS t = 4.885, adjusted p = 0.007, n = 12 mice; *paired t-test with Bonferroni correction*) (Fig 23e). Finally, we did not observe difference of the abundance of GABAergic projecting neurons along the anteroposterior axis of the MSDB (percentage of GAD+ projecting neurons over bins: Bregma 1.34 mm dHC: 69.39 ± 10.58 %, vHC: 76.76 ± 4.17 %; 1.12 mm dHC: 66.28 ± 6.72 %, vHC: 67.66 ± 6.42 %,; 0.9 mm: 53.11 ± 6.12 %, 57.86 ± 5.46 %; 0.69: 46.90 ± 15.53 %, 67.13 ± 1.30 %; 0.47 mm: 55.35 ± 12.23 %, 72.83 ± 6.60 %; n = 9 mice; *non-significant values of paired t-test with Bonferroni correction, mean ± SEM*)

4.2.3 *Majority of ChAT and GAD67 coexpressing MSDB neurons project to vHC*

Next, we quantified the cholinergic subpopulation by using ChAT immunostaining. As we know that mixed neurotransmitter releasing MSDB subpopulation target the hippocampus (Takács et al., 2018), we also tested ChAT colocalization with GAD67 (Fig 24a). Interestingly, we did not observe dorso-ventral projection bias of cholinergic septo-hippocampal neurons (PR of dHC projecting: 30.81(24.16-46.91) % vs vHC: 46.32(31.99-49.22) %; t = -1.054, p = 0.317, n = 11; *paired t-test, median(IQR)*) (Fig 24b), but in their dual neurotransmitter subpopulation. The vHC projecting ChAT+GAD+ neurons composed the majority of all ChAT+ projecting neurons (dHC: 27.18(18.91-35.88) % vs vHC: 61.39(59.75-68.46) %; t = -3.207, p = 0.049, n = 11) (Fig 24c). The total percentage of ChAT+ and ChAT+GAD+ dHC projecting neurons was similar to

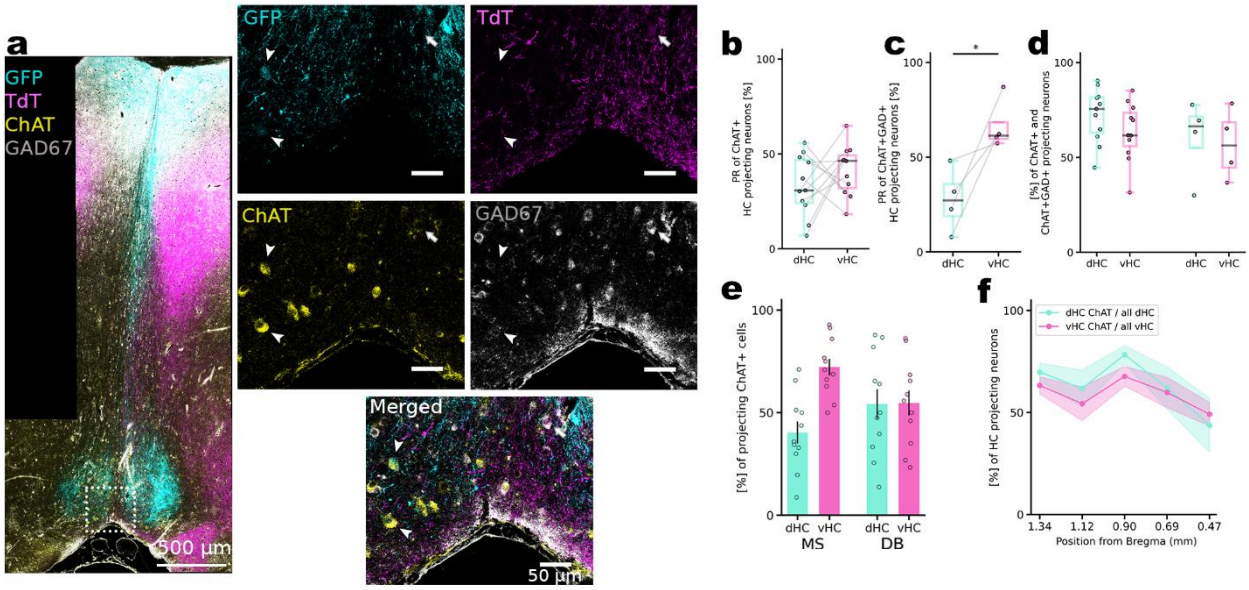

Figure 24, GAD67+ subpopulation of MSDB cholinergic neurons preferentially target vHC. A, (left) Confocal micrograph of the MSDB with retrograde labeling of (cyan) dHC, and (magenta) vHC projections, and additional immunohistochemistry against (yellow) ChAT, and (gray) GAD67. (right) Magnified images of the 4 channels and the merged micrograph of the area represented by the dashed rectangle on the left. It shows ChAT+GAD+ dHC projecting (full arrowhead), and ChAT+GAD+ vHC projecting (arrow) neurons in the DB. B, Paired ratio of the projecting neurons representing ChAT+ dHC or ChAT+ vHC projecting cells ratio among all ChAT+ projections. Individual connected datapoints represent individual animals. C, Same as in B, but with ChAT+GAD+ dHC or ChAT+GAD+ vHC projecting ratio among all ChAT+ projections. D, Percentage of (left) ChAT or (right) ChAT and GAD immunoreactivity of the retrogradely labeled neurons. E, Same as in B, but with dividing MSDB into MS and DB. F, Percentage of ChAT+ dHC or ChAT+ vHC along bregma positions.

vHC projecting ones (percentage of ChAT+ dHC neurons: 75.61(62.94-81.70) %, vHC: 61.70(55.95-73.54) %; t = 1.547, p = 0.153, n = 11; ChAT+GAD+ dHC neurons: 66.49(55.06-71.62) %, vHC: 56.32(44.73-68.58) %; t = 0.324, p = 0.767, n = 4) (Fig 24d). The PR ratio of cholinergic vHC projecting neurons originating from the MS was tendentiously higher compared to the cholinergic dHC projecting neurons, but not significant (PR of dHC MS: 40.30 ± 5.35 %, vHC MS: 72.19 ± 4.05 %, dHC DB: 54.14 ± 7.24 %, vHC DB: 54.66 ± 6.09 %; dHC MS vs vHC MS t = -3.320, p = 0.008, n = 11 mice; *paired t-test*) (Fig 24e). These observations remained homogeneous along the anteroposterior MSDB axis (percentage of ChAT+ projecting neurons over bins: Bregma 1.34 mm dHC: 69.82 ± 4.59 %, vHC: 63.27 ± 4.41 %; 1.12 mm dHC: 61.76 ± 11.55 %, vHC: 54.33 ± 10.37 %; 0.9 mm: 78.36 ± 4.70 %, 67.70 ± 5.09 %; 0.69: 62.07 ± 14.06 %, 59.83 ± 10.09 %; 0.47 mm: 43.75 ± 43.75 %, 49.15 ± 19.15 %; n = 11 mice; *non-significant values of paired t-test with Bonferroni correction, mean ± SEM*) (Fig 24f).

4.2.4 *CaMKII+ MSDB neurons equally innervate the dHC and vHC*

Lastly, we wanted to use the α-subunit of the Calcium-calmodulin dependent kinase 2 (CaMKII) as a marker for excitatory neurons, but as recent reports doubting the specificity of this subunit for cortical glutamatergic cells (Veres et al., 2023), we also tested whether they are specific for MSDB VGluT2 neurons. We perfused and coronally sectioned the brains of VGluT2-TdT mice, which were generated by crossing VGluT2-Cre mice with the TdTomato (TdT) reporter mouse line (Ai9) from the Allen Institute. In these offspring, VGluT2-expressing neurons innately expressed red fluorophore, TdT. To assess colocalization, we performed immunolabeling for CaMKII on these brain sections and quantified the overlap between TdT fluorescence and CaMKII expression. Surprisingly, we saw low overlap of the two markers, basically forming two distinct

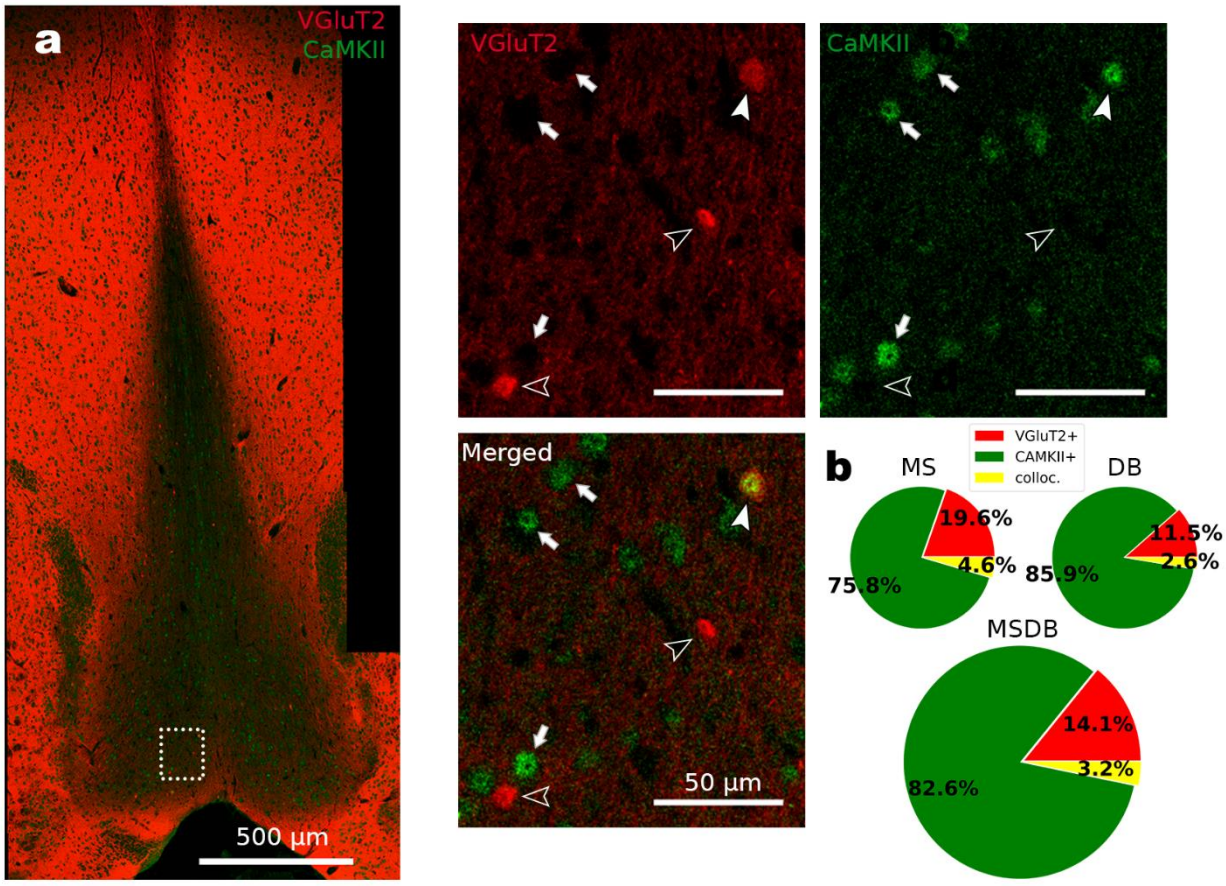

Figure 25, CaMKII is not specific for VGluT2+ MSDB neurons. A, (left) Confocal micrograph of the MSDB section of a reporter mouse, where red represents the innate TdT expression, and green is the CaMKII signal. (right) Magnified images of the 2 channels and the merged micrograph of the area represented by the dashed rectangle on the left. It shows TdT+ (empty arrowheads), CaMKII+ (arrows), and colocalized (full arrowhead) neurons. B, Pie chart showing generally low colocalization of TdT and CaMKII both in the (top left) MS, and (top right) DB.

populations (number of counted VGluT2+ cells: 285 ± 28, CAMKII+: 1406 ± 26, colocalized: 53 ± 7; n = 3 animals, n = 11 slices) (Fig 25). This amount of overlap was similar both in the MS and DB subparts (Fig 25b).

Although we noted that we are unable to tag VGluT2+ neurons with this marker, we were still curious about the ratio of septohippocampal cells expressing CaMKII (Fig 26a). From all of the CaMKII+ projecting neurons about half of them projected to dHC, and the other half to the vHC (PR of dHC projecting: 45.83(44.86-47.51) % vs vHC: 57.38(55.77-61.74) %; t = 0, p = 0.1, n = 3; *paired t-test, median(IQR)*) (Fig 26b), and the percentage of CaMKII+ projection to the dHC was proportional to the percentage of CaMKII+ projection to the vHC (Fig 26c) regarding the whole MSDB with its subregions (percentage of CaMKII + dHC neurons: 68.75(54.65-72.72) %, vHC: 67.61(49.29-68.94) %; t = 6.000, p = 0.7, n = 3) (Fig 26d) and along its anteroposterior axis (percentage of CaMKII+ projecting neurons over bins: Bregma 1.34 mm dHC: 63.89 ± 5.56

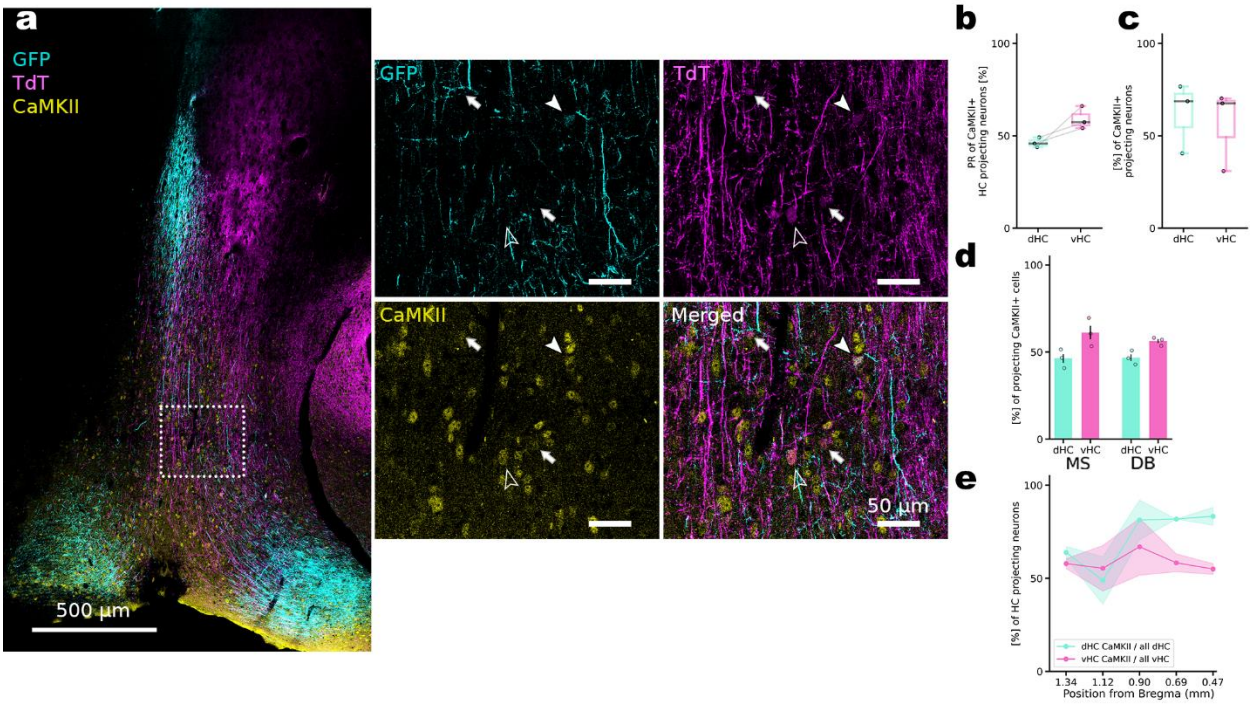

Figure 26, CaMKII+ MSDB neurons innervate the dHC and vHC equally. A, (left) Confocal micrograph of the MSDB with retrograde labeling of (cyan) dHC, and (magenta) vHC projections, and additional immunohistochemistry against (yellow) CaMKII. (right) Magnified images of the 3 channels and the merged micrograph of the area represented by the dashed rectangle on the left. It shows CaMKII+ dual projecting (full arrowhead), CaMKII+ vHC projecting (empty arrowhead), and CaMKII- vHC projecting (arrows) neurons in the DB. B, Paired ratio of the projecting neurons representing CaMKII+ dHC or CaMKII+ vHC projecting cells ratio among all CaMKII+ projections. Individual connected datapoints represent individual animals. C, Percentage of CaMKII+ dHC and vHC neurons. E, Same as in B, but with dividing MSDB into MS and DB. F, Percentage of CaMKII+ dHC or CaMKII+ vHC along bregma positions.

%, vHC: 57.92 ± 4.58 %; 1.12 mm dHC: 48.92 ± 15.62 %, vHC: 55.39 ± 14.99 %; 0.9 mm: 81.33 ± 13.13 %, 66.95 ± 18.71 %; 0.69: 81.82 ± 0.00 %, 58.33 ± 8.33 %; 0.47 mm: 83.33 ± 8.33 %, 55.00 ± 5.00 %; n = 3 mice; *non-significant values of paired t-test with Bonferroni correction, mean ± SEM*) (Fig 26e). This all suggest that the CaMKII+ MSDB subpopulation equally project to both poles of the HC, and is a distinct subpopulation than the VGluT2+ cells.

4.2.5 *Sparse population of VGluT2+ septohippocampal neurons*

To investigate the glutamatergic subpopulation of septohippocampal neurons, we used the previously mentioned reporter mouse line and adjusted our experimental protocol. We injected rAAV-hSyn-EGFP to either the dorsal or the ventral part of the unilateral hippocampus, and imaged the perfused sections (Fig 27a). As we could not normalize our dataset with the overall projection due to only working with one injection site, we measured the volume of the analysed tissue, and calculated cell density. Surprisingly, the density of VGluT2+ projecting neurons to the vHC was more than 3-fold higher compared to the density of dHC projecting ones (cell density of dHC projecting MSDB neurons: $6.154*10^{-8} \pm 1.719*10^{-8}$ cell/μm^3 vs vHC: $17.86*10^{-8} \pm 2.858*10^{-8}$ cell/μm^3; t = -2.750, p = 0.071, n = 4 animals for each group; *Student's t-test, median(IQR)*) (Fig 27b), and this difference was the most striking in the MS subregion (cell density of dHC projecting in MS: $9.732*10^{-8} \pm 1.654*10^{-8}$ cell/μm^3, vHC MS: $31.76*10^{-8} \pm 5.325*10^{-8}$ cell/μm^3, dHC DB: $3.971*10^{-8} \pm 1.997*10^{-8}$ cell/μm^3, vHC DB: $9.490*10^{-8} \pm 2.525*10^{-8}$ cell/μm^3; dHC MS vs vHC MS t = -3.422, p = 0.014, n = 4 mice for each group; *Student's t-test; mean ± SEM*) (Fig 27d). In line with the literature, among all projecting neurons, VGluT2+ subpopulation was the least represented (Müller & Remy, 2018). Furthermore, cumulative evidence of the metadata of papers investigating MSDB VGluT2 cells (Sotty et al., 2003; X. Wu et al., 2021), and our self-curiosity led us to test ChAT expression along with the TdT and GFP. We observed that the amount of projecting VGluT2 cells was very low, around 0-2 cells in each slice, almost all of them were colocalized with ChAT marker for both the dorsal and ventral projecting subpopulations (percentage of VGluT2+ dHC neurons: 20.60(4.93-36.94) %, vHC: 26.14(18.79-33.48) %; t = -0.441, p = 0. 675, n = 4; VGluT2+ChAT+ dHC neurons: 12.77(3.90-25.45) %, vHC: 21.22(15.02-29.34) %; t = -0.687, p = 0.518, n = 4) (Fig 27c). The low expression was constant along the anteroposterior axis of the MSDB (percentage of VGluT2+ projecting neurons over bins: Bregma

1.34 mm dHC: 27.12 ± 12.67 %, vHC: 44.50 ± 10.91 %; 1.12 mm dHC: 5.87 ± 2.70 %, vHC: 11.54 ± 2.43 %; 0.9 mm: 27.49 ± 13.59 %, 15.92 ± 4.93 %; 0.69: 9.90 ± 7.95 %, 30.43 ± 12.83 %; 0.47 mm: 6.25 ± 6.25 %, 25.92 ± 11.78 %; n = 4 mice; *non-significant values of paired t-test with Bonferroni correction, mean ± SEM*) (Fig 27e).

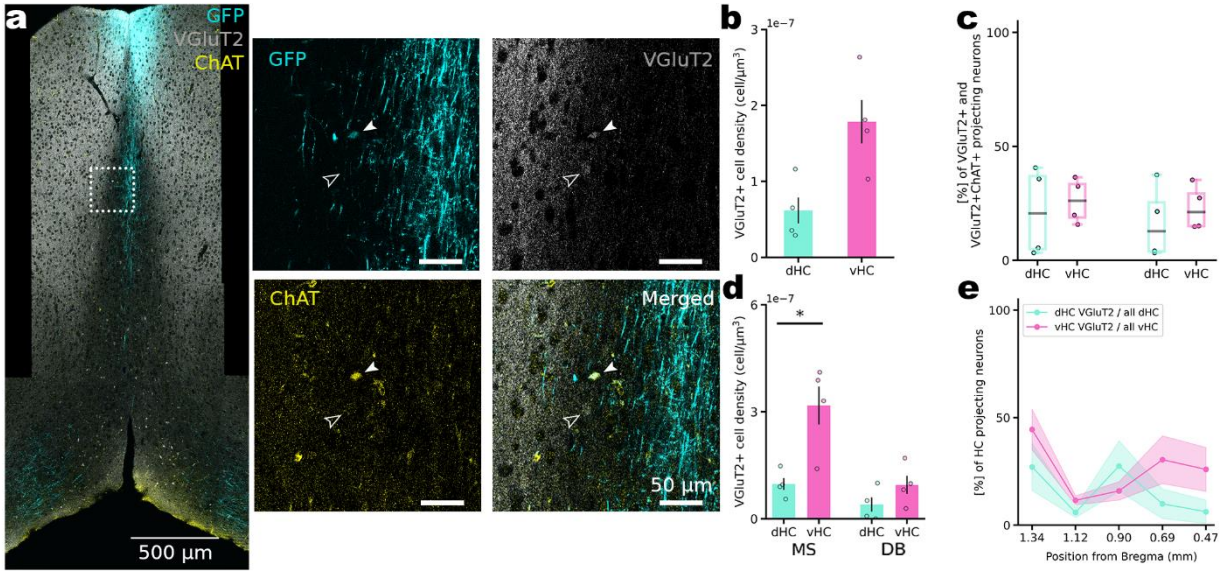

Figure 27, MS VGluT2+ projection is 3-fold denser to the vHC. A, (left) Confocal micrograph of the MSDB with retrograde labeling of (cyan) dHC projection, the reporter channel for (gray) VGluT2, and additional immunohistochemistry against (yellow) ChAT. (right) Magnified images of the 3 channels and the merged micrograph of the area represented by the dashed rectangle on the left. It shows a VGluT2+ChAT+ dHC projecting (full arrowhead), and a VGluT2+ChAT- non-projecting (empty arrowhead) neuron. B, Cell density of VGluT2+ projecting neurons. C, Percentage of (left) VGluT2+ or (right) VGluT2+ChAT+ dHC or vHC projecting neurons. D, Same as in B, but with dividing MSDB into MS and DB. E, Percentage of VGluT2+ dHC or VGluT2+ vHC along bregma positions.

Taken altogether, we showed that MSDB expresses a strong projection bias toward the vHC. The neurochemical identity of these projecting neurons revealed a proportional projection comparing the dHC to vHC. Further studies remained to be conducted on determining the postsynaptic targets of these projections in the HC, which could bring further understanding about this projecting pathway.

5. Discussion

The MSDB is regarded as a subcortical hub that bridges the sensory system and the limbic system, playing a role in a wide range of functions. This functional diversity can be better understood through two key aspects: (1) the variety of MSDB populations and their local interactions and (2) the projection patterns of these cells that transmit the computed output to target areas. In this thesis, we demonstrated that optogenetic activation of VGluT2+ MSDB neurons recruits non-VGluT2+ neurons, leading to persistent firing (PF). This firing matches the duration of photostimulation-induced CME and pupil dilation, two main behavioral variables linked to locomotion.

This persistent activity likely further supports cognitive functions such as working memory, motor planning, and decision-making, acting as a neural substrate for linking transient sensory stimuli with sustained motor and cognitive outputs. By dissecting these mechanisms utilizing large scale neural recordings, this work enhances our understanding of the MSDB's electrophysiological properties and functional roles. This thesis further explores the connectivity between the medial MSDB and the hippocampus, revealing differential innervation from the MSDB along the hippocampal dorsoventral axis. In summary, this work contributes to the growing body of literature that underscores the MSDB's role as a crucial node in integrating a wide range of behaviors. This integration supports not only hippocampal-dependent memory but also broader brain networks responsible for movement coordination and adaptive behavioral responses.

5.1 Transient photoexcitation of MSDB VGluT2 neurons mediate locomotion-related behaviors

Previous studies demonstrated that prolonged stimulation of VGluT2+ neurons in the MSDB, particularly at theta frequencies, can initiate locomotion (Fuhrmann et al., 2015; Kocsis et al., 2022; Mocellin et al., 2024). In this thesis, we examined the impact of shorter, more physiologically relevant stimulation durations on locomotion-related behavioral variables. Specifically, we used a 1 s light stimulus to excite the VGluT2+ population, which, in some cases, initiated running. Analyzing unsuccessful run initiations revealed movement-preparatory actions, such as CME (i.e. whisking) and pupil dilation. These observations suggest that even when the

excitatory/inhibitory (E/I) balance in the MSDB is insufficient to induce locomotion, this brief stimulation can elicit CME and subsequent pupil dilation. This effect may involve the MSDB-LH network, as LH orexin neurons are sufficient to induce pupil dilation, but also to elicit activity after the state of quiescence (Grujic et al., 2023; An et al., 2021). Indeed, our results revealed a functional connection between the two aspects of locomotion: a 1-second photoexcitation not only initiated running but, in most cases, also induced whisking, which was closely followed by pupil dilation.

Analyzing the ORX signal of LH neurons in the NAcc revealed a clear delay of ~500 ms between orexin activity and the onset of locomotion (Duffet et al., 2022). Previous evidence supports the notion that MSDB VGluT2+ neurons send excitatory projections to the LH, enabling transitions from sleep to active state (An et al., 2021). In line with this and other hypothesis (Liu et al., 2020), it is plausible that MSDB VGluT2+ cells directly innervate LH orexin neurons. This aligns with our data showing a strong speed-tuning effect in MSDB neurons and the understanding that the LH is not primarily a computational hub but rather a relay for transmitting input signals due to its low intra-area connectivity (Burdakov & Karnani, 2020). While LH ORX neurons are well-established drivers of pupil dilation, the direct pathway from the MSDB to the locus coeruleus (LC)—another brain region closely associated with pupil dilation—remains largely unexplored. Our tracing from the MSDB VGluT2 cells revealed a strong projection of these neurons directly to the LC (data not shown). Optogenetically targeting these fibers could reveal the functional significance of this pathway in autonomic regulations and arousal maintenance. It is likely that the pupil dilation effect observed with LH activation is complemented by MSDB-LH projections. The role of the MSDB-LH interconnections regarding pupil dynamics, however, remains an open question in our understanding. Moreover, during locomotion, both acetylcholine (ACh) and norepinephrine (NE) signals are present, with NE preceding ACh (Reimer et al., 2016). This temporal relationship suggests that the LC-to-MSDB projection may play a crucial role in locomotion initiation. Increased ACh signaling from the MSDB ascends through the visual cortex, mediating visual response by locomotion (Fu et al, 2014). Our results demonstrated that activation of MSDB VGluT2+ neurons induce arousal-related behaviors, evident in increased whisking and pupil dilation, even in the absence of locomotion. This finding raises questions about the functional significance of these arousal epochs without accompanying movement. Previous research (Vinck et al., 2015) has highlighted the role of such arousal states in enhancing perception and learning.

Thus, future studies should explore how MSDB VGluT2-induced arousal is linked to learning processes.

5.2 Persistent Activity in MSDB Neurons

Characterization of MSDB neurons revealed a persistently active neural population which was in close coordination with the whisking signal. This link suggests that the sensory input to MSDB is transferred via PF, because the length of PF in this area aligns with the length of the whisking signal. Notably, the same neuronal populations were activated during voluntary whisking, supporting the hypothesis that whisking behavior is driven through MSDB circuits. Complementing this finding, analysis of pupil signals revealed a delayed correlation with MSDB neural activity, suggesting that whisking and pupil dilation share a common origin in the MSDB before diverging at downstream targets. Supporting this hypothesis, Reimer et al. (2016) observed that pupil signals lag approximately 1 second behind LC noradrenergic activation. This could imply that while whisking signal is expressed immediately after our stimulation (with about 200 ms delay), the pupil signal needs to propagate through several downstream targets until actual dilation. Although our anatomical inspection did not identify MSDB VGluT2 terminals in either the V or VII cranial nerve nuclei (associated with whisking), we hypothesize that whisking-related CME signals are likely conveyed from the MSDB to cortical execution areas, such as the barrel cortex. Given its strong influence by whisking, this pathway could account for the observed short latency. This pathway divergence may function as a synchronization mechanism, ensuring that whisking aligns with locomotion. Supporting this idea, we observed that while running and pupil signal has a more variable relationship, whisking and pupil signals maintain a tighter coupling. Stimulated running followed both whisking and pupil signals, whereas voluntary movements displayed whisking preceding running, with pupil dilation synchronized to running. This synchronization may enhance visual perception during movement by modulating cortical sensory areas. Interestingly, stimulated CME signals emerged promptly (~300 ms after stimulation onset) and were generated by a subgroup of neurons, whereas locomotion initiation exhibited seconds long delay. This suggests that the recruitment of PF neurons plays a role in bridging preparatory whisking and running initiation. Supporting this, we showed that increased recruitment of PF neurons, accompanied by the downregulation of putative GABAergic neurons and higher CME magnitude, correlated with successful run initiation.

Both the intrinsic biophysical properties of individual neurons and the synaptic circuit dynamics have been shown to play mechanistic roles in persistent activity. Evidence supporting the involvement of intrinsic cellular conductances in generating persistent activity comes from a substantial body of research (Fransén et al., 2006; Jochems & Yoshida, 2015; Knauer et al., 2013; Navaroli et al., 2012; Pressler & Strowbridge, 2006). These studies demonstrated that transient intracellular depolarization can lead to persistent firing in specific neurons, even when synaptic transmission is pharmacologically blocked. Notably, many of these experiments involved the application of carbachol (a muscarinic receptor agonist), which is thought to mimic the increased acetylcholine levels associated with heightened attention and working memory. In contrast, other studies have highlighted the necessity of synaptic circuits to drive persistent activity (Inagaki et al., 2019; Hart & Huk, 2020), supported further by numerous computational models of persistent activity grounded in attractor network dynamics (Amit & Brunel, 1997; Barak & Tsodyks, 2007; Compte, 2006; Nachstedt & Tetzlaff, 2017; Zylberberg & Strowbridge, 2017). In our study, we observed prominent persistent activity following transient stimulation of MSDB VGluT2 neurons, even in the presence of synaptic blockers and without additional carbachol application. This finding suggests that MSDB VGluT2 neurons possess intrinsic biophysical properties that enable them to sustain firing independently. However, we also observed more pronounced persistent firing in an intact network condition, indicating that the network amplifies the persistence and prominence of sustained activity.

Numerous studies have explored the biophysical mechanisms underlying persistent activity. In many cortical neurons, persistent firing has been reported to likely involve a second messenger system that activates the underlying depolarizing response. Evidence supporting this hypothesis comes from studies showing that persistent firing is sensitive to calcium ion concentrations (Pressler & Strowbridge, 2006; Rahman & Berger, 2011; Lei et al., 2014). Despite significant efforts by several research groups (Haj-Dahmane & Andrade, 1999; Lei et al., 2014; Rahman & Berger, 2011; Tahvildari et al., 2008; Z. Zhang et al., 2011) to elucidate this mechanism, the exact calcium-dependent current enabling neurons to sustain firing after a stimulus remains unidentified. One proposed mechanism is a calcium-activated non-selective cation current (I_{CAN}), as suggested in studies by Pace et al. (2007) and Rubin et al. (2009). Our additional experiments manipulating extracellular calcium concentrations ($[Ca^{2+}]_o$) provided evidence that PF in the MSDB is driven by intrinsic membrane properties and depends on Ca^{2+}-mediated

mechanisms. This finding aligns with studies in other regions, such as the prefrontal cortex, where intrinsic mechanisms support sustained activity during working memory tasks (Goldman-Rakic, 1995), and the entorhinal cortex, where muscarinic receptor activation enhances intrinsic PF (Fransén et al., 2006). Several studies have reported that specific subtypes of transient receptor potential canonical (TRPC) channels may mediate I_{CAN} responses in cortical neurons (Yan et al., 2009; Z. Zhang et al., 2011; Reboreda et al., 2011; Lei et al., 2014). Additionally, a more recent study (O'Malley et al., 2020) demonstrated the involvement of TRPM channels in the persistent firing exhibited by thalamic reticular nucleus neurons. Future research should aim to elucidate the specific biophysical mechanisms that enable MSDB VGluT2 neurons to sustain persistent firing. Although the investigation of the intrinsic mechanisms and conductances underlying this persistent firing falls outside the scope of the current thesis, it remains a topic of great interest, given the diverse behavioral and cognitive functions associated with the MSDB. Furthermore, antagonizing other neuromodulators, such as norepinephrine (NE), remains to be explored. This would be intriguing, as earlier studies have demonstrated that a 1-second activation of the noradrenergic nucleus LC induces sustained activity in the MSDB (Segal, 1976). Finally, combining retrograde tracing in candidate brain regions—such as the preoptic area (Zhang et al., 2018), lateral hypothalamus (An et al., 2021), or ventral tegmental area (Mocellin et al., 2024)—with electrophysiological recordings of specific MSDB-projecting neurons could provide valuable insights into the projection patterns of persistently active neurons.

Persistent firing in VGluT2+ neurons may extend beyond memory functions to encompass processes such as reinforcement learning, locomotor state maintenance, and anticipatory coding during goal-directed behaviors. The MSDB circuits have long been implicated in coordinating hippocampal theta oscillations, a critical component for encoding spatial and temporal information (McNaughton et al., 2006; Vertes & Kocsis, 1997). Persistent activity observed in VGluT2+ neurons aligns with these roles, suggesting that these neurons act as integrators of motor planning and spatial coding. During locomotion, these neurons might synchronize hippocampal theta oscillations with stepping rhythms, enhancing spatial memory encoding and retrieval. Their coupling with pupil-linked arousal signals further suggests a role in modulating cortical states during attentive behaviors. Such integrative dynamics are critical for adaptive responses to complex environments, enabling animals to navigate efficiently while

processing sensory inputs. Future research should also explore how VGluT2+ neuron activity contributes to behavioral flexibility during rapid changes in environmental demands or task rules.

5.3 Septo-Hippocampal Connectivity

The increased MSDB activity during run initiation may reflect its role in preparing the hippocampal network for processing incoming sensory and motor-related signals, to enhance encoding by transferring theta oscillation. In this thesis, we explored the projections of septo-hippocampal neurons, and showed a strong general projection bias along the dorso-ventral axis of the HC. Specifically, MSDB neurons projects stronger input to the vHC compared to the dHC. This projection bias aligns with the broader functional dichotomy of the hippocampal axis: the dHC supports spatial navigation and memory, while the vHC is involved in emotional processing and encoding the valence of experiences.

A study examining the role of the MSDB as part of a secondary auditory pathway (G.-W. Zhang, Sun, et al., 2018) also highlights the significance of this distinction. The authors showed that disturbingly high dB noises, but not pure tones are represented in the MSDB. Additionally, other aversive stimulus like airpuff also rapidly activates MSDB subpopulations (G.-W. Zhang, Shen, et al., 2018), like cholinergic cells (Hangya et al., 2015). The vHC is coding the valence of the experience, therefore it is hypothesized, that the MSDB to vHC pathway should have a strong influence of aversive memory encoding. Specific experiments investigating this pathway may reveal how differential MSDB projections regulate specific hippocampal subdomains to optimize memory consolidation and spatial navigation during active exploration. The MSDB also projects to the VTA (Mocellin et al., 2024) and LHb (G.-W. Zhang, Shen, et al., 2018), brain regions associated with reward and aversion. However, it remains to be investigated whether the same neurons conveying these inputs also target the vHC. Future research is necessary to clarify the circuitry underlying the integration of inputs processing emotional information.

VGluT2+ neurons projecting to the dHC are particularly important for understanding how the MSDB regulates locomotion and spatial coding. This interplay between locomotion and spatial memory is central to adaptive navigation and environmental learning (O'Keefe & Burgess, 1996). This connection between locomotion and spatial memory is supported by studies

demonstrating that theta oscillations frequency dynamically adjust to match motor and environmental demands (Buzsáki, 2002; Fuhrmann et al., 2015). Additional exploration of how VGluT2+ neuron activity adapts during changes in task complexity or environmental uncertainty would provide valuable insights into the flexible role of the MSDB.

VGluT2+ septo-hippocampal neurons likely interact with local interneurons and pyramidal cells (Sotty et al., 2003; Colom et al., 2005; Huh et al., 2010), facilitating prolonged firing and theta synchronization. This dynamic integration may underlie behavioral state transitions, such as movement initiation or exploratory behavior. Future studies could further investigate how neuromodulators such as ACh or NE influence VGluT2+ neuron activity during locomotion and cognitive tasks. By coordinating theta oscillations with locomotor phases, VGluT2+ neurons likely enhance the precision of spatial coding in hippocampal circuits, facilitating navigation and memory consolidation. Altogether, these findings underscore the importance of VGluT2+ neurons as an interface between hippocampal spatial representation and motor planning circuits.

5.4 Broader Implications and Future Directions

Our in vivo study was performed in head-fixed animals, focusing on simple behavioral patterns outside of naturalistic environments. While this experimental approach yielded valuable insights, it also had limitations. Specifically, our study did not address the activity of the MSDB population during more complex behaviors, such as exploration, food-seeking, consumption, or defensive responses. These behaviors likely engage MSDB neurons differently than the limited paradigms we employed. An additional behavior of interest is rearing, which has been previously shown to involve MSDB VGluT2+ neuron activation (Mocellin et al., 2024). Due to the limitations of our experimental setup, we could not investigate all behavioral variables of interest.

Our study provides foundational insights into MSDB dynamics and their integration with hippocampal circuits. However, several questions remain open for future exploration. First, the causal roles of VGluT2+ neurons in specific behavioral paradigms should be examined using advanced techniques, such as Ca^{2+} imaging to monitor the same neurons across multiple behaviors, combined with optogenetic manipulations. These approaches could elucidate how VGluT2+ neuron activity supports locomotion, memory, and decision-making. Second, the interaction between intrinsic mechanisms and network dynamics underlying persistent activity warrants

further investigation. Computational models could clarify how synaptic inputs and neuromodulatory signals shape VGluT2+ neuron firing, providing a deeper understanding of their contributions to behavioral states. A particular focus on the role of cholinergic modulation could reveal how task-specific demands influence MSDB dynamics and downstream hippocampal activity.

From a translational perspective, the MSDB's role in regulating hippocampal dynamics suggests potential therapeutic applications. Dysfunction in MSDB circuits has been implicated in neurological and neuropsychiatric disorders such as epilepsy, anxiety, depression, and schizophrenia (Degroot & Treit, 2004; Takeuchi, Nagy, et al., 2021; Takeuchi, Harangozó, et al., 2021; Leung & Ma, 2022). Targeting MSDB activity through pharmacological or neuromodulatory interventions could provide new strategies for treating these conditions. Additionally, understanding how MSDB activity adapts to degenerative conditions, such as Alzheimer's disease, may inform interventions aimed at preserving spatial memory and cognitive flexibility. Also deeper understanding of locomotion initiation circuits could provide valuable insights that can help improve the lifestyle of the people with Parkinson's disease.

In summary, this study highlights the MSDB's multifaceted roles in coordinating neural and behavioral systems. By integrating findings on MSDB-driven locomotion, hippocampal dynamics, and persistent activity, this work lays the groundwork for future investigations into the broader implications of MSDB function in health and disease.

6. References

Adhikari, A., Topiwala, M. A., & Gordon, J. A. (2010). Synchronized Activity between the Ventral Hippocampus and the Medial Prefrontal Cortex during Anxiety. *Neuron*, *65*(2), 257–269. https://doi.org/10.1016/j.neuron.2009.12.002

Ain, B. R., Lubar, J. F., Moon, R. D., & Kulig, B. M. (1969). Effect of septal and neocortical damage on complex maze learning. *Physiology & Behavior*, *4*(2), 235–238. https://doi.org/10.1016/0031-9384(69)90085-7

Alreja, M. (1996). Excitatory actions of serotonin on GABAergic neurons of the medial septum and diagonal band of broca. *Synapse*, *22*(1), 15–27. https://doi.org/10.1002/(SICI)1098-2396(199601)22:1<15::AID-SYN2>3.0.CO;2-L

Amaral, D. G., & Kurz, J. (1985). An analysis of the origins of the cholinergic and noncholinergic septal projections to the hippocampal formation of the rat. *Journal of Comparative Neurology*, *240*(1), 37–59. https://doi.org/10.1002/cne.902400104

Amit, D. J., & Brunel, N. (1997). Model of global spontaneous activity and local structured activity during delay periods in the cerebral cortex. *Cerebral Cortex (New York, N.Y.: 1991)*, *7*(3), 237–252. https://doi.org/10.1093/cercor/7.3.237

An, S., Sun, H., Wu, M., Xie, D., Hu, S.-W., Ding, H.-L., & Cao, J.-L. (2021). Medial septum glutamatergic neurons control wakefulness through a septo-hypothalamic circuit. *Current Biology*, *31*(7), 1379-1392.e4. https://doi.org/10.1016/j.cub.2021.01.019

Anderson, R. W., & Strowbridge, B. W. (2014). Regulation of persistent activity in hippocampal mossy cells by inhibitory synaptic potentials. *Learning & Memory*, *21*(5), 263–271. https://doi.org/10.1101/lm.033829.113

Armstrong, D. M. (1986). Supraspinal contributions to the initiation and control of locomotion in the cat. *Progress in Neurobiology*, *26*(4), 273–361. https://doi.org/10.1016/0301-0082(86)90021-3

Armstrong, D. M., Saper, C. B., Levey, A. I., Wainer, B. H., & Terry, R. D. (1983). Distribution of cholinergic neurons in rat brain: Demonstrated by the immunocytochemical localization of choline acetyltransferase. *Journal of Comparative Neurology*, *216*(1), 53–68. https://doi.org/10.1002/cne.902160106

Barak, O., & Tsodyks, M. (2007). Persistent activity in neural networks with dynamic synapses. *PLoS Computational Biology*, *3*(2), e35. https://doi.org/10.1371/journal.pcbi.0030035

Barden, N., Mérand, Y., Rouleau, D., Moore, S., Dockray, G. J., & Dupont, A. (1981). Regional distributions of somatostatin and cholecystokinin-like immunoreactivities in rat and bovine brain. *Peptides*, *2*(3), 299–302. https://doi.org/10.1016/S0196-9781(81)80123-4

Beatty, J. (1982). Task-Evoked Pupillary Responses, Processing Load, and the Structure of Processing Resources. *Psychological Bulletin*, *91*(2), 276–292.

Berg, R. W., & Kleinfeld, D. (2003). Rhythmic whisking by rat: Retraction as well as protraction of the vibrissae is under active muscular control. *Journal of Neurophysiology*, *89*(1), 104–117. https://doi.org/10.1152/jn.00600.2002

Berger-Sweeney, J., Stearns, N. A., Murg, S. L., Floerke-Nashner, L. R., Lappi, D. A., & Baxter, M. G. (2001). Selective Immunolesions of Cholinergic Neurons in Mice: Effects on Neuroanatomy, Neurochemistry, and Behavior. *Journal of Neuroscience*, *21*(20), 8164–8173. https://doi.org/10.1523/JNEUROSCI.21-20-08164.2001

Berridge, C. W., & Waterhouse, B. D. (2003). The locus coeruleus-noradrenergic system: Modulation of behavioral state and state-dependent cognitive processes. *Brain Research. Brain Research Reviews*, *42*(1), 33–84. https://doi.org/10.1016/s0165-0173(03)00143-7

Biane, J. S., Ladow, M. A., Stefanini, F., Boddu, S. P., Fan, A., Hassan, S., Dundar, N., Apodaca-Montano, D. L., Zhou, L. Z., Fayner, V., Woods, N. I., & Kheirbek, M. A. (2023). Neural dynamics underlying associative learning in the dorsal and ventral hippocampus. *Nature Neuroscience*, *26*(5), 798–809. https://doi.org/10.1038/s41593-023-01296-6

Bittencourt, J. C., & Elias, C. F. (1998). Melanin-concentrating hormone and neuropeptide EI projections from the lateral hypothalamic area and zona incerta to the medial septal nucleus and spinal cord: A study using multiple neuronal tracers. *Brain Research*, *805*(1), 1–19. https://doi.org/10.1016/S0006-8993(98)00598-8

Bland, B. H., & Oddie, S. D. (2001). Theta band oscillation and synchrony in the hippocampal formation and associated structures: The case for its role in sensorimotor integration. *Behavioural Brain Research*, *127*(1–2), 119–136. https://doi.org/10.1016/S0166-4328(01)00358-8

Bortz, D. M., Feistritzer, C. M., Power, C. C., & Grace, A. A. (2022). Medial septum activation improves strategy switching once strategies are well-learned via bidirectional regulation of dopamine neuron population activity. *Neuropsychopharmacology*, *47*(12), 2090–2100. https://doi.org/10.1038/s41386-022-01387-1

Bott, J.-B., Robinson, J., Manseau, F., Gauthier-Lafrenière, E., & Williams, S. (2022). *Medial septum glutamate neurons are essential for spatial goal-directed memory* (p. 2022.03.16.484657). bioRxiv. https://doi.org/10.1101/2022.03.16.484657

Boyce, R., Glasgow, S. D., Williams, S., & Adamantidis, A. (2016). Causal evidence for the role of REM sleep theta rhythm in contextual memory consolidation. *Science*, *352*(6287), 812–816. https://doi.org/10.1126/science.aad5252

Bradshaw, J. (1967). Pupil Size as a Measure of Arousal during Information Processing. *Nature*, *216*(5114), 515–516. https://doi.org/10.1038/216515a0

Bramble, D. M., & Carrier, D. R. (1983). Running and Breathing in Mammals. *Science*, *219*(4582), 251–256. https://doi.org/10.1126/science.6849136

Brandon, M. P., Bogaard, A. R., Libby, C. P., Connerney, M. A., Gupta, K., & Hasselmo, M. E. (2011). Reduction of theta rhythm dissociates grid cell spatial periodicity from directional tuning. *Science (New York, N.Y.)*, *332*(6029), 595–599. https://doi.org/10.1126/science.1201652

Brioni, J. D., Decker, M. W., Gamboa, L. P., Izquierdo, I., & McGaugh, J. L. (1990). Muscimol injections in the medial septum impair spatial learning. *Brain Research*, *522*(2), 227–234. https://doi.org/10.1016/0006-8993(90)91465-S

Brown, G. E., & Remley, N. R. (1971). The effects of septal and olfactory bulb lesions on stimulus reactivity. *Physiology & Behavior*, *6*(5), 497–501. https://doi.org/10.1016/0031-9384(71)90196-x

Brudzynski, S. M., Wu, M., & Mogenson, G. J. (1993). Decreases in rat locomotor activity as a result of changes in synaptic transmission to neurons within the mesencephalic locomotor region. *Canadian Journal of Physiology and Pharmacology*, *71*(5–6), 394–406. https://doi.org/10.1139/y93-060

Burdakov, D., & Karnani, M. M. (2020). Ultra-sparse Connectivity within the Lateral Hypothalamus. *Current Biology: CB*, *30*(20), 4063-4070.e2. https://doi.org/10.1016/j.cub.2020.07.061

Busse, L. (2018). The influence of locomotion on sensory processing and its underlying neuronal circuits. *e-Neuroforum*, *24*(1), A41–A51. https://doi.org/10.1515/nf-2017-A046

Butcher, L. L., & Marchand, R. (1978). Dopamine neurons in pars compacta of the substantia nigra contain acetylcholinesterase: Histochemical correlations on the same brain section. *European Journal of Pharmacology*, *52*(3), 415–417. https://doi.org/10.1016/0014-2999(78)90301-1

Buzsáki, G. (1986). Hippocampal sharp waves: Their origin and significance. *Brain Research*, *398*(2), 242–252. https://doi.org/10.1016/0006-8993(86)91483-6

Buzsáki, G. (2002). Theta Oscillations in the Hippocampus. *Neuron*, *33*(3), 325–340. https://doi.org/10.1016/S0896-6273(02)00586-X

Caggiano, V., Leiras, R., Goñi-Erro, H., Masini, D., Bellardita, C., Bouvier, J., Caldeira, V., Fisone, G., & Kiehn, O. (2018). Midbrain circuits that set locomotor speed and gait selection. *Nature*, *553*(7689), 455–460. https://doi.org/10.1038/nature25448

Calandreau, L., Jaffard, R., & Desmedt, A. (2007). Dissociated roles for the lateral and medial septum in elemental and contextual fear conditioning. *Learning & Memory*, *14*(6), 422–429. https://doi.org/10.1101/lm.531407

Campbell, M. G., Ocko, S. A., Mallory, C. S., Low, I. I. C., Ganguli, S., & Giocomo, L. M. (2018). Principles governing the integration of landmark and self-motion cues in entorhinal cortical codes for navigation. *Nature Neuroscience*, *21*(8), 1096–1106. https://doi.org/10.1038/s41593-018-0189-y

Carvalho, M. M., Tanke, N., Kropff, E., Witter, M. P., Moser, M.-B., & Moser, E. I. (2020). A Brainstem Locomotor Circuit Drives the Activity of Speed Cells in the Medial Entorhinal Cortex. *Cell Reports*, *32*(10), 108123. https://doi.org/10.1016/j.celrep.2020.108123

Castañeda, M. T., Sanabria, E. R. G., Hernandez, S., Ayala, A., Reyna, T. A., Wu, J.-Y., & Colom, L. V. (2005). Glutamic acid decarboxylase isoforms are differentially distributed in the septal region of the rat. *Neuroscience Research*, *52*(1), 107–119. https://doi.org/10.1016/j.neures.2005.02.003

Cenquizca, L. A., & Swanson, L. W. (2007). Spatial organization of direct hippocampal field CA1 axonal projections to the rest of the cerebral cortex. *Brain Research Reviews*, *56*(1), 1–26. https://doi.org/10.1016/j.brainresrev.2007.05.002

Chakrabarti, S., Nambiar, J., & Schwarz, C. (2022). Adaptive Whisking in Mice. *Frontiers in Systems Neuroscience*, *15*. https://doi.org/10.3389/fnsys.2021.813311

Chen, G., King, J. A., Burgess, N., & O'Keefe, J. (2013). How vision and movement combine in the hippocampal place code. *Proceedings of the National Academy of Sciences*, *110*(1), 378–383. https://doi.org/10.1073/pnas.1215834110

Colom, L. V. (2006). Septal networks: Relevance to theta rhythm, epilepsy and Alzheimer's disease. *Journal of Neurochemistry*, *96*(3), 609–623. https://doi.org/10.1111/j.1471-4159.2005.03630.x

Colom, L. V., Castaneda, M. T., Reyna, T., Hernandez, S., & Garrido-sanabria, E. (2005). Characterization of medial septal glutamatergic neurons and their projection to the hippocampus. *Synapse*, *58*(3), 151–164. https://doi.org/10.1002/syn.20184

Compte, A. (2006). Computational and in vitro studies of persistent activity: Edging towards cellular and synaptic mechanisms of working memory. *Neuroscience*, *139*(1), 135–151. https://doi.org/10.1016/j.neuroscience.2005.06.011

Corkin, S. (1984). Lasting Consequences of Bilateral Medial Temporal Lobectomy: Clinical Course and Experimental Findings in H.M. *Seminars in Neurology*, *4*(02), 249–259. https://doi.org/10.1055/s-2008-1041556

Crochet, S., & Petersen, C. C. H. (2006). Correlating whisker behavior with membrane potential in barrel cortex of awake mice. *Nature Neuroscience*, *9*(5), 608–610. https://doi.org/10.1038/nn1690

Cui, G., Jun, S. B., Jin, X., Pham, M. D., Vogel, S. S., Lovinger, D. M., & Costa, R. M. (2013). Concurrent activation of striatal direct and indirect pathways during action initiation. *Nature*, *494*(7436), 238–242. https://doi.org/10.1038/nature11846

Czurkó, A., Hirase, H., Csicsvari, J., & Buzsáki, G. (1999). Sustained activation of hippocampal pyramidal cells by "space clamping" in a running wheel. *The European Journal of Neuroscience*, *11*(1), 344–352. https://doi.org/10.1046/j.1460-9568.1999.00446.x

da Silva, J. A., Tecuapetla, F., Paixão, V., & Costa, R. M. (2018). Dopamine neuron activity before action initiation gates and invigorates future movements. *Nature*, *554*(7691), 244–248. https://doi.org/10.1038/nature25457

Dadarlat, M. C., & Stryker, M. P. (2017). Locomotion Enhances Neural Encoding of Visual Stimuli in Mouse V1. *Journal of Neuroscience*, *37*(14), 3764–3775. https://doi.org/10.1523/JNEUROSCI.2728-16.2017

Dannenberg, H., Pabst, M., Braganza, O., Schoch, S., Niediek, J., Bayraktar, M., Mormann, F., & Beck, H. (2015). Synergy of direct and indirect cholinergic septo-hippocampal pathways coordinates firing in hippocampal networks. *The Journal of Neuroscience: The Official Journal of the Society for Neuroscience*, *35*(22), 8394–8410. https://doi.org/10.1523/JNEUROSCI.4460-14.2015

Degroot, A., & Treit, D. (2004). Anxiety is functionally segregated within the septo-hippocampal system. *Brain Research*, *1001*(1), 60–71. https://doi.org/10.1016/j.brainres.2003.10.065

Di Prisco, G. V., Pearlstein, E., Le Ray, D., Robitaille, R., & Dubuc, R. (2000). A Cellular Mechanism for the Transformation of a Sensory Input into a Motor Command. *The Journal of Neuroscience*, *20*(21), 8169–8176. https://doi.org/10.1523/JNEUROSCI.20-21-08169.2000

Duffet, L., Kosar, S., Panniello, M., Viberti, B., Bracey, E., Zych, A. D., Radoux-Mergault, A., Zhou, X., Dernic, J., Ravotto, L., Tsai, Y.-C., Figueiredo, M., Tyagarajan, S. K., Weber, B., Stoeber, M., Gogolla, N., Schmidt, M. H., Adamantidis, A. R., Fellin, T., … Patriarchi, T. (2022). A genetically encoded sensor for in vivo imaging of orexin neuropeptides. *Nature Methods*, *19*(2), 231–241. https://doi.org/10.1038/s41592-021-01390-2

Eggermann, E., Kremer, Y., Crochet, S., & Petersen, C. C. H. (2014). Cholinergic signals in mouse barrel cortex during active whisker sensing. *Cell Reports*, *9*(5), 1654–1660. https://doi.org/10.1016/j.celrep.2014.11.005

Eldar, E., Cohen, J. D., & Niv, Y. (2013). The effects of neural gain on attention and learning. *Nature Neuroscience*, *16*(8), 1146–1153. https://doi.org/10.1038/nn.3428

Elvander-Tottie, E., Eriksson, T. M., Sandin, J., & Ögren, S. O. (2006). N-methyl-d-aspartate receptors in the medial septal area have a role in spatial and emotional learning in the rat. *Neuroscience*, *142*(4), 963–978. https://doi.org/10.1016/j.neuroscience.2006.07.043

Espinosa, N., Caneo, M., Alonso, A., Moran, C., & Fuentealba, P. (2022). *Optogenetic stimulation of septal somatostatin neurons disrupts locomotory behavior and regulates hippocampus cholinergic theta oscillations* (p. 2022.09.30.510330). bioRxiv. https://doi.org/10.1101/2022.09.30.510330

Etienne, A. S., & Jeffery, K. J. (2004). Path integration in mammals. *Hippocampus*, *14*(2), 180–192. https://doi.org/10.1002/hipo.10173

Etter, G., van der Veldt, S., Choi, J., & Williams, S. (2023). Optogenetic frequency scrambling of hippocampal theta oscillations dissociates working memory retrieval from hippocampal spatiotemporal codes. *Nature Communications*, *14*(1), 410. https://doi.org/10.1038/s41467-023-35825-5

Fadda, F., Cocco, S., & Stancampiano, R. (2000). Hippocampal acetylcholine release correlates with spatial learning performance in freely moving rats. *NeuroReport*, *11*(10), 2265.

Fanselow, M. S., & Dong, H.-W. (2010). Are the Dorsal and Ventral Hippocampus Functionally Distinct Structures? *Neuron*, *65*(1), 7–19. https://doi.org/10.1016/j.neuron.2009.11.031

Ferreira-Pinto, M. J., Ruder, L., Capelli, P., & Arber, S. (2018). Connecting Circuits for Supraspinal Control of Locomotion. *Neuron*, *100*(2), 361–374. https://doi.org/10.1016/j.neuron.2018.09.015

Forloni, G., Grzanna, R., Blakely, R. D., & Coyle, J. T. (1987). Co-localization of N-acetyl-aspartyl-glutamate in central cholinergic, noradrenergic, and serotonergic neurons. *Synapse (New York, N.Y.)*, *1*(5), 455–460. https://doi.org/10.1002/syn.890010509

Franklin, K. B. J., & Paxinos, G. (2019). *Paxinos and Franklin's the Mouse Brain in Stereotaxic Coordinates, Compact: The Coronal Plates and Diagrams* (5th edition). Academic Press.

Fransén, E., Tahvildari, B., Egorov, A. V., Hasselmo, M. E., & Alonso, A. A. (2006). Mechanism of graded persistent cellular activity of entorhinal cortex layer v neurons. *Neuron*, *49*(5), 735–746. https://doi.org/10.1016/j.neuron.2006.01.036

Freund, T. F. (1989). GABAergic septohippocampal neurons contain parvalbumin. *Brain Research*, *478*(2), 375–381. https://doi.org/10.1016/0006-8993(89)91520-5

Freund, T. F., & Antal, M. (1988). GABA-containing neurons in the septum control inhibitory interneurons in the hippocampus. *Nature*, *336*(6195), 170–173. https://doi.org/10.1038/336170a0

Fu, Y., Tucciarone, J. M., Espinosa, J. S., Sheng, N., Darcy, D. P., Nicoll, R. A., Huang, Z. J., & Stryker, M. P. (2014). A Cortical Circuit for Gain Control by Behavioral State. *Cell*, *156*(6), 1139–1152. https://doi.org/10.1016/j.cell.2014.01.050

Fuhrmann, F., Justus, D., Sosulina, L., Kaneko, H., Beutel, T., Friedrichs, D., Schoch, S., Schwarz, M. K., Fuhrmann, M., & Remy, S. (2015). Locomotion, Theta Oscillations, and the Speed-Correlated Firing of Hippocampal Neurons Are Controlled by a Medial Septal Glutamatergic Circuit. *Neuron*, *86*(5), 1253–1264. https://doi.org/10.1016/j.neuron.2015.05.001

Funahashi, S., Bruce, C. J., & Goldman-Rakic, P. S. (1989). Mnemonic coding of visual space in the monkey's dorsolateral prefrontal cortex. *Journal of Neurophysiology, 61*(2), 331–349. https://doi.org/10.1152/jn.1989.61.2.331

Fuster, J. M. (1973). Unit activity in prefrontal cortex during delayed-response performance: Neuronal correlates of transient memory. *Journal of Neurophysiology*, *36*(1), 61–78. https://doi.org/10.1152/jn.1973.36.1.61

Garner, H. L., Whittington, M. A., & Henderson, Z. (2005). Induction by kainate of theta frequency rhythmic activity in the rat medial septum–diagonal band complex in vitro. *The Journal of Physiology*, *564*(1), 83–102. https://doi.org/10.1113/jphysiol.2004.080622

Garrido-Sanabria, E. R., Perez, M. G., Banuelos, C., Reyna, T., Hernandez, S., Castaneda, M. T., & Colom, L. V. (2007). Electrophysiological and morphological heterogeneity of slow firing neurons in medial septal/diagonal band complex as revealed by cluster analysis. *Neuroscience*, *146*(3), 931–945. https://doi.org/10.1016/j.neuroscience.2007.02.047

Gaspar, P., Berger, B., Lesur, A., Borsotti, J. P., & Febvret, A. (1987). Somatostatin 28 and neuropeptide Y innervation in the septal area and related cortical and subcortical structures of the human brain. Distribution, relationships and evidence for differential coexistence. *Neuroscience*, *22*(1), 49–73. https://doi.org/10.1016/0306-4522(87)90197-7

Girardeau, G., Benchenane, K., Wiener, S. I., Buzsáki, G., & Zugaro, M. B. (2009). Selective suppression of hippocampal ripples impairs spatial memory. *Nature Neuroscience*, *12*(10), 1222–1223. https://doi.org/10.1038/nn.2384

Goard, M., & Dan, Y. (2009). Basal forebrain activation enhances cortical coding of natural scenes. *Nature Neuroscience*, *12*(11), 1444–1449. https://doi.org/10.1038/nn.2402

Gogolák, G., Stumpf, C., Petsche, H., & Sterc, J. (1968). The firing pattern of septal neurons and the form of the hippocampal theta wave. *Brain Research*, *7*(2), 201–207. https://doi.org/10.1016/0006-8993(68)90098-x

Goldman-Rakic, P. S. (1995). Cellular basis of working memory. *Neuron*, *14*(3), 477–485. https://doi.org/10.1016/0896-6273(95)90304-6

Gothard, K. M., Skaggs, W. E., & McNaughton, B. L. (1996). Dynamics of Mismatch Correction in the Hippocampal Ensemble Code for Space: Interaction between Path Integration and Environmental Cues. *The Journal of Neuroscience*, *16*(24), 8027–8040. https://doi.org/10.1523/JNEUROSCI.16-24-08027.1996

Green, J. D., & Arduini, A. A. (1954). Hippocampal electrical activity in arousal. *Journal of Neurophysiology*, *17*(6), 533–557. https://doi.org/10.1152/jn.1954.17.6.533

Gritti, I., Manns, I. D., Mainville, L., & Jones, B. E. (2003). Parvalbumin, calbindin, or calretinin in cortically projecting and GABAergic, cholinergic, or glutamatergic basal forebrain neurons of the rat. *Journal of Comparative Neurology*, *458*(1), 11–31. https://doi.org/10.1002/cne.10505

Grujic, N., Tesmer, A., Bracey, E., Peleg-Raibstein, D., & Burdakov, D. (2023). Control and coding of pupil size by hypothalamic orexin neurons. *Nature Neuroscience*, *26*(7), 1160–1164. https://doi.org/10.1038/s41593-023-01365-w

Hagan, J. J., Salamone, J. D., Simpson, J., Iversen, S. D., & Morris, R. G. M. (1988). Place navigation in rats is impaired by lesions of medial septum and diagonal band but not nucleus basalis magnocellularis. *Behavioural Brain Research*, *27*(1), 9–20. Scopus. https://doi.org/10.1016/0166-4328(88)90105-2

Haghdoost-Yazdi, H., Pasbakhsh, P., Vatanparast, J., Rajaei, F., & Behzadi, G. (2009). Topographical and quantitative distribution of the projecting neurons to main divisions of the septal area. *Neurological Research*, *31*, 503–513. https://doi.org/10.1179/174313208X353712

Haj-Dahmane, S., & Andrade, R. (1996). Muscarinic Activation of a Voltage-Dependent Cation Nonselective Current in Rat Association Cortex. *Journal of Neuroscience*, *16*(12), 3848–3861. https://doi.org/10.1523/JNEUROSCI.16-12-03848.1996

Haj-Dahmane, S., & Andrade, R. (1999). Muscarinic receptors regulate two different calcium-dependent non-selective cation currents in rat prefrontal cortex. *The European Journal of Neuroscience*, *11*(6), 1973–1980. https://doi.org/10.1046/j.1460-9568.1999.00612.x

Hajszan, T., Alreja, M., & Leranth, C. (2004). Intrinsic vesicular glutamate transporter 2-immunoreactive input to septohippocampal parvalbumin-containing neurons: Novel glutamatergic local circuit cells. *Hippocampus*, *14*(4), 499–509. https://doi.org/10.1002/hipo.10195

Hallanger, A. E., & Wainer, B. H. (1988). Ascending projections from the pedunculopontine tegmental nucleus and the adjacent mesopontine tegmentum in the rat. *Journal of Comparative Neurology*, *274*(4), 483–515. https://doi.org/10.1002/cne.902740403

Hangya, B., Borhegyi, Z., Szilágyi, N., Freund, T. F., & Varga, V. (2009). GABAergic Neurons of the Medial Septum Lead the Hippocampal Network during Theta Activity. *Journal of Neuroscience*, *29*(25), 8094–8102. https://doi.org/10.1523/JNEUROSCI.5665-08.2009

Hangya, B., Ranade, S. P., Lorenc, M., & Kepecs, A. (2015). Central Cholinergic Neurons Are Rapidly Recruited by Reinforcement Feedback. *Cell*, *162*(5), 1155–1168. https://doi.org/10.1016/j.cell.2015.07.057

Harkany, T., Härtig, W., Berghuis, P., Dobszay, M. B., Zilberter, Y., Edwards, R. H., Mackie, K., & Ernfors, P. (2003). Complementary distribution of type 1 cannabinoid receptors and vesicular glutamate transporter 3 in basal forebrain suggests input-specific retrograde signalling by cholinergic neurons. *The European Journal of Neuroscience*, *18*(7), 1979–1992. https://doi.org/10.1046/j.1460-9568.2003.02898.x

Harris, K. D., & Thiele, A. (2011). Cortical state and attention. *Nature Reviews Neuroscience*, *12*(9), 509–523. https://doi.org/10.1038/nrn3084

Hart, E., & Huk, A. C. (2020). Recurrent circuit dynamics underlie persistent activity in the macaque frontoparietal network. *eLife*, *9*, e52460. https://doi.org/10.7554/eLife.52460

Harvey, J. A., & Lints, C. E. (1965). LESIONS IN THE MEDIAL FOREBRAIN BUNDLE: DELAYED EFFECTS ON SENSITIVITY TO ELECTRIC SHOCK. *Science (New York, N.Y.)*, *148*(3667), 250–252. https://doi.org/10.1126/science.148.3667.250

Hayat, A., & Feldman, S. (1974). Effects of sensory stimuli on single cell activity in the septum of the cat. *Experimental Neurology*, *43*(2), 298–313. https://doi.org/10.1016/0014-4886(74)90172-1

Henderson, Z., Lu, C. B., Janzsó, G., Matto, N., McKinley, C. E., Yanagawa, Y., & Halasy, K. (2010). Distribution and role of Kv3.1b in neurons in the medial septum diagonal band complex. *Neuroscience*, *166*(3), 952–969. https://doi.org/10.1016/j.neuroscience.2010.01.020

Henke, P. G. (1990). Hippocampal pathway to the amygdala and stress ulcer development. *Brain Research Bulletin*, *25*(5), 691–695. https://doi.org/10.1016/0361-9230(90)90044-Z

Hepler, D. J., Wenk, G. L., Cribbs, B. L., Olton, D. S., & Coyle, J. T. (1985). Memory impairments following basal forebrain lesions. *Brain Research*, *346*(1), 8–14. https://doi.org/10.1016/0006-8993(85)91088-1

Herkenham, M., & Nauta, W. J. (1979). Efferent connections of the habenular nuclei in the rat. *The Journal of Comparative Neurology*, *187*(1), 19–47. https://doi.org/10.1002/cne.901870103

Herman, A. M., Ortiz-Guzman, J., Kochukov, M., Herman, I., Quast, K. B., Patel, J. M., Tepe, B., Carlson, J. C., Ung, K., Selever, J., Tong, Q., & Arenkiel, B. R. (2016). A cholinergic basal forebrain feeding circuit modulates appetite suppression. *Nature*, *538*(7624), 253–256. https://doi.org/10.1038/nature19789

Herz, A., & Gogolák, G. (1965). Mikroelektrophoretische Untersuchungen am Septum des Kaninchens. *Pflüger's Archiv für die gesamte Physiologie des Menschen und der Tiere*, *285*(4), 317–330. https://doi.org/10.1007/BF00363232

Hess, E. H., & Polt, J. M. (1964). Pupil Size in Relation to Mental Activity during Simple Problem-Solving. *Science*, *143*(3611), 1190–1192. https://doi.org/10.1126/science.143.3611.1190

Himmelheber, A. M., Sarter, M., & Bruno, J. P. (2000). Increases in cortical acetylcholine release during sustained attention performance in rats. *Cognitive Brain Research*, *9*(3), 313–325. https://doi.org/10.1016/S0926-6410(00)00012-4

Hitti, F. L., & Siegelbaum, S. A. (2014). The hippocampal CA2 region is essential for social memory. *Nature*, *508*(7494), 88–92. https://doi.org/10.1038/nature13028

Howe, M. W., & Dombeck, D. A. (2016). Rapid signalling in distinct dopaminergic axons during locomotion and reward. *Nature*, *535*(7613), 505–510. https://doi.org/10.1038/nature18942

Hu, W., Li, Q., Li, B., Ma, K., Zhang, C., & Fu, X. (2020). Optogenetics sheds new light on tissue engineering and regenerative medicine. *Biomaterials*, *227*, 119546. https://doi.org/10.1016/j.biomaterials.2019.119546

Hughes, S. W., Cope, D. W., Tóth, T. I., Williams, S. R., & Crunelli, V. (1999). All thalamocortical neurones possess a T-type Ca2+'window' current that enables the expression of bistability-mediated activities. *The Journal of Physiology*, *517*(3), 805–815. https://doi.org/10.1111/j.1469-7793.1999.0805s.x

Huh, C. Y. L., Goutagny, R., & Williams, S. (2010). Glutamatergic neurons of the mouse medial septum and diagonal band of Broca synaptically drive hippocampal pyramidal cells: Relevance for hippocampal theta rhythm. *The Journal of Neuroscience: The Official Journal of the Society for Neuroscience*, *30*(47), 15951–15961. https://doi.org/10.1523/JNEUROSCI.3663-10.2010

Ikemoto, S. (2005). The supramammillary nucleus mediates primary reinforcement via GABA(A) receptors. *Neuropsychopharmacology: Official Publication of the American College of Neuropsychopharmacology*, *30*(6), 1088–1095. https://doi.org/10.1038/sj.npp.1300660

Ikemoto, S., Qin, M., & Liu, Z.-H. (2006). Primary Reinforcing Effects of Nicotine Are Triggered from Multiple Regions Both Inside and Outside the Ventral Tegmental Area. *Journal of Neuroscience*, *26*(3), 723–730. https://doi.org/10.1523/JNEUROSCI.4542-05.2006

Ikemoto, S., Witkin, B. M., Zangen, A., & Wise, R. A. (2004). Rewarding Effects of AMPA Administration into the Supramammillary or Posterior Hypothalamic Nuclei But Not the Ventral Tegmental Area. *Journal of Neuroscience*, *24*(25), 5758–5765. https://doi.org/10.1523/JNEUROSCI.5367-04.2004

Inagaki, H. K., Fontolan, L., Romani, S., & Svoboda, K. (2019). Discrete attractor dynamics underlies persistent activity in the frontal cortex. *Nature*, *566*(7743), 212–217. https://doi.org/10.1038/s41586-019-0919-7

Iriki, A., Tanaka, M., & Iwamura, Y. (1996). Attention-induced neuronal activity in the monkey somatosensory cortex revealed by pupillometrics. *Neuroscience Research*, *25*(2), 173–181. https://doi.org/10.1016/0168-0102(96)01043-7

Ito, H. T., Moser, E. I., & Moser, M.-B. (2018). Supramammillary Nucleus Modulates Spike-Time Coordination in the Prefrontal-Thalamo-Hippocampal Circuit during Navigation. *Neuron*, *99*(3), 576-587.e5. https://doi.org/10.1016/j.neuron.2018.07.021

Jacob, P.-Y., Gordillo-Salas, M., Facchini, J., Poucet, B., Save, E., & Sargolini, F. (2017). Medial entorhinal cortex and medial septum contribute to self-motion-based linear distance estimation. *Brain Structure & Function*, *222*(6), 2727–2742. https://doi.org/10.1007/s00429-017-1368-4

Jarzebowski, P., Tang, C. S., Paulsen, O., & Hay, Y. A. (2021). Impaired spatial learning and suppression of sharp wave ripples by cholinergic activation at the goal location. *eLife*, *10*, e65998. https://doi.org/10.7554/eLife.65998

Jayakumar, R. P., Madhav, M. S., Savelli, F., Blair, H. T., Cowan, N. J., & Knierim, J. J. (2019). Recalibration of path integration in hippocampal place cells. *Nature*, *566*(7745), 533–537. https://doi.org/10.1038/s41586-019-0939-3

Ji, H., & Shepard, P. D. (2007). Lateral habenula stimulation inhibits rat midbrain dopamine neurons through a GABAA receptor-mediated mechanism. *Journal of Neuroscience*, *27*(26), 6923–6930. Scopus. https://doi.org/10.1523/JNEUROSCI.0958-07.2007

Jo, Y.-H., Talmage, D. A., & Role, L. W. (2002). Nicotinic receptor-mediated effects on appetite and food intake. *Journal of Neurobiology*, *53*(4), 618–632. https://doi.org/10.1002/neu.10147

Jochems, A., & Yoshida, M. (2015). A Robust In Vivo-Like Persistent Firing Supported by a Hybrid of Intracellular and Synaptic Mechanisms. *PLOS ONE*, *10*(4), e0123799. https://doi.org/10.1371/journal.pone.0123799

Joshi, A., Denovellis, E. L., Mankili, A., Meneksedag, Y., Davidson, T. J., Gillespie, A. K., Guidera, J. A., Roumis, D., & Frank, L. M. (2023). Dynamic synchronization between hippocampal representations and stepping. *Nature*, *617*(7959), 125–131. https://doi.org/10.1038/s41586-023-05928-6

Joshi, A., Salib, M., Viney, T. J., Dupret, D., & Somogyi, P. (2017). Behavior-Dependent Activity and Synaptic Organization of Septo-hippocampal GABAergic Neurons Selectively Targeting the Hippocampal CA3 Area. *Neuron*, *6*(96), 1342-1357.e5. https://doi.org/10.1016/j.neuron.2017.10.033

Joshi, A., & Somogyi, P. (2020). Changing phase relationship of the stepping rhythm to neuronal oscillatory theta activity in the septo-hippocampal network of mice. *Brain Structure & Function*, *225*(2), 871–879. https://doi.org/10.1007/s00429-020-02031-8

Joshi, S., Li, Y., Kalwani, R. M., & Gold, J. I. (2016). Relationships between Pupil Diameter and Neuronal Activity in the Locus Coeruleus, Colliculi, and Cingulate Cortex. *Neuron*, *89*(1), 221–234. https://doi.org/10.1016/j.neuron.2015.11.028

Jung, M. W., Wiener, S. I., & McNaughton, B. L. (1994). Comparison of spatial firing characteristics of units in dorsal and ventral hippocampus of the rat. *Journal of Neuroscience*, *14*(12), 7347–7356. https://doi.org/10.1523/JNEUROSCI.14-12-07347.1994

Justus, D., Dalügge, D., Bothe, S., Fuhrmann, F., Hannes, C., Kaneko, H., Friedrichs, D., Sosulina, L., Schwarz, I., Elliott, D. A., Schoch, S., Bradke, F., Schwarz, M. K., & Remy, S. (2017). Glutamatergic synaptic integration of locomotion speed via septoentorhinal projections. *Nature Neuroscience*, *20*(1), 16–19. https://doi.org/10.1038/nn.4447

Kaneko, M., Fu, Y., & Stryker, M. P. (2017). Locomotion Induces Stimulus-Specific Response Enhancement in Adult Visual Cortex. *The Journal of Neuroscience*, *37*(13), 3532–3543. https://doi.org/10.1523/JNEUROSCI.3760-16.2017

Karnani, M. M., Schöne, C., Bracey, E. F., González, J. A., Viskaitis, P., Li, H.-T., Adamantidis, A., & Burdakov, D. (2020). Role of spontaneous and sensory orexin network dynamics in rapid locomotion initiation. *Progress in Neurobiology*, *187*, 101771. https://doi.org/10.1016/j.pneurobio.2020.101771

Kennedy, A., Kunwar, P. S., Li, L.-Y., Stagkourakis, S., Wagenaar, D. A., & Anderson, D. J. (2020). Stimulus-specific hypothalamic encoding of a persistent defensive state. *Nature*, *586*(7831), 730–734. https://doi.org/10.1038/s41586-020-2728-4

Kesner, A. J., Shin, R., Calva, C. B., Don, R. F., Junn, S., Potter, C. T., Ramsey, L. A., Abou-Elnaga, A. F., Cover, C. G., Wang, D. V., Lu, H., Yang, Y., & Ikemoto, S. (2021). Supramammillary neurons projecting to the septum regulate dopamine and motivation for environmental interaction in mice. *Nature Communications*, *12*(1), Article 1. https://doi.org/10.1038/s41467-021-23040-z

Kiehn, O., & Dougherty, K. (2013). Locomotion: Circuits and physiology. In *Neuroscience in the 21st Century* (pp. 1209–1236). Springer. https://doi.org/10.1007/978-1-4614-1997-6_42

King, C., Recce, M., & O'Keefe, J. (1998). The rhythmicity of cells of the medial septum/diagonal band of Broca in the awake freely moving rat: Relationships with behaviour and hippocampal theta. *European Journal of Neuroscience*, *10*(2), 464–477. https://doi.org/10.1046/j.1460-9568.1998.00026.x

Király, B., Domonkos, A., Jelitai, M., Lopes-dos-Santos, V., Martínez-Bellver, S., Kocsis, B., Schlingloff, D., Joshi, A., Salib, M., Fiáth, R., Barthó, P., Ulbert, I., Freund, T. F., Viney, T. J., Dupret, D., Varga, V., & Hangya, B. (2023). The medial septum controls hippocampal supra-theta oscillations. *Nature Communications*, *14*(1), Article 1. https://doi.org/10.1038/s41467-023-41746-0

Kirk, I. J., & McNaughton, N. (1991). Supramammillary cell firing and hippocampal rhythmical slow activity. *Neuroreport*, *2*(11), 723–725. https://doi.org/10.1097/00001756-199111000-00023

Kjelstrup, K. B., Solstad, T., Brun, V. H., Hafting, T., Leutgeb, S., Witter, M. P., Moser, E. I., & Moser, M.-B. (2008). Finite Scale of Spatial Representation in the Hippocampus. *Science*, *321*(5885), 140–143. https://doi.org/10.1126/science.1157086

Knauer, B., Jochems, A., Valero-Aracama, M. J., & Yoshida, M. (2013). Long-lasting intrinsic persistent firing in rat CA1 pyramidal cells: A possible mechanism for active maintenance of memory. *Hippocampus*, *23*(9), 820–831. https://doi.org/10.1002/hipo.22136

Knox, D., & Keller, S. M. (2016). Cholinergic neuronal lesions in the medial septum and vertical limb of the diagonal bands of Broca induce contextual fear memory generalization and impair acquisition of fear extinction. *Hippocampus*, *26*(6), 718–726. https://doi.org/10.1002/hipo.22553

Kocsis, B., & Kaminski, M. (2006). Dynamic changes in the direction of the theta rhythmic drive between supramammillary nucleus and the septohippocampal system. *Hippocampus*, *16*(6), 531–540. https://doi.org/10.1002/hipo.20180

Kocsis, B., & Li, S. (2004). In vivo contribution of h-channels in the septal pacemaker to theta rhythm generation. *The European Journal of Neuroscience*, *20*(8), 2149–2158. https://doi.org/10.1111/j.1460-9568.2004.03678.x

Kocsis, B., Martínez-Bellver, S., Fiáth, R., Domonkos, A., Sviatkó, K., Schlingloff, D., Barthó, P., Freund, T. F., Ulbert, I., Káli, S., Varga, V., & Hangya, B. (2022). Huygens synchronization of medial septal pacemaker neurons generates hippocampal theta oscillation. *Cell Reports*, *40*(5), 111149. https://doi.org/10.1016/j.celrep.2022.111149

Kocsis, B., & Vertes, R. P. (1997). Phase relations of rhythmic neuronal firing in the supramammillary nucleus and mammillary body to the hippocampal theta activity in urethane anesthetized rats. *Hippocampus*, *7*(2), 204–214. https://doi.org/10.1002/(SICI)1098-1063(1997)7:2<204::AID-HIPO7>3.0.CO;2-M

Koenig, J., Linder, A. N., Leutgeb, J. K., & Leutgeb, S. (2011). The spatial periodicity of grid cells is not sustained during reduced theta oscillations. *Science (New York, N.Y.)*, *332*(6029), 592–595. https://doi.org/10.1126/science.1201685

Köhler, C., & Eriksson, L. G. (1984). An immunohistochemical study of somatostatin and neurotensin positive neurons in the septal nuclei of the rat brain. *Anatomy and Embryology*, *170*(1), 1–10. https://doi.org/10.1007/BF00319452

Konopacki, J., MacIver, M. B., Bland, B. H., & Roth, S. H. (1987). Carbachol-induced EEG "theta" activity in hippocampal brain slices. *Brain Research*, *405*(1), 196–198. https://doi.org/10.1016/0006-8993(87)91009-2

Korotkova, T., Ponomarenko, A., Monaghan, C. K., Poulter, S. L., Cacucci, F., Wills, T., Hasselmo, M. E., & Lever, C. (2018). Reconciling the different faces of hippocampal theta: The role of theta oscillations in cognitive, emotional and innate behaviors. *Neuroscience and Biobehavioral Reviews*, *85*, 65–80. https://doi.org/10.1016/j.neubiorev.2017.09.004

Kramis, R., Vanderwolf, C. H., & Bland, B. H. (1975). Two types of hippocampal rhythmical slow activity in both the rabbit and the rat: Relations to behavior and effects of atropine, diethyl ether, urethane, and pentobarbital. *Experimental Neurology*, *49*(1 Pt 1), 58–85. https://doi.org/10.1016/0014-4886(75)90195-8

Kropff, E., Carmichael, J. E., Moser, M.-B., & Moser, E. I. (2015). Speed cells in the medial entorhinal cortex. *Nature*, *523*(7561), 419–424. https://doi.org/10.1038/nature14622

Kuhn, F., Mocellin, P., Pupe, S., Wang, L., Lemire, A. L., Sosulina, L., Barnstedt, O., Spruston, N., Cembrowski, M. S., & Remy, S. (2024). *Neuronal heterogeneity in the medial septum and diagonal band of Broca: Classes and continua* (p. 2024.08.27.609593). bioRxiv. https://doi.org/10.1101/2024.08.27.609593

Lamour, Y., Dutar, P., & Jobert, A. (1984). Septo-hippocampal and other medial septum-diagonal band neurons: Electrophysiological and pharmacological properties. *Brain Research*, *309*, 217–226. https://doi.org/10.1016/0006-8993(84)90588-2

Lawson, V. H., & Bland, B. H. (1993). The role of the septohippocampal pathway in the regulation of hippocampal field activity and behavior: Analysis by the intraseptal microinfusion of carbachol, atropine, and procaine. *Experimental Neurology*, *120*(1), 132–144. https://doi.org/10.1006/exnr.1993.1047

Leão, R. N., Targino, Z. H., Colom, L. V., & Fisahn, A. (2015). Interconnection and synchronization of neuronal populations in the mouse medial septum/diagonal band of Broca. *Journal of Neurophysiology*, *113*(3), 971–980. https://doi.org/10.1152/jn.00367.2014

Lee, E. H. Y., Lin, Y. P., & Yin, T. H. (1988). Effects of lateral and medial septal lesions on various activity and reactivity measures in rats. *Physiology & Behavior*, *42*(1), 97–102. https://doi.org/10.1016/0031-9384(88)90267-3

Lee, M. G., Chrobak, J. J., Sik, A., Wiley, R. G., & Buzsáki, G. (1994). Hippocampal theta activity following selective lesion of the septal cholinergic system. *Neuroscience*, *62*(4), 1033–1047. https://doi.org/10.1016/0306-4522(94)90341-7

Lei, Y.-T., Thuault, S. J., Launay, P., Margolskee, R. F., Kandel, E. R., & Siegelbaum, S. A. (2014). Differential contribution of TRPM4 and TRPM5 nonselective cation channels to the slow afterdepolarization in mouse prefrontal cortex neurons. *Frontiers in Cellular Neuroscience*, *8*. https://doi.org/10.3389/fncel.2014.00267

Leranth, C., & Frotscher, M. (1989). Organization of the septal region in the rat brain: Cholinergic-GABAergic interconnections and the termination of hippocampo-septal fibers. *Journal of Comparative Neurology*, *289*(2), 304–314. https://doi.org/10.1002/cne.902890210

Leung, L. S., & Ma, J. (2022). Medial Septum Modulates Consciousness and Psychosis-Related Behaviors Through Hippocampal Gamma Activity. *Frontiers in Neural Circuits*, *16*. https://doi.org/10.3389/fncir.2022.895000

Li, N., Daie, K., Svoboda, K., & Druckmann, S. (2016). Robust neuronal dynamics in premotor cortex during motor planning. *Nature*, *532*(7600), 459–464. https://doi.org/10.1038/nature17643

Li, X., Yu, H., Zhang, B., Li, L., Chen, W., Yu, Q., Huang, X., Ke, X., Wang, Y., Jing, W., Du, H., Li, H., Zhang, T., Liu, L., Zhu, L.-Q., & Lu, Y. (2022). Molecularly defined and functionally distinct cholinergic subnetworks. *Neuron*, *110*(22), 3774-3788.e7. https://doi.org/10.1016/j.neuron.2022.08.025

Lin, W., McKinney, K., Liu, L., Lakhlani, S., & Jennes, L. (2003). Distribution of Vesicular Glutamate Transporter-2 Messenger Ribonucleic Acid and Protein in the Septum-Hypothalamus of the Rat. *Endocrinology*, *144*(2), 662–670. https://doi.org/10.1210/en.2002-220908

Liu, D., Li, W., Ma, C., Zheng, W., Yao, Y., Tso, C. F., Zhong, P., Chen, X., Song, J. H., Choi, W., Paik, S.-B., Han, H., & Dan, Y. (2020). A common hub for sleep and motor control in the substantia nigra. *Science*, *367*(6476), 440–445. https://doi.org/10.1126/science.aaz0956

Lorens, S. A., & Brown, T. S. (1967). Influence of stimulation of the septal area on visual evoked potentials. *Experimental Neurology*, *17*(1), 86–90. https://doi.org/10.1016/0014-4886(67)90124-0

Loureiro, M., Lecourtier, L., Engeln, M., Lopez, J., Cosquer, B., Geiger, K., Kelche, C., Cassel, J.-C., & Pereira de Vasconcelos, A. (2012). The ventral hippocampus is necessary for expressing a spatial memory. *Brain Structure & Function*, *217*(1), 93–106. https://doi.org/10.1007/s00429-011-0332-y

Lu, C. B., Ouyang, G., Henderson, Z., & Li, X. (2011). Induction of θ-frequency oscillations in the rat medial septal diagonal band slice by metabotropic glutamate receptor agonists. *Neuroscience*, *177*, 1–11. https://doi.org/10.1016/j.neuroscience.2011.01.004

Manseau, F., Danik, M., & Williams, S. (2005). A functional glutamatergic neurone network in the medial septum and diagonal band area. *The Journal of Physiology*, *566*. https://doi.org/10.1113/jphysiol.2005.089664

Markram, H., & Segal, M. (1990). Electrophysiological characteristics of cholinergic and non-cholinergic neurons in the rat medial septum-diagonal band complex. *Brain Research*, *513*(1), 171–174. https://doi.org/10.1016/0006-8993(90)91106-Q

Matsumoto, M., & Hikosaka, O. (2007). Lateral habenula as a source of negative reward signals in dopamine neurons. *Nature*, *447*(7148), 1111–1115. https://doi.org/10.1038/nature05860

McGinley, M. J., David, S. V., & McCormick, D. A. (2015). Cortical Membrane Potential Signature of Optimal States for Sensory Signal Detection. *Neuron*, *87*(1), 179–192. https://doi.org/10.1016/j.neuron.2015.05.038

McNaughton, B. L., Battaglia, F. P., Jensen, O., Moser, E. I., & Moser, M.-B. (2006). Path integration and the neural basis of the "cognitive map." *Nature Reviews Neuroscience*, *7*(8), 663–678. https://doi.org/10.1038/nrn1932

Mikulovic, S., Restrepo, C. E., Siwani, S., Bauer, P., Pupe, S., Tort, A. B. L., Kullander, K., & Leão, R. N. (2018). Ventral hippocampal OLM cells control type 2 theta oscillations and response to predator odor. *Nature Communications*, *9*(1), 3638. https://doi.org/10.1038/s41467-018-05907-w

Mishima, K., Iwasaki, K., Tsukikawa, H., Matsumoto, Y., Egashira, N., Abe, K., Egawa, T., & Fujiwara, M. (2000). The Scopolamine-Induced Impairment of Spatial Cognition Parallels the Acetylcholine Release in the Ventral Hippocampus in Rats. *Japanese Journal of Pharmacology*, *84*(2), 163–173. https://doi.org/10.1254/jjp.84.163

Missault, S., De Waegenaere, S., Kosten, L., Van der Linden, A., Verhoye, M., & Keliris, G. (2022). *Selective cholinergic stimulation of the medial septum-diagonal band of Broca via DREADDs improves spatial learning in healthy rat*. https://doi.org/10.1101/2022.08.02.502516

Mitchell, S. J., Rawlins, J. N., Steward, O., & Olton, D. S. (1982). Medial septal area lesions disrupt theta rhythm and cholinergic staining in medial entorhinal cortex and produce impaired radial arm maze behavior in rats. *Journal of Neuroscience*, *2*(3), 292–302. https://doi.org/10.1523/JNEUROSCI.02-03-00292.1982

Mitsukawa, K., Lu, X., & Bartfai, T. (2010). Galanin, Galanin Receptors, and Drug Targets. In T. Hökfelt (Ed.), *Galanin* (pp. 7–23). Springer. https://doi.org/10.1007/978-3-0346-0228-0_2

Mocellin, P., Barnstedt, O., Luxem, K., Kaneko, H., Vieweg, S., Henschke, J. U., Dalügge, D., Fuhrmann, F., Karpova, A., Pakan, J. M. P., Kreutz, M. R., Mikulovic, S., & Remy, S. (2024). A septal-ventral tegmental area circuit drives exploratory behavior. *Neuron*, *112*(6), 1020-1032.e7. https://doi.org/10.1016/j.neuron.2023.12.016

Mocellin, P., & Mikulovic, S. (2021). The Role of the Medial Septum-Associated Networks in Controlling Locomotion and Motivation to Move. *Frontiers in Neural Circuits*, *15*, 699798. https://doi.org/10.3389/fncir.2021.699798

Mori, S. (1990). Naurophysiology of locomotion: Recent advances in the studies of posture and locomotion in cats. バイオメカニズム学会誌, *14*(Special), 9–25. https://doi.org/10.3951/sobim.14.9

Morris, N. P., Fyffe, R. E. W., & Robertson, B. (2004). Characterisation of hyperpolarization-activated currents (I(h)) in the medial septum/diagonal band complex in the mouse. *Brain Research*, *1006*(1), 74–86. https://doi.org/10.1016/j.brainres.2004.01.062

Moser, E. I. (1995). Learning-related changes in hippocampal field potentials. *Behavioural Brain Research*, *71*(1), 11-IN1. https://doi.org/10.1016/0166-4328(95)00051-8

Müller, C., & Remy, S. (2018). Septo–hippocampal interaction. *Cell and Tissue Research*, *373*(3), 565–575. https://doi.org/10.1007/s00441-017-2745-2

Nachstedt, T., & Tetzlaff, C. (2017). Working Memory Requires a Combination of Transient and Attractor-Dominated Dynamics to Process Unreliably Timed Inputs. *Scientific Reports*, *7*(1), 2473. https://doi.org/10.1038/s41598-017-02471-z

Navaroli, V. L., Zhao, Y., Boguszewski, P., & Brown, T. H. (2012). Muscarinic receptor activation enables persistent firing in pyramidal neurons from superficial layers of dorsal perirhinal cortex. *Hippocampus*, *22*(6), 1392–1404. https://doi.org/10.1002/hipo.20975

Neale, J. H., Bzdega, T., & Wroblewska, B. (2000). N-Acetylaspartylglutamate: The most abundant peptide neurotransmitter in the mammalian central nervous system. *Journal of Neurochemistry*, *75*(2), 443–452. https://doi.org/10.1046/j.1471-4159.2000.0750443.x

Niederschuh, S. J., Witte, H., & Schmidt, M. (2015). The role of vibrissal sensing in forelimb position control during travelling locomotion in the rat (*Rattus norvegicus*, Rodentia). *Zoology*, *118*(1), 51–62. https://doi.org/10.1016/j.zool.2014.09.003

Niell, C. M., & Stryker, M. P. (2010). Modulation of Visual Responses by Behavioral State in Mouse Visual Cortex. *Neuron*, *65*(4), 472–479. https://doi.org/10.1016/j.neuron.2010.01.033

O'Keefe, J., & Burgess, N. (1996). Geometric determinants of the place fields of hippocampal neurons. *Nature*, *381*(6581), 425–428. https://doi.org/10.1038/381425a0

O'Keefe, J., & Dostrovsky, J. (1971). The hippocampus as a spatial map. Preliminary evidence from unit activity in the freely-moving rat. *Brain Research*, *34*(1), 171–175. https://doi.org/10.1016/0006-8993(71)90358-1

O'Keefe, J., & Nadel, L. (1979). The cognitive map as a hippocampus. *Behavioral and Brain Sciences*, *2*(4), 520–533. https://doi.org/10.1017/S0140525X00064256

O'Keefe, J., & Recce, M. L. (1993). Phase relationship between hippocampal place units and the EEG theta rhythm. *Hippocampus*, *3*(3), 317–330. https://doi.org/10.1002/hipo.450030307

Okuyama, T., Kitamura, T., Roy, D. S., Itohara, S., & Tonegawa, S. (2016). Ventral CA1 neurons store social memory. *Science (New York, N.Y.)*, *353*(6307), 1536–1541. https://doi.org/10.1126/science.aaf7003

O'Malley, J. J., Seibt, F., Chin, J., & Beierlein, M. (2020). TRPM4 Conductances in Thalamic Reticular Nucleus Neurons Generate Persistent Firing during Slow Oscillations. *Journal of Neuroscience*, *40*(25), 4813–4823. https://doi.org/10.1523/JNEUROSCI.0324-20.2020

Ortiz-Guzman, J., Swanson, J. L., Tantry, E. K., Kochukov, M., Ung, K., Addison, A. P., Srivastava, S., Belfort, B. D., Ji, E., Dooling, S. W., Chen, S. A., Tong, Q., & Arenkiel, B. R. (2024). Cholinergic Basal Forebrain Connectivity to the Basolateral Amygdala Modulates Food Intake. *eNeuro*, *11*(3). https://doi.org/10.1523/ENEURO.0369-23.2024

Otsuka, T., Murakami, F., & Song, W.-J. (2001). Excitatory Postsynaptic Potentials Trigger a Plateau Potential in Rat Subthalamic Neurons at Hyperpolarized States. *Journal of Neurophysiology*, *86*(4), 1816–1825. https://doi.org/10.1152/jn.2001.86.4.1816

Pachitariu, M., Sridhar, S., Pennington, J., & Stringer, C. (2024). Spike sorting with Kilosort4. *Nature Methods*, *21*(5), 914–921. https://doi.org/10.1038/s41592-024-02232-7

Pang, K. C. H., Jiao, X., Sinha, S., Beck, K. D., & Servatius, R. J. (2011). Damage of GABAergic neurons in the medial septum impairs spatial working memory and extinction of active avoidance: Effects on proactive interference. *Hippocampus*, *21*(8), 835–846. https://doi.org/10.1002/hipo.20799

Panula, P., Revuelta, A. V., Cheney, D. L., Wu, J.-Y., & Costa, E. (1984). An immunohistochemical study on the location of GABAergic neurons in rat septum. *Journal of Comparative Neurology*, *222*(1), 69–80. https://doi.org/10.1002/cne.902220107

Paxinos, G., Watson, C. R. R., & Emson, P. C. (1980). AChE-stained horizontal sections of the rat brain in stereotaxic coordinates. *Journal of Neuroscience Methods*, *3*(2), 129–149. https://doi.org/10.1016/0165-0270(80)90021-7

Petsche, H., Gogolak, G., & van Zwieten, P. A. (1965). Rhythmicity of septal cell discharges at various levels of reticular excitation. *Electroencephalography and Clinical Neurophysiology*, *19*(1), 25–33. https://doi.org/10.1016/0013-4694(65)90004-0

Petsche, H., Stumpf, Ch., & Gogolak, G. (1962). The significance of the rabbit's septum as a relay station between the midbrain and the hippocampus I. The control of hippocampus arousal activity by the septum cells. *Electroencephalography and Clinical Neurophysiology*, *14*(2), 202–211. https://doi.org/10.1016/0013-4694(62)90030-5

Petty, G. H., Kinnischtzke, A. K., Hong, Y. K., & Bruno, R. M. (2021). Effects of arousal and movement on secondary somatosensory and visual thalamus. *eLife*, *10*, e67611. https://doi.org/10.7554/eLife.67611

Petzold, A., van den Munkhof, H. E., Figge-Schlensok, R., & Korotkova, T. (2023). Complementary lateral hypothalamic populations resist hunger pressure to balance nutritional and social needs. *Cell Metabolism*, *35*(3), 456-471.e6. https://doi.org/10.1016/j.cmet.2023.02.008

Peyron, C., Tighe, D. K., van den Pol, A. N., de Lecea, L., Heller, H. C., Sutcliffe, J. G., & Kilduff, T. S. (1998). Neurons containing hypocretin (orexin) project to multiple neuronal systems. *The Journal of Neuroscience: The Official Journal of the Society for Neuroscience*, *18*(23), 9996–10015. https://doi.org/10.1523/JNEUROSCI.18-23-09996.1998

Pickel, V. M., Segal, M., & Bloom, F. E. (1974). A radioautographic study of the efferent pathways of the nucleus locus coeruleus. *Journal of Comparative Neurology*, *155*(1), 15–41. https://doi.org/10.1002/cne.901550103

Pimpinella, D., Mastrorilli, V., Giorgi, C., Coemans, S., Lecca, S., Lalive, A. L., Ostermann, H., Fuchs, E. C., Monyer, H., Mele, A., Cherubini, E., & Griguoli, M. (2021). Septal cholinergic input to CA2 hippocampal region controls social novelty discrimination via nicotinic receptor-mediated disinhibition. *eLife*, *10*, e65580. https://doi.org/10.7554/eLife.65580

Pressler, R. T., & Strowbridge, B. W. (2006). Blanes Cells Mediate Persistent Feedforward Inhibition onto Granule Cells in the Olfactory Bulb. *Neuron*, *49*(6), 889–904. https://doi.org/10.1016/j.neuron.2006.02.019

Quirk, C. R., Zutshi, I., Srikanth, S., Fu, M. L., Devico Marciano, N., Wright, M. K., Parsey, D. F., Liu, S., Siretskiy, R. E., Huynh, T. L., Leutgeb, J. K., & Leutgeb, S. (2021). Precisely timed theta oscillations are selectively required during the encoding phase of memory. *Nature Neuroscience*, *24*(11), 1614–1627. https://doi.org/10.1038/s41593-021-00919-0

Ragozzino, M. E., Unick, K. E., & Gold, P. E. (1996). Hippocampal acetylcholine release during memory testing in rats: Augmentation by glucose. *Proceedings of the National Academy of Sciences of the United States of America*, *93*(10), 4693–4698. https://doi.org/10.1073/pnas.93.10.4693

Rahman, J., & Berger, T. (2011). Persistent activity in layer 5 pyramidal neurons following cholinergic activation of mouse primary cortices. *European Journal of Neuroscience*, *34*(1), 22–30. https://doi.org/10.1111/j.1460-9568.2011.07736.x

Ranade, S., Hangya, B., & Kepecs, A. (2013). Multiple Modes of Phase Locking between Sniffing and Whisking during Active Exploration. *The Journal of Neuroscience*, *33*(19), 8250–8256. https://doi.org/10.1523/JNEUROSCI.3874-12.2013

Raut, R. V., Rosenthal, Z. P., Wang, X., Miao, H., Zhang, Z., Lee, J.-M., Raichle, M. E., Bauer, A. Q., Brunton, S. L., Brunton, B. W., & Kutz, J. N. (2023). *Arousal as a universal embedding for spatiotemporal brain dynamics* (p. 2023.11.06.565918). bioRxiv. https://doi.org/10.1101/2023.11.06.565918

Rawlins, J. N., Feldon, J., & Gray, J. A. (1979). Septo-hippocampal connections and the hippocampal theta rhythm. *Experimental Brain Research*, *37*(1), 49–63. https://doi.org/10.1007/BF01474253

Reboreda, A., Jiménez-Díaz, L., & Navarro-López, J. D. (2011). TRP Channels and Neural Persistent Activity. In Md. S. Islam (Ed.), *Transient Receptor Potential Channels* (pp. 595–613). Springer Netherlands. https://doi.org/10.1007/978-94-007-0265-3_32

Reimer, J., Froudarakis, E., Cadwell, C. R., Yatsenko, D., Denfield, G. H., & Tolias, A. S. (2014). Pupil fluctuations track fast switching of cortical states during quiet wakefulness. *Neuron*, *84*(2), 355–362. https://doi.org/10.1016/j.neuron.2014.09.033

Reimer, J., McGinley, M. J., Liu, Y., Rodenkirch, C., Wang, Q., McCormick, D. A., & Tolias, A. S. (2016). Pupil fluctuations track rapid changes in adrenergic and cholinergic activity in cortex. *Nature Communications*, *7*(1), Article 1. https://doi.org/10.1038/ncomms13289

Robbins, T. W., & Everitt, B. J. (1996). Neurobehavioural mechanisms of reward and motivation. *Current Opinion in Neurobiology*, *6*(2), 228–236. https://doi.org/10.1016/S0959-4388(96)80077-8

Robinson, J. C., Ying, J., Hasselmo, M. E., & Brandon, M. P. (2023). Optogenetic Silencing of Medial Septal GABAergic Neurons Disrupts Grid Cell Spatial and Temporal Coding in the Medial Entorhinal Cortex. *bioRxiv: The Preprint Server for Biology*, 2023.11.08.566228. https://doi.org/10.1101/2023.11.08.566228

Robinson, J., Manseau, F., Ducharme, G., Amilhon, B., Vigneault, E., Mestikawy, S. E., & Williams, S. (2016). Optogenetic Activation of Septal Glutamatergic Neurons Drive Hippocampal Theta Rhythms. *Journal of Neuroscience*, *36*(10), 3016–3023. https://doi.org/10.1523/JNEUROSCI.2141-15.2016

Roland, J. J., Stewart, A. L., Janke, K. L., Gielow, M. R., Kostek, J. A., Savage, L. M., Servatius, R. J., & Pang, K. C. H. (2014). Medial Septum-Diagonal Band of Broca (MSDB) GABAergic Regulation

of Hippocampal Acetylcholine Efflux Is Dependent on Cognitive Demands. *Journal of Neuroscience*, *34*(2), 506–514. https://doi.org/10.1523/JNEUROSCI.2352-13.2014
Sainsbury, R. S., Heynen, A., & Montoya, C. P. (1987). Behavioral correlates of hippocampal type 2 theta in the rat. *Physiology & Behavior*, *39*(4), 513–519. https://doi.org/10.1016/0031-9384(87)90382-9
Salib, M., Joshi, A., Katona, L., Howarth, M., Micklem, B. R., Somogyi, P., & Viney, T. J. (2019). GABAergic Medial Septal Neurons with Low-Rhythmic Firing Innervating the Dentate Gyrus and Hippocampal Area CA3. *The Journal of Neuroscience*, *39*(23), 4527–4549. https://doi.org/10.1523/JNEUROSCI.3024-18.2019
Schliebs, R., & Arendt, T. (2011). The cholinergic system in aging and neuronal degeneration. *Behavioural Brain Research*, *221*(2), 555–563. https://doi.org/10.1016/j.bbr.2010.11.058
Schultz, W., Dayan, P., & Montague, P. R. (1997). A neural substrate of prediction and reward. *Science (New York, N.Y.)*, *275*(5306), 1593–1599. https://doi.org/10.1126/science.275.5306.1593
Schultz, W., Romo, R., Ljungberg, T., Mirenowicz, J., Hollerman, J. R., & Dickinson, A. (1994). *Reward-related Signals Carried by Dopamine Neurons*. https://doi.org/10.7551/mitpress/4708.003.0019
Segal, M. (1976). Brain stem afferents to the rat medial septum. *The Journal of Physiology*, *261*. https://doi.org/10.1113/jphysiol.1976.sp011577
Segal, M. (1986). Properties of rat medial septal neurones recorded in vitro. *The Journal of Physiology*, *379*(1), 309–330. https://doi.org/10.1113/jphysiol.1986.sp016255
Segal, M., & Landis, S. (1974). Afferents to the hippocampus of the rat studied with the method of retrograde transport of horseradish peroxidase. *Brain Research*, *78*(1), 1–15. https://doi.org/10.1016/0006-8993(74)90349-7
Senut, M. C., De Bilbao, F., & Lamour, Y. (1990). Medial septal neurons containing *N*-acetyl-aspartyl-glutamate-like immunoreactivity project to the hippocampal formation in the rat. *Neuroscience Letters*, *113*(1), 12–16. https://doi.org/10.1016/0304-3940(90)90486-S
Senut, M. C., Menetrey, D., & Lamour, Y. (1989). Cholinergic and peptidergic projections from the medial septum and the nucleus of the diagonal band of broca to dorsal hippocampus, cingulate cortex and olfactory bulb: A combined wheatgerm agglutinin-apohorseradish peroxidase-gold immunohistochemical study. *Neuroscience*, *30*(2), 385–403. https://doi.org/10.1016/0306-4522(89)90260-1
Shen, L., Zhang, G.-W., Tao, C., Seo, M. B., Zhang, N. K., Huang, J. J., Zhang, L. I., & Tao, H. W. (2022). A bottom-up reward pathway mediated by somatostatin neurons in the medial septum complex underlying appetitive learning. *Nature Communications*, *13*(1), Article 1. https://doi.org/10.1038/s41467-022-28854-z
Shik, M. L., Severin, F. V., & Orlovskiĭ, G. N. (1966). Control of walking and running by means of electric stimulation of the midbrain. *Biofizika*. https://www.semanticscholar.org/paper/%5BControl-of-walking-and-running-by-means-of-of-the-Shik-Severin/8a2996cc3d98ceb171f4c014b4ebce76bdb7977c
Simon, A. P., Poindessous-Jazat, F., Dutar, P., Epelbaum, J., & Bassant, M.-H. (2006). Firing Properties of Anatomically Identified Neurons in the Medial Septum of Anesthetized and Unanesthetized Restrained Rats. *Journal of Neuroscience*, *26*(35), 9038–9046. https://doi.org/10.1523/JNEUROSCI.1401-06.2006
Skaggs, W. E., McNaughton, B. L., Wilson, M. A., & Barnes, C. A. (1996). Theta phase precession in hippocampal neuronal populations and the compression of temporal sequences. *Hippocampus*, *6*(2), 149–172. https://doi.org/10.1002/(SICI)1098-1063(1996)6:2<149::AID-HIPO6>3.0.CO;2-K
Sofroniew, N. J., Cohen, J. D., Lee, A. K., & Svoboda, K. (2014). Natural Whisker-Guided Behavior by Head-Fixed Mice in Tactile Virtual Reality. *The Journal of Neuroscience*, *34*(29), 9537–9550. https://doi.org/10.1523/JNEUROSCI.0712-14.2014

Sofroniew, N. J., & Svoboda, K. (2015). Whisking. *Current Biology*, *25*(4), R137–R140. https://doi.org/10.1016/j.cub.2015.01.008
Sotty, F., Danik, M., Manseau, F., Laplante, F., Quirion, R., & Williams, S. (2003). Distinct electrophysiological properties of glutamatergic, cholinergic and GABAergic rat septohippocampal neurons: Novel implications for hippocampal rhythmicity. *The Journal of Physiology*, *551*(Pt 3), 927. https://doi.org/10.1113/jphysiol.2003.046847
Staib, J. M., Della Valle, R., & Knox, D. K. (2018). Disruption of medial septum and diagonal bands of Broca cholinergic projections to the ventral hippocampus disrupt auditory fear memory. *Neurobiology of Learning and Memory*, *152*, 71–79. https://doi.org/10.1016/j.nlm.2018.05.009
Stancampiano, R., Cocco, S., Cugusi, C., Sarais, L., & Fadda, F. (1999). Serotonin and acetylcholine release response in the rat hippocampus during a spatial memory task. *Neuroscience*, *89*(4), 1135–1143. https://doi.org/10.1016/s0306-4522(98)00397-2
Starzl, T. E., Taylor, C. W., & Magoun, H. W. (1951). ASCENDING CONDUCTION IN RETICULAR ACTIVATING SYSTEM, WITH SPECIAL REFERENCE TO THE DIENCEPHALON. *Journal of Neurophysiology*, *14*(6), 461–477. https://doi.org/10.1152/jn.1951.14.6.461
Strange, B. A., Witter, M. P., Lein, E. S., & Moser, E. I. (2014). Functional organization of the hippocampal longitudinal axis. *Nature Reviews. Neuroscience*, *15*(10), 655–669. https://doi.org/10.1038/nrn3785
Swanson, L. W., & Cowan, W. M. (1977). An autoradiographic study of the organization of the efferent connections of the hippocampal formation in the rat. *The Journal of Comparative Neurology*, *172*(1), 49–84. https://doi.org/10.1002/cne.901720104
Swanson, L. W., & Cowan, W. M. (1979). The connections of the septal region in the rat. *Journal of Comparative Neurology*, *186*(4), 621–655. https://doi.org/10.1002/cne.901860408
Sweeney, P., Li, C., & Yang, Y. (2017). Appetite suppressive role of medial septal glutamatergic neurons. *Proceedings of the National Academy of Sciences*, *114*(52), 13816–13821. https://doi.org/10.1073/pnas.1707228114
Sweeney, P., & Yang, Y. (2016). An Inhibitory Septum to Lateral Hypothalamus Circuit That Suppresses Feeding. *Journal of Neuroscience*, *36*(44), 11185–11195. https://doi.org/10.1523/JNEUROSCI.2042-16.2016
Tahvildari, B., Alonso, A. A., & Bourque, C. W. (2008). Ionic Basis of on and off Persistent Activity in Layer III Lateral Entorhinal Cortical Principal Neurons. *Journal of Neurophysiology*, *99*(4), 2006–2011. https://doi.org/10.1152/jn.00911.2007
Tai, S. K., Ma, J., & Leung, L. S. (2014). Medial Septal Cholinergic Neurons Modulate Isoflurane Anesthesia. *Anesthesiology*, *120*(2), 392–402. https://doi.org/10.1097/ALN.0b013e3182a7cab6
Takács, V. T., Cserép, C., Schlingloff, D., Pósfai, B., Szőnyi, A., Sos, K. E., Környei, Z., Dénes, Á., Gulyás, A. I., Freund, T. F., & Nyiri, G. (2018). Co-transmission of acetylcholine and GABA regulates hippocampal states. *Nature Communications*, *9*(1), 2848. https://doi.org/10.1038/s41467-018-05136-1
Takeuchi, Y., Harangozó, M., Pedraza, L., Földi, T., Kozák, G., Li, Q., & Berényi, A. (2021). Closed-loop stimulation of the medial septum terminates epileptic seizures. *Brain*, *144*(3), 885–908. https://doi.org/10.1093/brain/awaa450
Takeuchi, Y., Nagy, A. J., Barcsai, L., Li, Q., Ohsawa, M., Mizuseki, K., & Berényi, A. (2021). The Medial Septum as a Potential Target for Treating Brain Disorders Associated With Oscillopathies. *Frontiers in Neural Circuits*, *15*. https://doi.org/10.3389/fncir.2021.701080
Tamamaki, N., Yanagawa, Y., Tomioka, R., Miyazaki, J.-I., Obata, K., & Kaneko, T. (2003). Green fluorescent protein expression and colocalization with calretinin, parvalbumin, and somatostatin in the GAD67-GFP knock-in mouse. *Journal of Comparative Neurology*, *467*(1), 60–79. https://doi.org/10.1002/cne.10905
Tao, S., Wang, Y., Peng, J., Zhao, Y., He, X., Yu, X., Liu, Q., Jin, S., & Xu, F. (2021). Whole-Brain Mapping the Direct Inputs of Dorsal and Ventral CA1 Projection Neurons. *Frontiers in Neural Circuits*, *15*, 643230. https://doi.org/10.3389/fncir.2021.643230

Tappaz, M. L., Brownstein, M. J., & Palkovits, M. (1976). Distribution of glutamate decarboxylase in discrete brain nuclei. *Brain Research*, *108*(2), 371–379. https://doi.org/10.1016/0006-8993(76)90193-1

Teles-Grilo Ruivo, L., & Mellor, J. (2013). Cholinergic modulation of hippocampal network function. *Frontiers in Synaptic Neuroscience*, *5*. https://www.frontiersin.org/articles/10.3389/fnsyn.2013.00002

Terrazas, A., Krause, M., Lipa, P., Gothard, K. M., Barnes, C. A., & McNaughton, B. L. (2005). Self-Motion and the Hippocampal Spatial Metric. *The Journal of Neuroscience*, *25*(35), 8085–8096. https://doi.org/10.1523/JNEUROSCI.0693-05.2005

Tesmer, A. L., Li, X., Bracey, E., Schmandt, C., Polania, R., Peleg-Raibstein, D., & Burdakov, D. (2024). Orexin neurons mediate temptation-resistant voluntary exercise. *Nature Neuroscience*, *27*(9), 1774–1782. https://doi.org/10.1038/s41593-024-01696-2

Torii, S. (1961). Two types of pattern of hippocampal electrical activity induced by stimulation of hypothalamus and surrounding parts of rabbit's brain. *The Japanese Journal of Physiology*, *11*, 147–157. https://doi.org/10.2170/jjphysiol.11.147

Tóth, K., & Freund, T. F. (1992). Calbindin D28k-containing nonpyramidal cells in the rat hippocampus: Their immunoreactivity for GABA and projection to the medial septum. *Neuroscience*, *49*(4), 793–805. https://doi.org/10.1016/0306-4522(92)90357-8

Uhl, G. R., Kuhar, M. J., & Snyder, S. H. (1977). Neurotensin: Immunohistochemical localization in rat central nervous system. *Proceedings of the National Academy of Sciences of the United States of America*, *74*(9), 4059–4063. https://doi.org/10.1073/pnas.74.9.4059

Ullsperger, M., & von Cramon, D. Y. (2003). Error monitoring using external feedback: Specific roles of the habenular complex, the reward system, and the cingulate motor area revealed by functional magnetic resonance imaging. *The Journal of Neuroscience*, *23*(10), 4308–4314. https://doi.org/10.1523/jneurosci.23-10-04308.2003

Unal, G., Crump, M. G., Viney, T. J., Éltes, T., Katona, L., Klausberger, T., & Somogyi, P. (2018). Spatio-temporal specialization of GABAergic septo-hippocampal neurons for rhythmic network activity. *Brain Structure and Function*, *223*(5), 2409–2432. https://doi.org/10.1007/s00429-018-1626-0

Unal, G., Joshi, A., Viney, T. J., Kis, V., & Somogyi, P. (2015). Synaptic Targets of Medial Septal Projections in the Hippocampus and Extrahippocampal Cortices of the Mouse. *The Journal of Neuroscience: The Official Journal of the Society for Neuroscience*, *35*(48), 15812–15826. https://doi.org/10.1523/JNEUROSCI.2639-15.2015

Vandecasteele, M., Varga, V., Berényi, A., Papp, E., Barthó, P., Venance, L., Freund, T. F., & Buzsáki, G. (2014). Optogenetic activation of septal cholinergic neurons suppresses sharp wave ripples and enhances theta oscillations in the hippocampus. *Proceedings of the National Academy of Sciences*, *111*(37), 13535–13540. https://doi.org/10.1073/pnas.1411233111

Vanderwolf, C. H. (1969). Hippocampal electrical activity and voluntary movement in the rat. *Electroencephalography and Clinical Neurophysiology*, *26*(4), 407–418. https://doi.org/10.1016/0013-4694(69)90092-3

Venditto, S. J. C., Le, B., & Newman, E. L. (2019). Place cell assemblies remain intact, despite reduced phase precession, after cholinergic disruption. *Hippocampus*, *29*(11), 1075–1090. https://doi.org/10.1002/hipo.23100

Veres, J. M., Andrasi, T., Nagy-Pal, P., & Hajos, N. (2023). CaMKIIα Promoter-Controlled Circuit Manipulations Target Both Pyramidal Cells and Inhibitory Interneurons in Cortical Networks. *eNeuro*, *10*(4), ENEURO.0070-23.2023. https://doi.org/10.1523/ENEURO.0070-23.2023

Vertes, R. P. (1982). Brain stem generation of the hippocampal EEG. *Progress in Neurobiology*, *19*(3), 159–186. https://doi.org/10.1016/0301-0082(82)90005-3

Vertes, R. P. (1992). PHA-L analysis of projections from the supramammillary nucleus in the rat. *Journal of Comparative Neurology*, *326*(4), 595–622. https://doi.org/10.1002/cne.903260408

Vertes, R. P., & Kocsis, B. (1997). Brainstem-diencephalo-septohippocampal systems controlling the theta rhythm of the hippocampus. *Neuroscience*, *81*(4), 893–926. https://doi.org/10.1016/s0306-4522(97)00239-x

Vinck, M., Batista-Brito, R., Knoblich, U., & Cardin, J. A. (2015a). Arousal and Locomotion Make Distinct Contributions to Cortical Activity Patterns and Visual Encoding. *Neuron*, *86*(3), 740–754. https://doi.org/10.1016/j.neuron.2015.03.028

Vinck, M., Batista-Brito, R., Knoblich, U., & Cardin, J. A. (2015b). Arousal and Locomotion Make Distinct Contributions to Cortical Activity Patterns and Visual Encoding. *Neuron*, *86*(3), 740–754. https://doi.org/10.1016/j.neuron.2015.03.028

Vollan, A. Z., Gardner, R. J., Moser, M.-B., & Moser, E. I. (2024). *Left-right-alternating theta sweeps in the entorhinal-hippocampal spatial map* (p. 2024.05.16.594473). bioRxiv. https://doi.org/10.1101/2024.05.16.594473

Wang, C.-A., & Munoz, D. P. (2015). A circuit for pupil orienting responses: Implications for cognitive modulation of pupil size. *Current Opinion in Neurobiology*, *33*, 134–140. https://doi.org/10.1016/j.conb.2015.03.018

Watson, T. C., Obiang, P., Torres-Herraez, A., Watilliaux, A., Coulon, P., Rochefort, C., & Rondi-Reig, L. (2019). Anatomical and physiological foundations of cerebello-hippocampal interaction. *eLife*, *8*, e41896. https://doi.org/10.7554/eLife.41896

Wee, R. W. S., Mishchanchuk, K., AlSubaie, R., Church, T. W., Gold, M. G., & MacAskill, A. F. (2024). Internal-state-dependent control of feeding behavior via hippocampal ghrelin signaling. *Neuron*, *112*(2), 288-305.e7. https://doi.org/10.1016/j.neuron.2023.10.016

Wells, C. E., Amos, D. P., Jeewajee, A., Douchamps, V., Rodgers, J., O'Keefe, J., Burgess, N., & Lever, C. (2013). Novelty and anxiolytic drugs dissociate two components of hippocampal theta in behaving rats. *The Journal of Neuroscience: The Official Journal of the Society for Neuroscience*, *33*(20), 8650–8667. https://doi.org/10.1523/JNEUROSCI.5040-12.2013

Wetzel, W., Ott, T., & Matthies, H. (1978). Periodic behavioral changes during hippocampal theta rhythm elicited by septal stimulation in rats. *Neuroscience*, *3*(8), 755–760. https://doi.org/10.1016/0306-4522(78)90071-4

Whishaw, I. Q., & Vanderwolf, C. H. (1973). Hippocampal EEG and behavior: Change in amplitude and frequency of RSA (Theta rhythm) associated with spontaneous and learned movement patterns in rats and cats. *Behavioral Biology*, *8*(4), 461–484. https://doi.org/10.1016/S0091-6773(73)80041-0

Winson, J. (1978). Loss of hippocampal theta rhythm results in spatial memory deficit in the rat. *Science*, *201*(4351), 160–163. Scopus. https://doi.org/10.1126/science.663646

Winter, S. S., Mehlman, M. L., Clark, B. J., & Taube, J. S. (2015). Passive Transport Disrupts Grid Signals in the Parahippocampal Cortex. *Current Biology*, *25*(19), 2493–2502. https://doi.org/10.1016/j.cub.2015.08.034

Wu, J.-L., Li, Z.-M., Chen, H., Chen, W.-J., Hu, N.-Y., Jin, S.-Y., Li, X.-W., Chen, Y.-H., Yang, J.-M., & Gao, T.-M. (2024). Distinct septo-hippocampal cholinergic projections separately mediate stress-induced emotional and cognitive deficits. *Science Advances*, *10*(45), eado1508. https://doi.org/10.1126/sciadv.ado1508

Wu, X., Morishita, W., Beier, K. T., Heifets, B. D., & Malenka, R. C. (2021). 5-HT modulation of a medial septal circuit tunes social memory stability. *Nature*, *599*(7883), 96–101. https://doi.org/10.1038/s41586-021-03956-8

Xia, J.-M., Fan, B.-Q., Yi, X.-W., Ni, W.-W., Zhou, Y., Chen, D.-D., Yi, W.-J., Feng, L.-L., Xia, Y., Li, S.-S., Qu, W.-M., Han, Y., Huang, Z.-L., & Li, W.-X. (2024). Medial Septal Glutamatergic Neurons Modulate States of Consciousness during Sevoflurane Anesthesia in Mice. *Anesthesiology*, *140*(1), 102–115. https://doi.org/10.1097/ALN.0000000000004798

Xu, M., Chung, S., Zhang, S., Zhong, P., Ma, C., Chang, W.-C., Weissbourd, B., Sakai, N., Luo, L., Nishino, S., & Dan, Y. (2015). Basal forebrain circuit for sleep-wake control. *Nature Neuroscience*, *18*(11), 1641–1647. https://doi.org/10.1038/nn.4143

Yamada-Hanff, J., & Bean, B. P. (2013). Persistent Sodium Current Drives Conditional Pacemaking in CA1 Pyramidal Neurons under Muscarinic Stimulation. *Journal of Neuroscience*, *33*(38), 15011–15021. https://doi.org/10.1523/JNEUROSCI.0577-13.2013

Yan, H.-D., Villalobos, C., & Andrade, R. (2009). TRPC Channels Mediate a Muscarinic Receptor-Induced Afterdepolarization in Cerebral Cortex. *Journal of Neuroscience*, *29*(32), 10038–10046. https://doi.org/10.1523/JNEUROSCI.1042-09.2009

Ye, J., Witter, M. P., Moser, M.-B., & Moser, E. I. (2018). Entorhinal fast-spiking speed cells project to the hippocampus. *Proceedings of the National Academy of Sciences*, *115*(7), E1627–E1636. https://doi.org/10.1073/pnas.1720855115

Yoshida, M., Fransén, E., & Hasselmo, M. E. (2008). mGluR-dependent persistent firing in entorhinal cortex layer III neurons. *European Journal of Neuroscience*, *28*(6), 1116–1126. https://doi.org/10.1111/j.1460-9568.2008.06409.x

Yoshida, M., & Hasselmo, M. E. (2009). Persistent Firing Supported by an Intrinsic Cellular Mechanism in a Component of the Head Direction System. *The Journal of Neuroscience*, *29*(15), 4945–4952. https://doi.org/10.1523/JNEUROSCI.5154-08.2009

Zhang, G.-W., Shen, L., Zhong, W., Xiong, Y., Zhang, L. I., & Tao, H. W. (2018). Transforming Sensory Cues into Aversive Emotion via Septal-Habenular Pathway. *Neuron*, *99*(5), 1016-1028.e5. https://doi.org/10.1016/j.neuron.2018.07.023

Zhang, G.-W., Sun, W.-J., Zingg, B., Shen, L., He, J., Xiong, Y., Tao, H. W., & Zhang, L. I. (2018). A Non-canonical Reticular-Limbic Central Auditory Pathway via Medial Septum Contributes to Fear Conditioning. *Neuron*, *97*(2), 406-417.e4. https://doi.org/10.1016/j.neuron.2017.12.010

Zhang, Z., Reboreda, A., Alonso, A., Barker, P. A., & Séguéla, P. (2011). TRPC channels underlie cholinergic plateau potentials and persistent activity in entorhinal cortex. *Hippocampus*, *21*(4), 386–397. https://doi.org/10.1002/hipo.20755

Zhu, C., Yao, Y., Xiong, Y., Cheng, M., Chen, J., Zhao, R., Liao, F., Shi, R., & Song, S. (2017). Somatostatin Neurons in the Basal Forebrain Promote High-Calorie Food Intake. *Cell Reports*, *20*(1), 112–123. https://doi.org/10.1016/j.celrep.2017.06.007

Zutshi, I., Brandon, M. P., Fu, M. L., Donegan, M. L., Leutgeb, J. K., & Leutgeb, S. (2018). Hippocampal Neural Circuits Respond to Optogenetic Pacing of Theta Frequencies by Generating Accelerated Oscillation Frequencies. *Current Biology*, *28*(8), 1179-1188.e3. https://doi.org/10.1016/j.cub.2018.02.061

Zylberberg, J., & Strowbridge, B. W. (2017). Mechanisms of Persistent Activity in Cortical Circuits: Possible Neural Substrates for Working Memory. *Annual Review of Neuroscience*, *40*, 603–627. https://doi.org/10.1146/annurev-neuro-070815-014006